



## **Orthogonal Generalized Frequency Division Multiplexing (OGFDM)**

Submitted for the Degree of  
Doctor of Philosophy  
At the University of Northampton

Year 2019

Author's Full Name

**Mohammad R. Kadhum**

© [Mohammad R. Kadhum] [year of completion (degree award) 2020].

This thesis is copyright material and no quotation from it may be published without proper acknowledgement.

*“If you don't design your own life plan, chances are you'll fall into someone else's plan. And guess what they have planned for you? Not much.”*

*Jim Rohn*

## **DECLARATION**

*I hereby declare that the work described in this thesis is original work undertaken by me for the degree of Doctor of Philosophy, at the Department of Computing (Computer Networks Engineering)- University of Northampton, United Kingdom. No part of the material described in this thesis has been submitted for any award of any other degree or qualification in this or any other University or College of advanced education.*

***Mohammad R. Kadhum***

## **ACKNOWLEDGMENTS**

*I'd like to thank my God for supporting me during my challenge time. I also thank my supervisor and lovely family for their backing during my PhD journey.*

## PUBLICATIONS

During the 4-years of the research study in the Department of Computing (Computer Network Engineering) at the University of Northampton, the following papers were published:

- 1) Kadhum, M. R. et al. (2018) ‘Digital Chunk Processing with Orthogonal GFDM Doubles Wireless Channel Capacity’, in *Proceeding of computing conference 2018, London*, pp. 1–6.
- 2) Kadhum, M. R. Kanakis, T. and Crockett, R. (2019a) ‘Dynamic Bit Loading with the OGFDM Waveform Maximises Bit-Rate of Future Mobile Communications’, in *Proceeding of computing conference 2019, London*, pp. 1–6.
- 3) Kadhum, M. R. Kanakis, T. and Crockett, R. (2019b) ‘Intra Channel Interference Avoidance with The OGFDM Boosts Channel Capacity of Future Wireless Mobile Communication’, in *Proceeding of computing conference 2019, London*, pp. 1–6.
- 4) Kadhum, M. R. (2019) ‘New Multi-Carrier Candidate Waveform For the 5G Physical Layer of Wireless Mobile Networks’, in *Proceeding of 2019 Wireless Days (WD) conference, Manchester*, IEEE, pp. 1–7.
- 5) Kadhum, M. R. (2020) ‘Upgrading Physical Layer of Multi-Carrier OGFDM Waveform for Improving Wireless Channel Capacity of 5G Mobile Networks and Beyond’, information Article, 11(1). Available at: <https://www.mdpi.com/2078-2489/11/1/35>.

## ABSTRACT

This thesis focuses on introducing a novel technique of the transmission waveform termed as orthogonal generalized frequency division multiplexing (OGFDM) for increasing the wireless channel capacity without the need for extra bandwidth (BW) size or power consumption. The new wireless waveform (OGFDM) tends to obtain a better BW efficiency which in turn can increase highly the wireless channel capacity in comparison with the generalized frequency division multiplexing (GFDM) and cyclic-prefix orthogonal frequency division multiplexing (CP-OFDM). The main feature of the OGFDM is developing the physical layer of future mobile networks by achieving the orthogonality between non-orthogonal filters, removing the interference between adjacent frequency subcarriers, and gaining a flexible bit loading scheme. Since the key downsides of the 4G waveform (CP-OFDM), several alternative transmission waveforms have been investigated for improving transmission techniques of the upcoming communication networks (5G and beyond). This, as a result, comes up with introducing the GFDM as the best candidate waveform for the 5G air interface. Nevertheless, due to ignoring the orthogonality with the GFDM, the BW efficiency is severely affected which in turn causes in extremely reducing the gained channel capacity (research gap). For this reason, the proposed OGFDM waveform aims to improve wireless channel capacity by investigating different levels of processing and carrier schemes. As such, three key levels called as filtration level, oversampling level, and modulation level are adopted for a variant range of OGFDM carriers like a single carrier, couple carrier, quadruple carrier, and multi-carrier system. Regarding the single carrier OGFDM system where the filtration level is developed, the orthogonality is attained between the non-orthogonal filters of the GFDM frequency subcarriers. The core idea behind this novel technique is increasing the efficiency of the applied BW which in turn can double the capacity of the channel at the acceptable level of the bit error rate (BER). Concerning the couple carrier OGFDM system where the oversampling level is developed, the double oversampling mode is applied side by side with the normal one. As a result, the OGFDM waveform can efficiently avoid the interference between adjacent frequency subcarriers improving the quality of service under bad transmission states. As regards the quadruple carrier OGFDM system where the modulation level is improved, a flexible modulation scheme is utilized rather than the fixed modulation formats. Consequently, multilevel modulation shapes are optimally assigned to gain an enhanced channel capacity in accordance with the realistic transmission state. To achieve a higher BW efficiency, the preliminary multi-carrier system that combines the three levels of processing in one uniformed physical platform is introduced. To demonstrate the main advantages of OGFDM waveform, the multicarrier system is further extended and compared with the GFDM (5G technology) and CP-OFDM (LTE Ericsson technology). Hence, the multi-carrier OGFDM can double, boost, and yet maximize the bit-rate of the transmission relative to the GFDM and CP-OFDM at the acceptable level of the BER. The MATLAB simulation and Visio tools are utilized to validate the results and represent them graphically.

## Table of contents:

Quotation	I
Declaration	II
Acknowledgment	III
Publications	IV
Abstract	V
Table of contents	VI
List of Figures	VIII
List of tables	XI
List of abbreviations	XII
Chapter 1: Thesis Overview	1
1.1 Historical View	1
1.2 Background	4
1.3 Thesis Contribution	6
Chapter 2: Wireless Waveforms Literature Review	10
2.1 Cyclic-Prefix Orthogonal Frequency Division Multiplexing	10
2.1.1 CP-OFDM Transceiver	10
2.1.2 CP-OFDM in 4G Cellular Communications	12
2.1.3 Basic CP-OFDM Parameterization in Long Term Evolution system	13
2.1.4 Potential Downsides of CP-OFDM	15
2.2 Waveform Candidates for the Future Generation of Mobile	17
2.2.1 Modern Motivations	17
2.2.2 Filter Bank Multi-Carrier	18
2.2.3 Universal Filtered Multi-Carrier	20
2.2.4 Filtered OFDM	22
2.2.5 Generalized Frequency Division Multiplexing	24
2.2.6 Comparison of the 5G candidate waveforms	26
2.2.7 Main Scenarios of Future Mobile Networks	28
Chapter 3: Processing Levels of OGFDM Waveform	33

3.1 Filtration Level	33
3.1.1 Introduction	33
3.1.2 System Model	35
3.1.3 Experimental Results	45
3.2 Oversampling Level	50
3.2.1 Introduction	50
3.2.2 System Model	51
3.2.3 Experimental Results	58
3.3 Modulation Level	63
3.3.1 Introduction	63
3.3.2 System Model	65
3.3.3 Experimental Results	71
3.4 Summary	74
Chapter 4: Multi-Carrier Stages of OGFDM Waveform	76
4.1 Preliminary Stage	76
4.1.1 Introduction	76
4.1.2 System Model	79
4.1.3 Experimental Results	84
4.2 Upgraded Stage	92
4.2.1 Introduction	92
4.2.2 System Model	94
4.2.3 Experimental Results	100
4.3 Summary	118
Chapter 5: Conclusion and Future Work	119
5.1 Conclusion	119
5.2 Future Work	123
References	124
Appendix	130

## List of figures:

Figure 1.1: Bell's harmonic telegraph system	2
Figure 2.1: CP-OFDM transceiver system	10
Figure 2.2: Cyclic prefix of CP-OFDM	11
Figure 2.3: Orthogonality in the CP-OFDM	12
Figure 2.4: Modern requirements of future mobile networks	17
Figure 2.5: Apply the filter for the FBMC subcarriers	19
Figure 2.6: Block diagram for the FBMC transmitter	19
Figure 2.7: Apply the filter for the UFMC subcarriers	21
Figure 2.8: Block diagram for the UFMC transmitter	21
Figure 2.9: Apply the filter for the F-OFDM subcarriers	22
Figure 2.10: Block diagram for the F-OFDM transmitter	23
Figure 2.11: Apply the filter for the GFDM subcarriers	24
Figure 2.12: Block diagram for the GFDM transmitter	25
Figure 2.13: Main scenarios of future mobile networks	29
Figure 3.1.1: Block diagram of single carrier OGFDM transmitter	36
Figure 3.1.2: Block diagram of single carrier OGFDM receiver	36
Figure 3.1.3: Bandwidth efficiency with both RRC and Hilbert filters (1 <sup>st</sup> case)	41
Figure 3.1.4: Orthogonal Hilbert filters vs non-orthogonal RRC filter (1st case)	42
Figure 3.1.5: Bandwidth efficiency with both RRC and Hilbert filters (2 <sup>nd</sup> case)	43
Figure 3.1.6: Orthogonal Hilbert filters vs non-orthogonal RRC filter (2 <sup>nd</sup> case)	44
Figure 3.1.7: Effect of the filter coefficients on the BER system performance	47
Figure 3.1.8: Roll-off effect on BER system performance	47
Figure 3.1.9: Combination of cosine and sine filter responses in the frequency domain	48
Figure 3.1.10: Higher (double) channel capacity of single carrier OGFDM than the GFDM	49
Figure 3.1.11: Similar SNR for both single carrier OGFDM and GFDM	49
Figure 3.2.1: Transmitter of the couple carriers OGFDM with ICIA	52
Figure 3.2.2: Receiver side of the couple carriers OGFDM with the ICIA	53
Figure 3.2.3: Normal oversampling for 4 filtered subcarriers	55
Figure 3.2.4: Double oversampling for 4 filtered subcarriers	56

Figure 3.2.5: Channel capacity vs roll-off factor of OGFDM with normal /double oversampling	60
Figure 3.2.6: BW efficiency of the OGFDM with normal /double oversampling vs the SNR	62
Figure 3.3.1: DBL system for the transmitter side of the quadruple carriers OGFDM	66
Figure 3.3.2: DBL system for the receiver side of the quadruple carriers OGFDM	67
Figure 3.3.3: Apply the DBL system for induced SNR between two successive modulation formats	72
Figure 3.3.4: Maximising achieved bit-rate with the DBL system (LB, MB, HB) and BER equals to ( $10^{-3}$ )	74
Figure 4.1.1: Wireless transmission system of the multi-carrier OGFDM	79
Figure 4.1.2: Wireless reception system of the multi-carrier OGFDM	81
Figure 4.1.3: Normal case (OV=K)	83
Figure 4.1.4: Double case (OV=2K)	84
Figure 4.1.5: Transmission spectrum for a single carrier in the OGFDM system	86
Figure 4.1.6: Transmission spectrum of the multi-carrier OGFDM	86
Figure 4.1.7: Channel capacity of the multi-carrier OGFDM vs GFDM. with $F_{DAC} = 4$ GHz	87
Figure 4.1.8: BER of variant roll-off factor with typical oversampling	88
Figure 4.1.9: BER of variant roll-off factor with double oversampling	89
Figure 4.1.10: BW efficiency of the multi-carrier OGFDM with typical and double oversampling	90
Figure 4.1.11: Improved channel capacities (C1, C2, C3) with the adaptive modulation of the OGFDM	91
Figure 4.2.1: Wireless transmitter side of the multi-carrier OGFDM system with layer and level processing	95
Figure 4.2.2: Wireless receiver side of the multi-carrier OGFDM system with layer and level processing	97
Figure 4.2.3: Case 1(initial): $F_{DAC} = 2$ GHz, $K=16$	101
Figure 4.2.4: Case 2: $F_{DAC} = 2$ GHz, $K=32$	101
Figure 4.2.5: Case 3: $F_{DAC} = 4$ GHz, $K=16$	102
Figure 4.2.6: Case 4: $F_{DAC} = 4$ GHz, $K=32$	102
Figure 4.2.7: Case 5: $F_{DAC} = 6$ GHz, $K=32$	103
Figure 4.2.8: Channel capacity of the multi-carrier OGFDM vs GFDM with diverse sampling frequency	105
Figure 4.2.9: Similar achieved SNR for both multi-carrier OGFDM and GFDM	106
Figure 4.2.10: Channel capacity of upgraded OGFDM vs GFDM with normal and double oversampling	108
Figure 4.2.11: BW efficiency of multi-carrier OGFDM vs GFDM with normal and double oversampling	110
Figure 4.2.12: Three significant adaptive areas, LB, MB, and HB between 128 & 256 QAM	111
Figure 4.2.13: Utilization of adaptive modulations in the multi-carrier OGFDM and GFDM	113

Figure 4.2.14: SNR level difference between the OGFDM and the CP-OFDM (Ericsson technology)	114
Figure 4.2.15: Channel capacity difference between multi-carrier OGFDM and CP-OFDM (Ericsson technology)	115
Figure 4.2.16: BW efficiency difference between the OGFDM and CP-OFDM (Ericsson technology) in good transmission condition	116
Figure 4.2.17: BW efficiency difference between the OGFDM and CP-OFDM (Ericsson technology) in bad transmission condition	117
Figure 4.2.18: Difference in channel capacity between the OGFDM and CP-OFDM (Ericsson technology) for adaptive and fixed modulations	117

## **List of tables:**

Table 2.1: Comparison between the main candidate waveforms for 5G mobile including the OGFDM	26
Table 3.1.1: System parameters for the single carrier OGFDM	46
Table 3.2.1: System parameters for the couple carriers OGFDM	59
Table 3.3.1: System parameters for the quadruple carriers OGFDM	71
Table 4.1.1: System parameters for the multi-carrier OGFDM	85
Table 4.2.1: System parameters for the upgraded multi-carrier OGFDM	100
Table 4.2.2: Comparison of expansion trials for multi-carrier OGFDM system	103

## **List of abbreviations:**

FDM	frequency division multiplexing
OFDM	orthogonal frequency division multiplexing
BW	bandwidth
BER	bit error rate
AWGN	additive white gaussian noise
SNR	signal to noise ratio
QAM	quadrature amplitude modulation
IFFT	inverse fast Fourier transform
FFT	fast Fourier transform
ISI	inter-symbol interference
ICI	inter-carrier interference
PAPR	peak-to-average-power ratio
OOB	out of band
FBMC	filter bank multi-carrier
UFMC	universal filtered multi-carrier
F-OFDM	filtered OFDM
GFDM	generalized frequency division multiplexing
CP-OFDM	cyclic-prefix OFDM
RRC	root raised cosine
OGFDM	orthogonal generalized frequency division multiplexing
DCP	digital chunk processing
ICIA	intra-channel interference avoidance
DBL	dynamic bit loading
4G	fourth generation of mobile
5G	fifth generation of mobile
ADC	analog to digital converter
DAC	digital to analog converter

# **Chapter 1: Thesis Overview**

On the brink of sophisticated generations of mobile starting with the fifth generation (5G) and moving on to the future mobile technologies, the necessity for developing the wireless telecommunications waveform is extremely required. The main reason beyond this is to support the future digital lifestyle that principally needs for higher wireless channel capacity than the currently applied.

Due to the main downsides of the 4G waveform, cyclic prefix orthogonal frequency division multiplexing (CP-OFDM), the wireless research community been investigated alternative transmission techniques for improving waveform of the upcoming communication networks. This, as a result, comes up with presenting the generalized frequency division multiplexing (GFDM) for the 5G air interface. Nevertheless, since ignoring the orthogonality with the considered GFDM, the bandwidth (BW) efficiency is severely impacted which in turn causes in highly reducing the gained channel capacity (research gap).

This thesis focuses on introducing a novel technique of the transmission waveform termed as orthogonal generalized frequency division multiplexing (OGFDM) for developing the physical layer of future mobile networks. Therefore, the new wireless transmission waveform can obtain a better BW efficiency by achieving the orthogonality between non-orthogonal filters, adopting improved manipulations for removing the interference and gaining a flexible bit loading scheme. The advanced levels of processing for the OGFDM come up with highly increasing the achieved channel capacity in comparison with the GFDM and CP-OFDM.

## **1.1 Historical View**

The history of the telecommunication system that utilizing various frequency domain comes back to 1870s where Alexander Graham Bell started his research on the Harmonic Telegraphy. Thus, due to competition among telegraph companies which aim to rapidly increase their profits, the researchers of that time sought new ways for enhancing the capacity of transmission by separating channel into a set of non-interfered subchannels. Hence, the necessity for coping with market needs stimulated inventors like Bell to develop a progressive kind of telegraphy (harmonic/multiple channels) that are called now the Frequency Division Multiplexing (FDM) (Schwartz, 2009). The basic harmonic telegraph system including

transmitter and receiver sides side by side with the system inventor (Bell) is shown in Figure 1.1.

After that (about one century), Baudot started his investigation on employing a new way for channel participating which essentially depends on time participation rather than frequency. Hence, moving to a more dynamic way where subscribers can turn regularly by employing time slots. It's worth noting that, the need for this kind of multiplexing which named as time division multiplexing (TDM), was because of inefficiently utilized telegraph line due to significantly wasted gaps between adjacent subchannels. From the frequency domain perspective, the TDM can be represented as a single frequency carrier where the BW can be totally given for one user on each period (Boute, 1985).

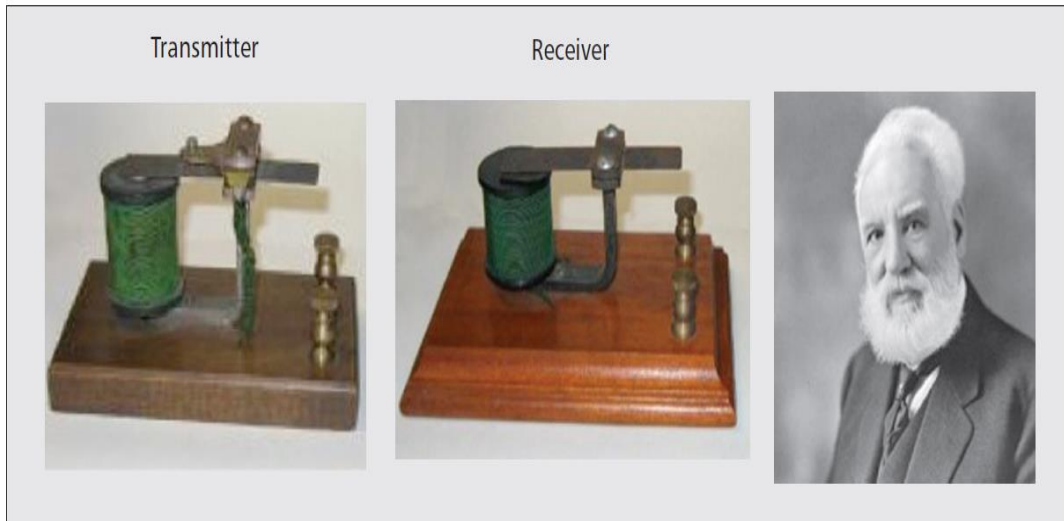


Figure 1.1: Bell's harmonic telegraph system (Schwartz, 2009).

The proposed system with the TDM significantly suffered from transmission limitation which essentially resulted from the impact of the inter-symbol interference (ISI) on the signal speed. Thus, a wider BW of the channel can come up with a greater potentiality of the ISI. To manipulate this quite important issue, the concentrating was backed to the FDM, that fundamentally transmitting data via its narrowed subchannels with a less frequency fading. As such, due to channel capacity restriction with the TDM transmission, the research was turned again to the FDM (Feig, 1990).

Utilizing the FDM, each subchannel can be a little bit affected by the channel response which approximately can be addressed by using a constant pilot (complex number) with previously

determined amplitude and phase. As a result, an easy equalization is achieved via multiplying the received complex numbers by the inverse of the estimated channel response. It's worth pointing that the saved effort of the equalization process compensates roughly the enlarged complexity of the FDM transmission. Nevertheless, the inefficient usage of the channel BW with the FDM waveform motivated researchers to think about a new waveform with advanced features which physically can support extra channel capacity.

The first theoretical study for simultaneous and orthogonal transmission was introduced in 1966. Thus, a new developed multicarrier scheme for real data transmission and without ISI and Inter-Channel Interference (ICI) called OFDM is invented by Robert W. Chang. Afterward, he patented his invention (OFDM) in 1970 (Casas and Leung, 1992).

Until late of the 1960s, the required number of frequency subcarriers for parallel modulations and demodulation of the OFDM is still large. To address this issue, Saltzberg applied a significant adaptation on the OFDM, particularly at the modulation level, to be compatible with the complex number transmission. Hence, employing the QAM system instead of the OQAM at the modulation/demodulation stages of the OFDM. As a result, a less computational complexity system can be obtained with the QAM due to reducing the needed number of parallel subcarriers (Howald, Kesler and Kam, 1998).

In 1971, a breakthrough processing was achieved in the OFDM where the fast Fourier transform (FFT) was used for the first time with the OFDM by Weinstein, Ebert, and Salz to achieve the orthogonality in the frequency domain. This is, accordingly, came up with easier, more efficient and lower complexity implementation of the OFDM system (Son *et al.*, 2002).

About one decade later, in 1980, another important enhancement was applied on the OFDM, principally at the protection level, by Peled and Ruiz. Thus, introducing an advanced guard interval for the OFDM waveform named as cyclic prefix to widely mitigate the multipath phenomena and support the Multiple-Input Multiple-Output (MIMO) transmission. It is important pointing that, the previously applied guard method of the FDM tended to employ unused bands (no-information spaces) in the frequency domain and windowing scheme (raised cosine) in the time domain to address both ICI and ISI respectively. Hence, with the CP-OFDM, the cyclic extension is used instead of utilizing free guard places in frequency domain (Yang, Cheng and Wang, 2005).

The introduced cyclic prefix can effectively manipulate the orthogonality of dispersive transmission channel, particularly, when the employed extension is longer than the impulse response of the channel, hence, improving the level of transmission for severe conditions. However, the proposed cyclic prefix came up with a loss in signal energy due to proportionally repeated part of the original signal. Besides, the reserved bands at the available BW caused in wasting the offered spaces for each launched symbol (Maham, 2006).

Utilizing these two significant milestones (cyclic prefix and FFT) in the CP-OFDM side by side with a developed level of the digital signal processing, the proposed waveform was highly recommended for the improved telecommunications system. Nevertheless, despite the long history of the CP-OFDM existence, it was selected last decade by the telecommunications companies (Bai *et al.*, 2010).

## 1.2 Background

The principal system design of the fourth generation (4G) mobile waveform (CP-OFDM) including the key stages of transmission is presented in the following chapters. Thus, converting the digital data to complex numbers, transforming data from the frequency domain to the time domain, supplying the signal with time protection and then moving from the digital to the analog domain are explored. Hence, demonstrating the fundamental responsibilities of the modulation/demodulation processes, inverse fast Fourier transform (IFFT) stage, supplementary cyclic prefix, and sampling frequency converters. Thus, channel BW distribution, multiplexing operation and orthogonality implementation of frequency subcarriers are discussed. In addition, the key advantages of employing the CP-OFDM in the 4G system design of mobile are listed. As such, the impact of core factors like the spectral efficiency, multi-path transmission and multiple-user access on the system performance are expressed demonstrating why CP-OFDM was elected for the fourth generation of mobile. Thus, exploring the effect of the orthogonality on improving the BW efficiency, cyclic prefix robustness against multi-path phenomena, and multiple access competence on multiple-user system.

The employment of the basic CP-OFDM parameterization in Long Term Evolution (LTE) system are also discussed. Hence, the important design criteria of the cellular system based

CP-OFDM are basically investigated in terms of the maximum probable propagation delay, and maximum expected Doppler effect. Thus, demonstrates how the vital CP-OFDM parameters like subcarrier spacing, sampling frequency, Doppler frequency, transmit time interval, cyclic prefix, and spectrum efficiency, are utilized in the LTE system for both the frequency and time domains. As such, exploring how the transmission and mobility considerations can essentially influence on selecting suitable system parameters, for instance, the optimum length of cyclic prefix and size of frequency subcarrier spacing.

On the other hand, the potential downsides of the CP-OFDM are examined as well. Even though that CP-OFDM can achieve all 4G mobile requirements, it still has proven limitations that would restrict the development of future mobile networks. Thus, the key limitations of CP-OFDM like cyclic prefix overhead, sensitivity to frequency offsets, high peak-to-average-power-ratio (PAPR), and large out of band (OOB) emission are presented.

As a result, alternative waveforms are investigated showing how the candidate waveforms possibly address the weaknesses of the presently used CP-OFDM. Consequently, the system model counting the main stages of processing like modulation, filtration, etc., are explored for the main candidate waveforms of 5G mobile. Thus, highlighting the various methods of applying the filtration level on each introduced waveform like filter bank multi-carrier (FBMC), universal filtered multi-carrier (UFMC), filtered OFDM (F-OFDM) and GFDM.

To clearly identify the research gap, the main advantages and disadvantages of these four candidate waveforms are discussed signifying the key differences among them in terms of the filtration level. That means, indicating the benefit of utilizing the applied filter for an orthogonal frequency subcarrier like the FBMC, set of orthogonal frequency subcarriers like the UFMC and F-OFDM, and non-orthogonal frequency subcarriers like the GFDM. However, the side effect of adding filter is mentioned explaining the principle reasons beyond some issues like the computational complexity, spread energy, and suitability for different types of applications. Besides, the impact of the orthogonality and cyclic prefix on the BW efficiency for each waveform is covered. Moreover, a proper comparison, for the key parameters of the 5G candidate waveforms including our proposed waveform, is delivered to clarify more about the key variances among them.

Significant scenarios of future mobile networks that represent essential motivations for introducing a group of candidate waveforms are also investigated. As such, highlighting the compatibility between the main predicated applications of the next mobile networks and the GFDM that is considered currently as the 5G waveform. Hence, the CP-OFDM incompatibility in achieving the new requirements is principally discussed in comparison with GFDM successes toward upcoming services. It's worth noting that the next needs of mobile networks that exceed the higher capabilities of the 4G are classified into four key applications. Consequently, the modern scenarios like the Bit-pipe Communication, Machine Type Communications, Tactile Internet, and Wireless Regional Area Network are basically demonstrated. That's means, the utilization of these proposed applications and their challenges are explained in terms of the high channel capacity, short transmission latency, massive machines connectivity, and availability in sparsely populated regions.

### **1.3 Thesis Contribution**

The aim of this research is to develop a novel technique for improving the future wireless communication transmission waveform. The proposed OGFDM waveform is thoroughly investigated from different perspectives of processing and carrier schemes. As such, three key levels are adopted for the OGFDM waveform (filtration level, oversampling level, modulation level), which are mainly considered for a variant range of carriers as a single carrier, couple carrier, quadruple carrier, and multi-carrier system.

Concerning the single carrier system, the first experiment for developing the filtration level of the OGFDM waveform is achieved between the filtered frequency subcarriers. Therefore, depending on the great properties of the Hilbert transforms, orthogonality is attained between the non-orthogonal filters of the GFDM frequency subcarriers. The core idea behind this novel technique is to increase the efficiency of the applied BW which in turn can double the capacity of the channel at an acceptable level of the bit error rate (BER). In terms of the system model, the basic system structure of the OGFDM transceiver including two filtered frequency subcarriers working on a single frequency centre is introduced. Besides, principal differences between the conventional root raised cosine (RRC) and developed Hilbert filters are investigated as well. Thus, two important cases are considered to explain the influence of utilizing the orthogonal filters (Hilbert) in the frequency subcarriers level comparing to the non-orthogonal filter (RRC). In addition, the relationship between the main filter parameters

and the optimal system performance is stated in the physical layer of an electrical back-to-back wireless transmission system. The level of treatment that contains all filter management processes is called herein as a digital chunk processing (DCP). By means of the simulation, the effect of utilizing the developed Hilbert filters on the overall system performance for both the channel capacity and BER is explored in the presence of an additive white gaussian noise (AWGN) channel.

With respect to the couple carrier system, the first development of the oversampling level with four adjacent filters of the frequency subcarriers that are adopted for two frequency centres at the OGFDM waveform, is realized. Since the interference management of the wireless mobile network is a significant topic, the traditional method of the interference elimination is no longer suitable. As a result, the OGFDM waveform aims to introduce a novel approach for manipulating the interference for the in-phase / out-phase filters of the adjacent frequency subcarriers. Consequently, depending on the oversampling factor, the interference is effectively avoided between the applied filtered subcarriers improving the quality of transmission under the heavily interfered states. Hence, employing a supportive method can principally consider the conditions of the propagation to avoid the unwanted effect of the roll-off ( $\alpha$ ) factor that in turn can play a big role in improving the available BW efficiency. In terms of the system model, the correlation between the oversampling factor and the Hilbert filter rolling parameter is theoretically investigated. In addition, the key impact of the new oversampling manipulation on the system performance including both the maximum bit-rate and the BER is experimentally achieved. Moreover, the required operations for treating the oversampling level and controlling the relationship with the other related levels are combined in the one block that is termed herein as intra-channel interference avoidance. Furthermore, to estimate the system performance under the AWGN channel, a computer simulation is presented in the physical layer of an electrical back-to-back wireless system.

With reference to the quadruple carrier system, the first improvement of the modulation level with eight adjacent filters of the frequency subcarriers accommodated in four frequency centres of the OGFDM waveform is obtained. Therefore, a hybrid modulation format that is substantially based on an adaptive distribution of bits specification is utilized. As the employment of the fixed modulation schemes causes in a bit-rate restriction for the telecommunication performance, the positive impact of using a flexible modulation scheme as an alternative solution is investigated. Consequently, depending on the changeable channel

conditions, an adaptable boost of the channel capacity can be reached with an adjustable range of the applied modulation formats. Hence, multilevel modulation shapes are optimally assigned to gain an enhanced channel capacity in accordance with the realistic transmission state. In addition, for various levels of the Signal to Noise Ratio (SNR), the influence of adopting a dynamic bit loading on the system performance (maximum bit-rate and acceptable BER) under the AWGN, is investigated. Moreover, the key operations that are needed for the modulation level processing are indicated in one part that is named herein as the dynamic bit loading. In terms of the experimental simulation, a numerical code is used to examine the system performance with the AWGN channel in the physical layer of a wireless electrical back-to-back system.

For the multi-carrier system, a combination of the three levels of processing (filtration, oversampling, and modulation) in one uniformed physical platform, where eight frequency centres can support sixteen frequency subcarriers of the OGFDM waveform, is demonstrated. Utilizing this developed design of the multi-carrier OGFDM, the system performance in terms of the channel capacity and BER performance is further improved. Therefore, at the acceptable level of the BER, the introduced multi-carrier OGFDM can double, boost and yet maximize the bit-rate of the transmission in comparison with the standard GFDM. This is principally realized due to significant operations that are mainly applied for the filtration level, oversampling level, and modulation level of the enhanced multi-carrier system. As such, depending on the advanced Hilbert Filters, orthogonality can be offered as a sophisticated solution for the non-orthogonal filtration of the GFDM system. Consequently, a double bit-rate can be achieved with the multi-carrier OGFDM in relative to the GFDM. In addition, employing an adjustable oversampling process, an extra improvement can be obtained for the overall channel capacity which in turn can play a major role in sustaining the transmission reliability in the worst channel conditions. Moreover, by using a flexible modulation scheme with the announced multi-carrier system, the maximum bit-rate of transmission can be reached at the venial limit of error. Hence, in contrast to the conventional fixed format, the adaptive bit loading can exploit the improved SNR for supporting an additional channel capacity. Additionally, in contrast to the single carrier OGFDM, the multi-carrier OGFDM can fundamentally promote the BW efficiency by offering a durable time period for the transmission. The key multi-carrier system parameters are basically stated in accordance with the optimum system performance. Furthermore, the processing levels of the multi-carrier OGFDM are experimentally demonstrated in the physical layer of an electrical back-to-back

wireless transceiver system. A computer simulation is presented to evaluate the system performance in terms of the BER & channel capacity in the presence of the AWGN.

To demonstrate the main advantages of OGFDM system, the proposed system is further upgraded and compared with other significant waveforms. Since the future mobile networks tend extensively to cope up with the accelerated and exceptional growth of the upcoming market challenges, the proposed scheme of the OGFDM aims to enlarge the number of mobile subscribers yet sustaining each one with a high level of transmission capacity. Therefore, the expanded multi-carrier OGFDM can improve the performance of the future wireless network that targets equally the broad sharing operation (scalability) and elevated transmission rate. Furthermore, the key OGFDM features, like orthogonality, interference avoidance and flexible bit loading can better support transmission efficiency, higher robustness and lower latency than the current waveform. Consequently, investigating the impact of utilizing the advanced Hilbert filters, normal and double oversampling manipulation and dynamic and fixed modulation formats on both the raised sampling frequency and increased number of the subcarriers. To highlight the main advantages of the developed OGFDM, the system performance is compared with the filtered GFDM (5G technology) and CP-OFDM (LTE Ericsson technology). Furthermore, a computer simulation is achieved for the extended system of the OGFDM waveform to experimentally evaluate the transmission performance in terms of the channel capacity and the BER. The improved physical layer of the OGFDM is examined in an electrical back-to-back wireless transmission system.

The rest of this thesis is structured as follows: a detailed literature review is presented in Chapter 2. The main processing levels of the OGFDM are presented in Chapter 3. In Chapter 4 the multi-carrier stages of the OGFDM are demonstrated and compared with GFDM and CP-OFDM. The findings of this thesis and future work are summarised in Chapter 5.

# Chapter 2: Wireless Waveforms Literature Review

## 2.1 Cyclic-Prefix Orthogonal Frequency Division Multiplexing

### 2.1.1 CP-OFDM Transceiver

CP-OFDM is a wireless multi-carrier transmission waveform, able to divide an available channel BW into  $N$  number of parallel frequency subcarriers and achieve the orthogonality for them. The multiplexing between utilized subcarriers can be applied in both, frequency and time domains (Ballal, Chadha and Satam, 2013).

With respect to the ideal design of the CP-OFDM transceiver, it's clear from Figure 2.1, particularly, at the transmitter side, the digital data is converted to constellations (complex numbers) using one of the applied modulation formats. A complex number is responsible for generating the amplitude and phase for an employed frequency subcarrier. The CP-OFDM waveform works on both, the low modulation formats like phase shift keying (PSK) and high modulation schemes such as 16, 32, 64 quadrature amplitude modulation (QAM). With higher modulation schemes, the channel capacity is widely improved. However, a higher SNR is required than the lower schemes of modulation. After that, a serial to parallel converter is used to produce  $K$  streams of generated constellations that corresponding to  $K$  frequency subcarriers.

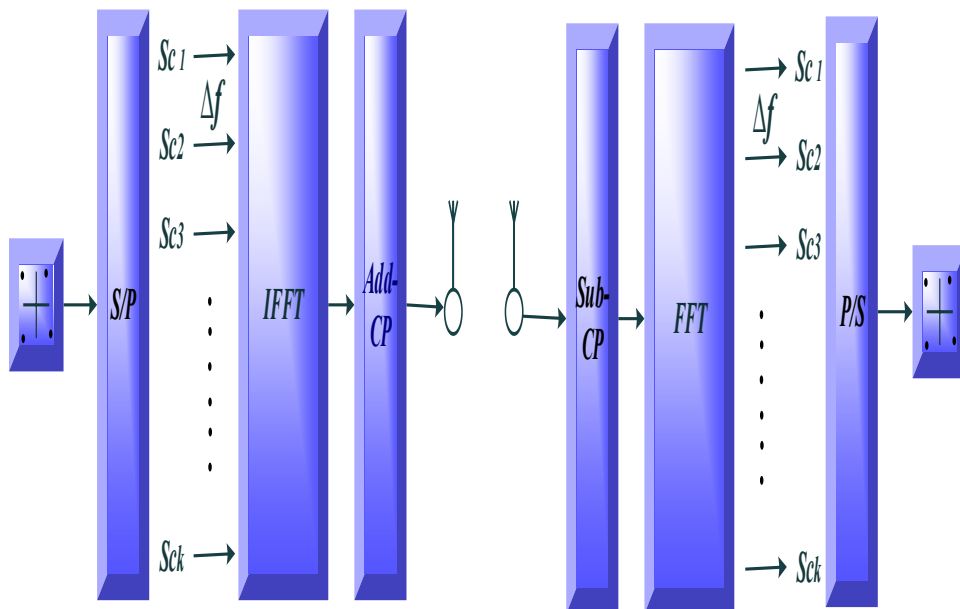


Figure 2.1: CP-OFDM transceiver system (Stern and Fischer, 2014).

Employing the IFFT, each parallel input group of complex numbers in the frequency domain is converted to one CP-OFDM output symbol in the time domain. Inside the IFFT, original frequency subcarriers are convoluted with a similar number of unused frequency subcarriers (conjugates), side by side with the central carrier (DC) that is fixed to zero. In the time domain, the cyclic prefix which represents a copy of the symbol tail, is placed at the head of each symbol, increasing the robustness against ISI resulted from the multipath transmission. The total duration of every transmitted symbol ( $T_{Symbol}$ ) is further expanded due to this addition of the cyclic prefix. Thus, if the number of transmitted samples ( $N_s$ ) increased, the time specified for each CP-OFDM symbol is enlarged since  $T_{Symbol} = N_s * d_t$ , where  $d_t$  represents the sampling duration of applied samples (Stern and Fischer, 2014). An example of adding the cyclic prefix between two adjacent symbols is shown in Figure 2.2.

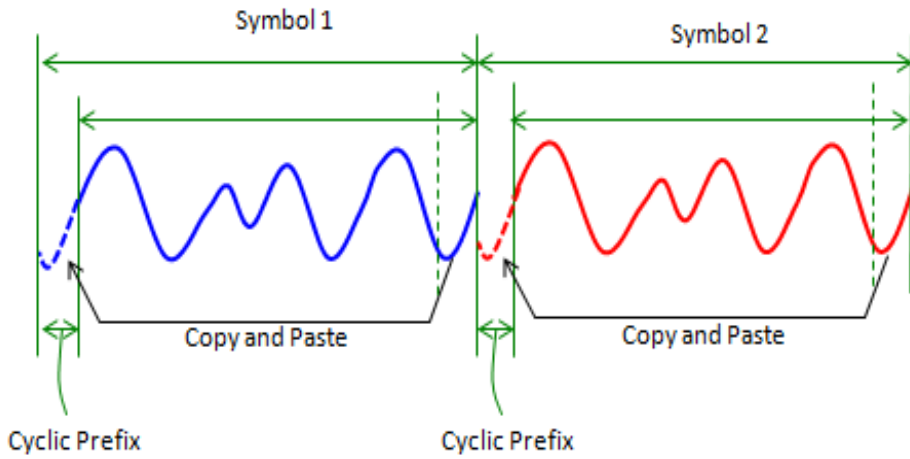


Figure 2.2: Cyclic prefix of CP-OFDM (Ouzzif, 2009).

Ultimately, an appropriate sampling frequency, called digital to analog converter (DAC), is employed to convert the signal from the digital to the analog domain then to be transmitted over the air interface. It's worth noting that propagated wireless signal faces different levels of noise through its journey from the transmitter to receiver. As such, signal attenuation depends not only the nature of the transmitted signal but also the features of the employed channel. Thus, channel noise with either the line of sight or non-line of sight transmission can impact the maximum bit-rate of a received signal (Mera and Estrada, 2009).

At the receiver side, where inverse operations are performed, an equivalent analog to digital converter (ADC) sampler, is used altering the analog signal into the digital domain. The cyclic prefix is later removed to obtain the original signal. Then, it is converted from the time domain

to the frequency domain utilizing the FFT. As such, each received sample is converted back to its corresponding complex number. The original digital data are recovered in the binary form employing one of the available modulation schemes. The CP-OFDM model is introduced in an electrical back to-back wireless transmission system (Jin *et al.*, 2016).

As it is seen in Figure 2.3, the spacing between frequency subcarriers  $\Delta f$  is selected accurately to avoid the frequency selective case, hence, attain a minimum cross-talk to produce the orthogonality for applied subcarriers, where,  $\Delta f = F_{DAC}/N$ . As such, in the frequency domain, the orthogonal subcarriers come up with a flat gain which can be easily recovered at the receiver side of the CP-OFDM (Debbabi, Siala and Boujema, 2005).

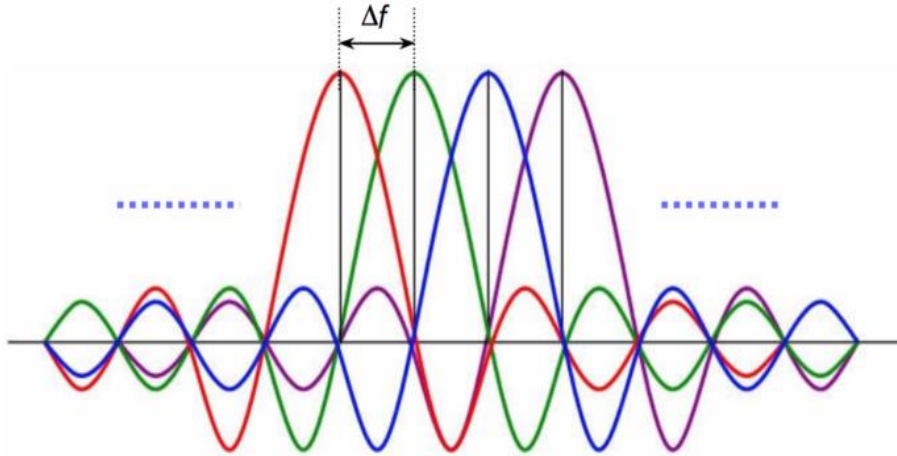


Figure 2.3: Orthogonality in the CP-OFDM (Ballal, Chadha and Satam, 2013).

### 2.1.2 CP-OFDM in 4G Cellular Communications

The key advantages of utilizing the CP-OFDM in the system design of the fourth generation (4G) of mobile can be listed as follows:

#### Spectral Efficiency

Due to the orthogonal design of the multi-carrier transmission system, the available BW can be utilized efficiently. Thus, instead of only separating the BW into frequency subcarriers and isolating them by generating guard bands, the orthogonal subcarriers are narrowly overlapped, achieving a minimum level of cross-talk. The obtained band spaces that result from this operation are used for accommodating an extra number of subcarriers, hence, come up with a higher channel capacity (Ballal, Chadha and Satam, 2013).

### **Robustness Against Multi-Path Transmission**

To cope with possible ISI due to multi-path transmission, long duration of the symbol is required employing a suitable cyclic prefix for this purpose. This combination (main subcarriers and added cyclic prefix) results in a low complexity receiver where usage of one-tap equalization is appropriate. Thus, probable changes in amplitudes and phases of the received signal are manipulated simply (Umatani, Ohno and Itami, 2010).

### **Multiple-User Access System**

Orthogonal Frequency Division Multiple Access (OFDMA) is used to support many users by allocating one or more of BW blocks to a user, each one of these blocks includes multiple frequency subcarriers. This efficient access system not only sustains individual users in the frequency domain but also can organize resources sharing in the time domain by offering a fixed 1ms Transmit Time Interval (TTI) for every group of symbols (Nusairat, Li and Member, 2012).

#### **2.1.3 Basic CP-OFDM Parameterization in Long Term Evolution system**

The key design criteria of the cellular system based CP-OFDM, LTE, are essentially based on the maximum probable propagation delay ( $T_d$ ), the maximum expected Doppler frequency ( $F_d$ ) and utilized cell size. It's worth noting that, the transmission features and mobility considerations which are represented by the propagation delay and the Doppler frequency have an influence on choosing the length of cyclic prefix ( $T_{CP}$ ) and BW of frequency subcarrier ( $\Delta f$ ). Accordingly, the ISI can be prevented when  $T_{CP} \geq T_d$  and a low ICI due to Doppler impact is kept when  $F_d/\Delta f \ll 1$ . In addition, the relation between the cyclic prefix time and the subcarrier spacing can basically affect the efficiency of the spectrum, thus, an efficient BW usage can be achieved when  $T_{CP}, \Delta f \ll 1$ .

The following example demonstrates how the key CP-OFDM parameters are utilized with the LTE system in both the frequency domain and the time domain (Gessner *et al.*, 2012):

### **Subcarrier Spacing**

In the LTE system, the spacing of each CP-OFDM subcarrier is accurately decided, where, worldwide deployments of LTE use a standard  $\Delta f$  equivalents to 15 kHz. In addition, due to the proportional relation inversely between the subcarrier spacing and the symbol duration,

the time specified for every CP-OFDM symbol is assigned to 66.7  $\mu$ s. Moreover, the subcarrier BW and thus symbol time are specified similarly in both LTE Uplink and Downlink.

### **Sampling Frequency**

The required size of sampling frequency is essentially decided by depending on the subcarrier spacing and number of input subcarriers to the IFFT. In the LTE, where subcarrier BW equals to 15 kHz, and about 2048 frequency subcarriers are employed, the essential sampling frequency can reach to 30.72 MHz, where,  $F_{DAC}$  results from multiplying the number of applied subcarriers by the subcarrier spacing. Besides, since the relation between the sampling frequency and sampling time ( $dt$ ) is proportional inversely, the sampling time corresponding to the applied  $F_{DAC}$  (30.72 MHz) is set to 32.55 ns.

### **Doppler Frequency**

With LTE, different bands of frequency are deployed, hence, various range of bands are utilized between 700 MHz up to around 2.7 GHz. Nevertheless, a standard carrier frequency ( $f_c = 2$  GHz) was applied initially for all related simulation processes. Noteworthy, both the frequency centre and the velocity ( $v$ ) that the system can sustain have an impact on the maximum level of Doppler frequency. In this context, LTE tends to support a high velocity up to 300 km/h which is known as 'High-Speed Train' scenario. Considering that  $F_d = f_c \cdot v/c$ , where  $c$  represents the speed of light, a maximum Doppler with LTE can reach to about 555 Hz. Accordingly, the ICI due to mobility is ignored, as the ratio of the recorded Doppler to the agreed subcarrier spacing (15 kHz) is much less than 1. Thus, to achieve the required criteria, the  $\Delta f$  should be specified well to accommodate any probable influence of the Doppler phenomena.

### **Transmit Time Interval**

In LTE, each radio frame with 10 ms duration contains 10 subframes, thus, a duration of 1 ms length is specified for each utilized subframe. Besides, every subframe corresponds to one defined TTI, hence, each TTI equivalent to 1 ms. Considering that 15 CP-OFDM symbols are decided for one subframe with the LTE, the utilized TTI can include 30.720 samples. Thus, the total number of transmitted samples results from multiplying the number of symbols per each subframe by the number of subcarriers in one symbol, that is corresponding

herein to 2048 subcarriers. Furthermore, every subframe is extra partitioned into two slots of time, each with 0.5 ms. As such, a half TTI should contain 15360 samples. Nevertheless, as just 2048 samples are assigned per an CP-OFDM symbol, only 7 symbols can be accommodated by one-time slot, causing in unused 1024 samples. To address this issue in the LTE, the cyclic prefix concept is introduced to exploit the ignored spaces of samples.

### Cyclic Prefix

Concerning the unused samples (1024), LTE decided that the unemployed samples can be distributed, as a cyclic prefix, among the 7 accepted CP-OFDM symbols to be compatible with the given time (0.5 ms). The intended samples are scattered in a special way, where the first CP-OFDM symbol can have 160 samples as a cyclic prefix while 144 samples are allocated for the other 6 symbols. Utilizing the determined sampling time (32.55 ns), the cyclic prefix durations for both the first CP-OFDM symbol and the remaining 6 symbols are 5.2  $\mu$ s and 4.7  $\mu$ s, respectively. It's worth pointing that, the maximum expected propagation delay depends on the multipath phenomena, hence, it greatly differs depending on the nature of transmission area whether it is a rural area where about 991 ns delay are recorded or a city centre with delay reaches up to 3.7  $\mu$ s. However, the selected time for cyclic prefix with LTE is determined well to accommodate any probable ISI.

### Spectral Efficiency

To come up with high spectral efficiency with LTE, the assigned value of the cyclic prefix must be determined perfectly. Thus, ensure that the product of the applied  $\Delta f$  and the introduced cyclic prefix is much lower than 1. As the smaller is the better, the employed cyclic prefix (4.7  $\mu$ s) and the given value of subcarrier spacing (15 kHz) can basically obtain a good spectrum use.

#### 2.1.4 Potential Downsides of CP-OFDM

Even with achieving all 4G mobile requirements listed in section 2.1.3, CP-OFDM still has proven limitations make it not the most suitable waveform for the predicated scenarios for the future generation of mobile networks. For this reason, researchers are working on introducing alternative waveforms able to complement the weak points of the currently applied CP-OFDM (Schaich *et al.*, 2014). The main limitations of CP-OFDM can be discussed one by one as following:

## Cyclic Prefix Overhead

It can be seen in Figure 2.2, the cyclic prefix is a copy of the symbol's tail positioned at its beginning to avoid any probable ISI, however, the redundant extension of the cyclic prefix increases the overhead of CP-OFDM symbol by adding the same content twice. Hence, the required supplement leads to expand the duration of each symbol by  $T_{cp}$ . As such, a longer symbol duration in the time domain corresponds to an extra BW waste in the frequency domain (Chen *et al.*, 2015).

## Sensitivity to Frequency Offsets

In CP-OFDM, the orthogonality assumes that a similar frequency reference ( $F_{DAC}$ ) is utilized at both transmitter and receiver sides. However, the orthogonality is lost due to frequency offsets caused by local oscillator drifts. As such, variations of voltage and temperature can play a big role in changing the subcarrier spacing resulting in a subcarrier leakage (ICI) (Boshehba, Badran and Mahmoud, 2013).

## High Peak-to-Average-Power Ratio

Typically, the combined frequency subcarriers have a variant phase to each other. Nevertheless, occasionally, the summation of individual frequency subcarriers that all have simultaneously the same value results in raising the output power to the peak. Due to the big number of frequency subcarriers with CP-OFDM system like LTE, the resulted peak can be very high relative to the average power. Hence, whenever the number of infected subcarriers is increased, the raised peak value can significantly affect the efficiency of a power amplifier (Kundu, 2014).

## Out of Band Emission

Adjacent to the desired peak of the CP-OFDM spectra, unwanted side lobes appear causing in the OOB emission. These spectral spikes, in turn, affect severely the spectrum efficiency of available BW (Lizárraga, Dowhuszko and Sauchelli, 2012).

## 2.2 Waveform Candidates for the Future Generation of Mobile

### 2.2.1 Modern Motivations

The key restrictions of the CP-OFDM, that were discussed in section 2.1.4, can cause large shortcomings in supporting the predicted challenges of future mobile technology. Thus, as is seen in Figure 2.4, modern requirements of wireless mobile networks (enhanced mobile broadband, ultra-reliable and low latency communication, and massive machine type communications) need high capabilities beyond the currently utilized CP-OFDM. As a result, the wireless research community has conducted its efforts to achieve the targeted designs and cope with the identified drawbacks by suggesting developed concepts in the physical layer of the future networks. Recently, new candidate waveforms have been investigated and gained the most attentiveness. In contrast to CP-OFDM, the core idea beyond all these explored systems is applying various digital filters. The four candidate waveforms can come up with innovative treatments for the utilized resources and from different filtration perspectives. As such, applying new filtration techniques decrease significantly the OOB radiations and then enhance spectrum efficiency. However, using diverse shaping filters can affect the orthogonality by spreading energy between adjacent frequency subcarriers causing in the ICI. More details about the filtration techniques, and how they are applied with different candidate waveforms are demonstrated in the following sections.

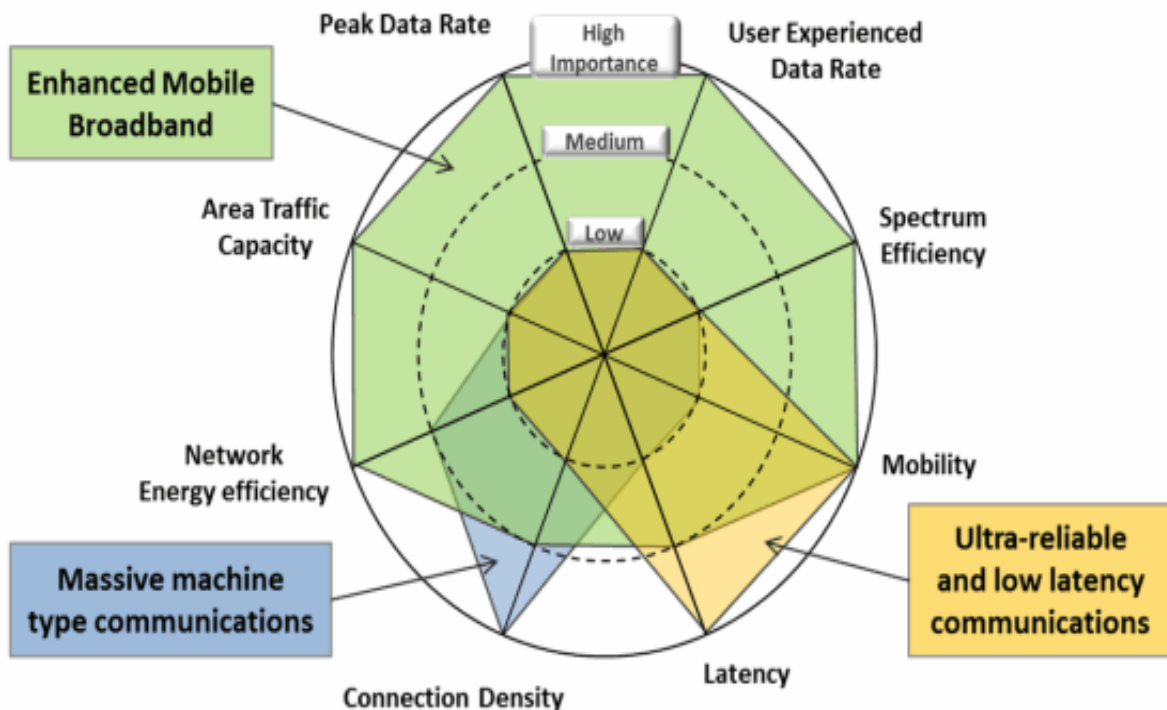


Figure 2.4: Modern requirements of future mobile networks (Tran, Shimodaira and Sakaguchi, 2016).

## 2.2.2 Filter Bank Multi-Carrier

FBMC is a wireless transmission waveform suitable for the physical layer of future mobile technology that is having some advantages over CP-OFDM. The main change with this proposed technique is replacing the traditional multi-carrier system of CP-OFDM with a filtered multi-carrier scheme at both transmitter and receiver sides. In the FBMC, the waveform consists of a set of parallel data, spread over a bank of modulated filters, where filtering operation is applied on a frequency subcarrier level. Moreover, the parameterization of the prototype filter, particularly, overlap factor, is chosen carefully to reduce channel leakage between adjacent frequency subcarriers (Kim and Rautio, 2016).

As is shown in Figure 2.5,  $N$  prototype filter is created based on the conventional cosine filter (RRC), with a specific roll-off factor, where  $N$  is equivalent to the number of orthogonal subcarriers. Thus, the filter bank is achieved by shifting the frequency centre of the proposed filter  $N$  times over orthogonal subcarriers of the FBMC. To explain more about this introduced waveform, it is seen in Figure 2.6, after applying one of the modulation schemes, the complex numbers of each frequency subcarrier are prepared, side by side with their conjugates to be a suitable input to the IFFT. At this stage, the frequency domain constellations are converted to the time domain samples.

After that, each frequency subcarrier is filtered individually using a narrow BW filter with a long-time duration. This, however, makes it more suitable for long-time applications than short-burst applications. It's worth noting that, with this filtered system, the orthogonality is impacted due to spread energy between adjacent frequency subcarriers which are resulting in the ICI. Nevertheless, non-contiguous subcarriers (odd, even) are still orthogonal to each other (Kim and Rautio, 2016). The convoluted subcarriers are then combined for moving from digital to analog domain using an appropriate DAC. At the receiver side, reverse operations are performed to retrieve the main data of signal.

Recently, another implementation of FBMC with Offset-QAM (OQAM) signalling, is investigated (He *et al.*, 2018). The proposed alternative can support the orthogonality in the time domain by cancelling the interference and improving the spectrum efficiency. Thus, introducing an orthogonal transmission system without the need for protecting durations (cyclic prefix). However, not having the cyclic prefix makes it unable to process MIMO easily.

In addition, with OQAM, the transceiver model has a higher complexity than CP-OFDM, particularly, the size of FFT, which is typically enlarged by a factor of 2, (He *et al.*, 2018).

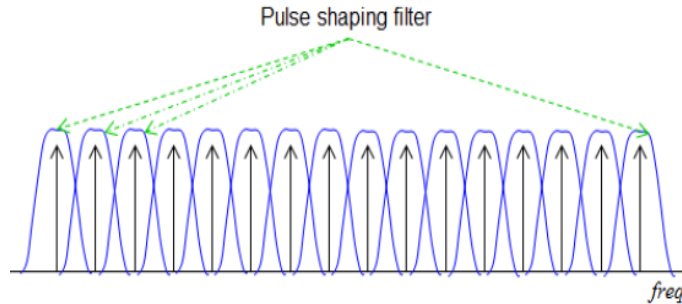


Figure 2.5: Apply the filter for the FBMC subcarriers (Kim and Rautio, 2016).

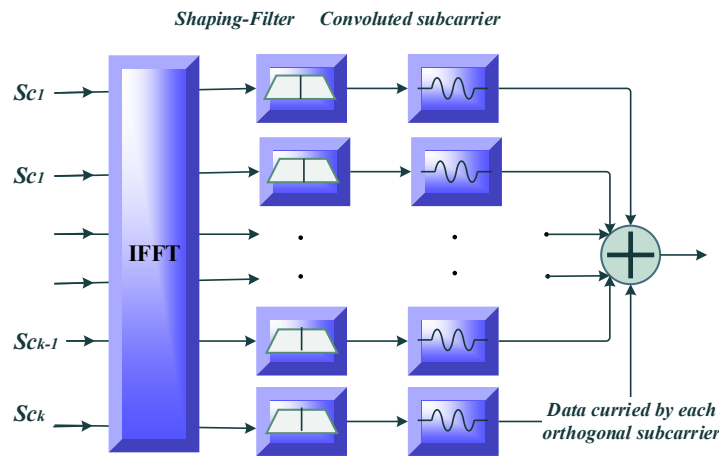


Figure 2.6: Block diagram for the FBMC transmitter (Kim and Rautio, 2016).

The main advantages and disadvantages of FBMC can be summarized as following, (Kim and Rautio, 2016), (He *et al.*, 2018):

### **Advantages:**

- Small side lobes for each orthogonal subcarrier due to utilized filtration.
- Support for long time applications.
- Good spectrum efficiency with an ability to remove cyclic prefix with the OQAM leading to extra BW use.

### **Disadvantages:**

- Computational complexity with the FFT.
- Orthogonality is affected due to spread energy among frequency subcarriers.
- Inefficient for short bursts services.

### 2.2.3 Universal Filtered Multi-Carrier

Like previous introduced waveform (FBMC), the UFMC is also constructed on the filtering technique. The main differentiation is how the filter is applied. In contrast to FBMC, as it is shown in Figure 2.7, the UFMC collects frequency subcarriers into groups (sub-bands) which are then filtered, hence, the UFMC represents a combination of both the CP-OFDM waveform and the prototype filter, in which, each group of frequency subcarriers is filtered efficiently. The filtering procedure results in reducing the OOB emission for each sub-band. Parameterization of the filter and the number of frequency subcarriers with each sub-band are similar and depend on the specification of the intended design, thus, use more or fewer frequency subcarriers with the created sub-bands is compatible and decided based on the required applications (Zhang *et al.*, 2017).

The UFMC scheme can be designed between two extremes (multi-block, single block). Concerning the first one, it's applied by dividing the CP-OFDM spectrum into a set of blocks/sub-bands with one subcarrier or more for each block. The determined sub-bands are then filtered improving spectral behaviour at sub-band boundaries; hence, various blocks are spectrally separated like the FBMC. With reference to the second one, it's produced by applying one filter for the whole CP-OFDM BW considering it as a single big block that contains all frequency subcarriers. Hence, it is an improvement for the spectral properties of the conventional CP-OFDM by decreasing the OOB emission. Consequently, the UFMC can be considered as a compromise between the FBMC and the CP-OFDM.

As it is seen in Figure 2.8, the transmitter side of the UFMC initializes its procedure by converting binary digits of input data into complex numbers using one of the most common modulation formats. The number of utilized subcarriers and their subcarrier spacings are decided similarly for all applied blocks. The distributed complex numbers in the frequency domain are transformed to the time domain using the IFFT. In addition, specific guard time intervals (cyclic prefix) are added equivalently to the processed blocks to avoid the impact of the multipath transmission. The filtering operation for every sub-band is employed according to the respective position of it and within the overall accessible range of frequencies considering that the length of the filter is uniform herein and depends on the width of sub-band. The convolution of every sub-band with the filter is performed individually and then accumulated with other convoluted blocks at the superposition level.

At the receiver part, the transmitted blocks are received, and the inverse of all corresponding transmitter operations is executed to retrieve the original signal. Worth noting, the FFT window size is essentially increased due to previously added zero side by side with the conjugates of the main complex numbers causing in high complexity. Ultimately, the channel estimation and equalization can be applied in a similar way as the CP-OFDM to improve the quality of the received signal (Naga Rani and Santhi Rani, 2017).

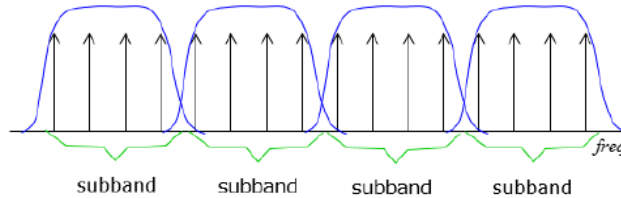


Figure 2.7: Apply the filter for the UFMC subcarriers (Geng, Xiong and Cheng, 2015).

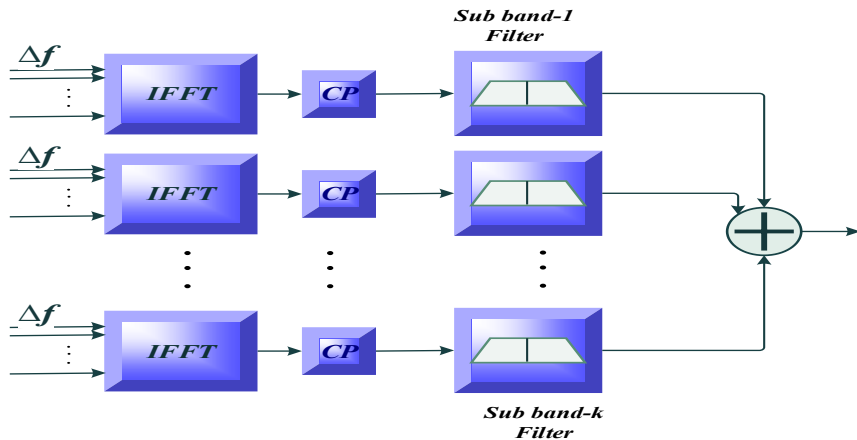


Figure 2.8: Block diagram for the UFMC transmitter (Naga Rani and Santhi Rani, 2017)

The main advantages and disadvantages of UFMC can be summarized as following (Zhang *et al.*, 2017) (Teja, 2018):

### **Advantages:**

- Good spectrum efficiency.
- Well suited for a short burst / low latency transmission.
- Enhance the OOB emission for each filtered block.

### **Disadvantages:**

- Orthogonality is lost partially makes it unsuitable for huge data rates.
- Increased receiver complexity due to FFT operation (computational complexity)
- Interference is due to partially overlapped sub-bands.

## 2.2.4 Filtered OFDM

F-OFDM is an introduced waveform for future mobile applications, which is very similar to the UFMC but with more flexibility due to creating flexible-parameter blocks of frequency subcarriers. The key difference with the F-OFDM is applying further steps not considered before in the UFMC as specifying a diverse filter for each sub-band and applying the block parameterization in a more elastic way. Thus, for each block, utilized parameters like the spacing of frequency subcarrier, guard time interval and transmission period (TTI), are determined in a different way.

As a result, user applications can work with variant sub-band features resulting in a more flexible transmission system (Wu *et al.*, 2016). Hence, the resilient structure of this waveform can cope with developed types of services due to its ability to support variation. For example, in the vehicle-to-vehicle application, the duration of a symbol is decreased while the spacing of frequency subcarrier is increased to deliver an extra-low latency. Principally, all alternative waveforms apply a sort of the filtration, however, the variance among them, is how the filter is used. Thus, in F-OFDM, the term 'Filtered' doesn't refer to any special significance.

With respect to the way that the filter is applied, it is shown in Figure 2.9, that the available channel BW can be separated into multiple filtered sub-bands, each one with different characteristics. The convoluted sub-band is composed of a set of frequency subcarriers with different frequency spacing.

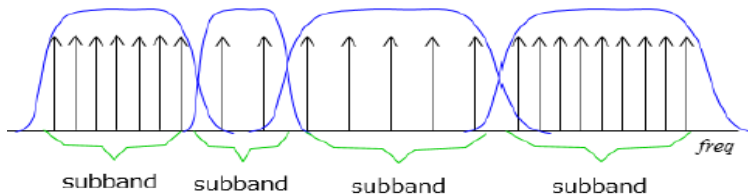


Figure 2.9: Apply the filter for the F-OFDM subcarriers (Wu *et al.*, 2016).

To explain more about the investigated waveform, it is shown in Figure 2.10, particularly, on the transmitter side, the complex numbers, which are originally come from the modulation process, are arranged in a parallel group of sub-bands. Inside each sub-band, a variant number of frequency subcarriers with changeable subcarrier spacings are designed according to required applications. Thus, a large subcarrier BW causes in a low symbol duration and vice versa.

Utilizing the IFFT, the prepared sub-band is converted from the frequency domain to the time domain. After that, a suitable cyclic prefix is differently decided for every processed block to prevent any probable ISI. It's worth mentioning that the assigned TTI of each block depends fundamentally on the previously decided spacing of subcarriers. As such, flexible (short/ long) TTI is given for a set of symbols/blocks depending on their own duration. The supplemented blocks are convoluted with their adaptable filters to reduce the unwanted OOB. The filtered blocks are combined to be prepared for transformation from the digital to the analog domain using an appropriate DAC. On the receiver side, reverse operations are applied to retrieve the original data (Weitkemper *et al.*, 2016).

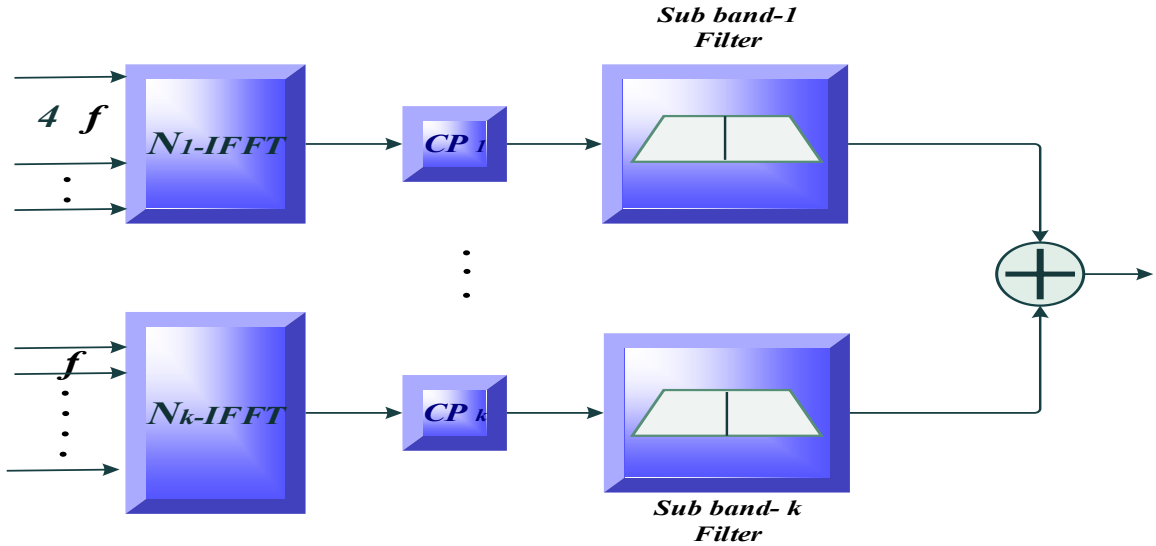


Figure 2.10: Block diagram for the F-OFDM transmitter (Weitkemper *et al.*, 2016).

The main advantages and disadvantages of F-OFDM can be summarized as following (Wu *et al.*, 2016), (Jayan and Nair, 2018):

### **Advantages:**

- Good spectrum efficiency like the UFMC and FBMC.
- Flexibility in dealing with variant applications (long/short).
- Improved OOB emission for each block.

### **Disadvantages:**

- Partially losing orthogonality makes it inapplicable with high data rates.
- Computational complexity due to Large FFT size.
- Interference due to partly overlapping sub-bands.

## 2.2.5. Generalized Frequency Division Multiplexing

The main motivation behind the GFDM is using a multi-carrier filter bank in a more flexible way. Thus, with GFDM, the spectrum region is separated non-orthogonally into a set of spectral segments where a developed method is utilized to reduce the emission. As such, the restrictions of orthogonality, particularly, that are related to subcarrier spacing, are removed, and the filtration process is applied for each GFDM subcarrier. As a result, recently, the enhanced GFDM, is considered as the 5G waveform for the mobile networks. Hence, the selected technique displays a motivating way for coping with the new challenges predicated for the future wireless mobile system, keeping it as an acceptable waveform for the next generation of mobile (Han, Sung and Lee, 2017).

However, removing the orthogonality between frequency subcarriers can cause an inefficient management for the available BW which in turn can extensively decrease the channel capacity (research area). Hence, the system performance in terms of the maximum bit-rate is badly affected. As such, GFDM comes up with more flexibility but less BW efficiency (Demel, Bockelmann and Dekorsy, 2017)

As is seen in Figure 2.11, the RRC shaping filter is utilized flexibly on the subcarrier level of the GFDM waveform. Hence, a non-orthogonal filtration stage can be achieved by convoluting every frequency subcarrier with its specified filter.

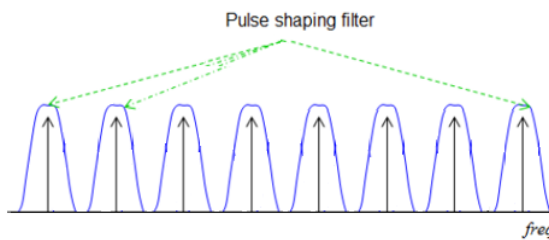


Figure 2.11: Apply the filter for the GFDM subcarriers (Li *et al.*, 2016)

As is shown in Figure 2.12, on the transmitter side, particularly, at the modulation step, the binary stream (0,1) are translated to a set of tokens (complex numbers) in the frequency domain. The generated constellations are mapped from serial to parallel direction and then to be converted into a group of samples in the time domain. After that, each subcarrier is oversampled by a factor of  $K$  where  $K$  represents the total number of applied frequency subcarriers.

At the filtration stage, every oversampled subcarrier is convoluted individually by its corresponding filter. Worth noting, orthogonality is no longer achieved with every frequency subcarrier considering that the characteristics of each frequency subcarrier can be changed. Thus, comparing to the FBMC, the filter is employed for each non-orthogonal subcarrier with a probability of variance BW for each employed frequency subcarrier. In this context, the probable overlap between adjacent frequency subcarriers can increase the interference level in a similar way to other introduced waveforms but without involving the orthogonality.

In the GFDM, each data block with  $N$  size is composed of several sub-symbols ( $K$  frequency of subcarriers and  $M$  time slots) where  $N$  equals to  $K \cdot M$ . To increase robustness against the ISI, the entire block but not the symbol is driven by the cyclic prefix results in reducing the cyclic prefix overhead comparing with the CP-OFDM. The length of the symbol duration is more flexible and can be fitted with a variant range of applications. Hence, a small number of the subcarriers can be used with short time-critical applications and vice versa. Then after, all convoluted subcarriers are combined to be prepared for transformation from the digital domain to the analog domain using a suitable  $F_{DAC}$ .

At the receiver side, opposite operations with extra recovering tools are employed to make sure that the original signal is received well. Hence, to improve the performance, in terms of the BER, an interference cancellation and equalization techniques are required at the reception part. Nevertheless, this improvement leads to increasing the complexity of the receiver (Towliat, Mohammad and Asgari, 2018).

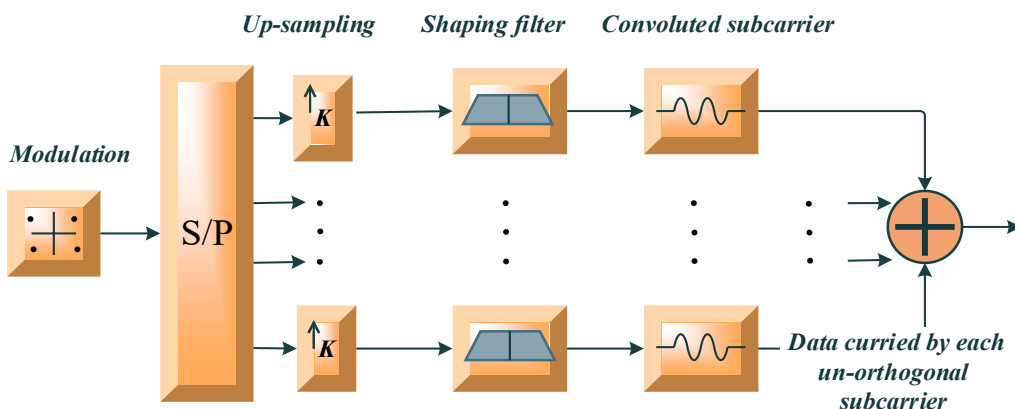


Figure 2.12: Block diagram for the GFDM transmitter (Li *et al.*, 2016).

The main advantages and disadvantages of the GFDM can be summarized as following (Demel, Bockelmann and Dekorsy, 2017), (Nimr *et al.*, 2018):

### **Advantages:**

- Lower PAPR compared to other waveforms.
- Low out-of-band emission for each non-orthogonal subcarrier.
- Support both long and short terms applications.
- Efficient usage for the cyclic prefix.

### **Disadvantages:**

- Computational complexity due to complex receiver design.
- Less BW efficiency due removing the orthogonality.

### **2.2.6 Comparison of the 5G candidate waveforms**

As shown in Table 2.1, to summarize the key differences between the main candidate waveforms (CP-OFDM, FBMC, UFMC, F-OFDM, and GFDM) (Wunder *et al.*, 2014), (Demel, Bockelmann and Dekorsy, 2017) (Nimr *et al.*, 2018) (Zaidi *et al.*, 2018) (Habibi *et al.*, 2019), and our proposed waveform (OGFDM) (Kadhum, 2020) in terms of the orthogonality, filter's level, filter's type, cyclic prefix, and the spectrum efficiency, the following comparison is introduced.

Table 2.1

Comparison between the main candidate waveforms for 5G mobile including the OGFDM.

<b>C.W Par</b>	<b>CP-OFDM</b>	<b>FBMC</b>	<b>UFMC</b>	<b>F-OFDM</b>	<b>GFDM</b>	<b>OGFDM Ch. 3 &amp; 4</b>
<b>Orthogonality</b>	Subcarriers	Subcarriers	Subcarriers	Subcarriers	None	Filters
<b>Filter level</b>	Non	Subcarrier	Fixed group	Flexible group	Subcarrier	Subcarrier
<b>Filter Type</b>	None	RRC	RRC	RRC	RRC	Hilbert
<b>Cyclic Prefix</b>	Symbol	None	Sub-band (Fixed size)	Sub-band (Flexible size)	Block/ None	Block/ None
<b>Spectrum Efficiency</b>	Good	Good	Good	Good	Average	V. Good

Regarding the orthogonality, most of the compared waveforms applied it on the frequency subcarrier level, nevertheless, the disadvantages of achieving it on the frequency subcarrier far outweigh the advantages, causing in removing the orthogonality with the 5G waveform (GFDM) (Habibi *et al.*, 2019). Worth noting that with the proposed OGFDM that is investigated thoroughly in the next chapters (3 and 4), the orthogonality is achieved again but on the filtration level, resulting in a better OOB emission and an improved BW efficiency.

Concerning the filtration level, it is noticed that with the LTE waveform (CP-OFDM), the filtration process is not applied, while it is introduced for the orthogonal and non-orthogonal frequency subcarrier level of other 5G candidates like the FBMC and the GFDM respectively. In addition, an extra expansion is performed by applying the filters for each set of frequency subcarriers as in the UFMC with fixed parameters and the F-OFDM with a flexible parameterization. Moreover, the supportive filters with developed features (Hilbert filters) are employed for each non-orthogonal frequency subcarrier converting the generalized waveform (GFDM) (Han, Sung and Lee, 2017) to orthogonal one as with the proposed OGFDM.

With reference to the type of applied filter, all the 5G filtered candidate waveforms like FBMC, UFMC, F-OFDM, and GFDM used the most common non-orthogonal cosine filter (RRC) (Han, Sung and Lee, 2017), while the proposed OGFDM replaced it with advanced orthogonal filters (Hilbert pair) that combine both orthogonality and filtration features. By adopting such a kind of the developed filters, the OGFDM can achieve a lower OOB and higher wireless channel capacity in comparison with both the orthogonal and the non-orthogonal 5G candidate waveforms.

On the topic of the applied cyclic prefix, some waveforms use it for each symbol duration like with the CP-OFDM where the obtained channel capacity is affected badly due to wasting large BW spaces, some of them add the cyclic prefix for each group (fixed / flexible) of frequency subcarriers as with the UFMC and F-OFDM (Naga Rani and Santhi Rani, 2017), and others apply it to the whole block of transmission or completely remove it (the best option) like with the GFDM, FBMC (Liu and Jiang, 2016), and the proposed OGFDM.

Ultimately, with respect to the spectrum efficiency, the orthogonal candidate waveforms like the CP-OFDM, FBMC, UFMC, and F-OFDM deliver a good spectrum efficiency. Nevertheless, the flexible GFDM still suffers from a sharp decline in the BW efficiency due to removing the orthogonality between adjacent frequency subcarriers (Gaspar, Mendes, *et al.*, 2015). On the other hand, the proposed OGFDM improves the spectrum efficiency by utilizing the advanced Hilbert filters that provide a very good BW usage due to introducing the orthogonality side by side with the filtration level for non-orthogonal frequency subcarriers.

## 2.2.7 Main Scenarios of Future Mobile Networks

Due to the key limitations of the CP-OFDM that were discussed in previous section, the existing cellular communication waveform (CP-OFDM) will not be able to reach the market demands beyond 2020 (Agiwal, Roy and Saxena, 2016) (Michailow *et al.*, 2014) (Wunder *et al.*, 2014). As such, the new applications of the 5G mobile networks and beyond have led to investigate new candidate waveforms, comparing their features, and then concluding that the flexible GFDM waveform is the 5G mobile waveform (Habibi *et al.*, 2019). Thus, the compatibility between the principle scenarios of future mobile networks and the best waveform (GFDM) is demonstrated.

As is shown in Figure 2.13, the predicted scenarios of 5G mobile networks have introduced new challenges for upcoming wireless networks (Gaspar, Mendes, *et al.*, 2015). One of the important challenges, that is proposed for future networks of mobile, is the ‘Bit-pipe Communication’ which essentially relates to the higher channel capacities and what the best possible ways are to increase it. Hence, the new scenario can involve successful approaches that tend to improve BW efficiency and move to a higher frequency sampler. Thus, it includes new solutions for improving the maximum bit-rate of transmission for data-hungry applications like the TV stream, videos, 3D contents, etc. As such, the employment of the CP-OFDM is yet doubtful with the proposed standards for upcoming mobile networks (Michailow *et al.*, 2014) (Hazareena, 2018). Hence, it's hard to believe that the CP-OFDM without supportive filtering can cope with the developed mechanism of mobile transceiver due to high OOB emission, waste spaces by the cyclic prefix and strict relation between adjacent subcarriers (Wunder *et al.*, 2014) (Agiwal, Roy and Saxena, 2016). Consequently, the future generation of mobile should depend on an advanced transmission waveform with an efficient ability to address the intend emission, unwanted BW consumption, and restrictions of orthogonality.



Figure 2.13: Main scenarios of future mobile networks (Gaspar, Gaspar, *et al.*, 2015).

In this context, the GFDM waveform that is recommended currently for 5G mobile networks can be introduced to accommodate the higher channel capacity of future wireless applications (Nimr *et al.*, 2018). To explain more about this, the GFDM, with several dBs of OOB emission below the CP-OFDM, can efficiently support the requirements of the dynamic spectrum allocation (Li *et al.*, 2016). In addition, with a large block of the GFDM symbols, the effect of the cyclic prefix on the aggregated channel capacity is minimized. Thus, efficient use of the cyclic prefix can improve the system performance in terms of the maximum bit-rate (Prabu *et*

*al.*, 2016). Moreover, due to the flexibility, the GFDM can manage easily both vacant allocation and fragmented spectrum of shifted media.

Another proposed scenario for future mobile networks is Machine Type Communications, in which, connected machines/objects can operate and communicate intelligently and autonomously. It's worth noting that, the majority of existing Machine Type Communication applications rely on wireless short-range technologies like Bluetooth. However, the modern type of this application that depend on the cellular wide area systems will strongly dominate the future market domain. The smart objects of Machine Type Communications environment that work with either peer to peer or client-server topologies are usually powered by limited lifetime batteries. Due to the large consumption of power, the cellular Machine Type Communications networks cannot pass across all steps of the synchronization. For this reason, the modern Machine Type Communications devices should be accommodated by a reliable communication system yet keeping an efficient use of the BW. As a result, it is hardly achieved this with the CP-OFDM due to allocating one cyclic prefix per each symbol. Hence, a good level of protection can be applied with the CP-OFDM but with extra BW waste due to allocating part of the spectrum for guard intervals (Chen *et al.*, 2015). As the number of connected Machine Type Communications devices is related to the available BW spaces, inefficient use of the BW due to the cyclic prefix, the OOB emission, etc., can limit the intended expansion of future Machine Type Communications networks. Therefore, the GFDM with one cyclic prefix for each block (several symbols) can be much better than the conventional CP-OFDM in covering any misalignment in time yet offering an efficient spectrum (Towliat, Mohammad and Asgari, 2018). Thus, the improved usage of BW can play a big role in increasing the number of communicated devices for upcoming mobile networks (Liu *et al.*, 2017). In addition, the gained BW spaces that are obtained due to the amended level of the OOB can add further enhancement to the Machine Type Communications networks by offering new band spaces for new devices. Moreover, the flexibility in subcarrier spacings and the ability to reallocate the spectrum can be an additional improvement to the future mobile networks. Thus, extra numbers of devices are attached to the obtainable bands after the shifting process.

The third predicted scenario for future mobile networks is the Tactile Internet, which is used for controlling real-time applications with a requirement of low latency, 1 ms round-trip at most. The low latency is estimated based on the ideal delay of tactile interaction of both virtual

and real objects. Most of the today's mobile technology tend to apply one interface (touch screen) for input and feedback operations, however, the modern generation of mobile go further to integrate several interfaces for visual, auditory and haptic interactions. The main purpose behind this variety is to manage a wide range of virtual and real online applications which is efficiently controlling health, smart houses, augmented games, etc. From Tactile Internet perspective, poor quality of service can result from too large round-trip latency that is required for covering the inserted command, online processing, and feedback. The overall round-trip latency of the CP-OFDM is still higher than the proposed threshold limit of the modern Tactile Internet latency. The key reasons beyond this are, CP-OFDM subcarriers work with a narrow frequency spacing and its symbols are yet protected by a long cyclic prefix for each one (Boshehba, Badran and Mahmoud, 2013). Because of the reverse relation between the symbol duration and the allocated subcarrier spacing, the determined time of every CP-OFDM symbol is accordingly increased result in enlarging the needed duration of latency. To address this issue, the GFDM is utilized to meet the intended limits of the future latency due to increasing the subcarrier spacing and efficient use of the cyclic prefix, hence, allocating a small amount of time per the symbol (Aijaz, 2016). It's worth noting that moving the radio frequency to the mm-wave can essentially improve the latency of the upcoming mobile generation since the specified BW of the frequency subcarrier is extra expanded resulting in short time duration of each transmitted symbol and then a small latency.

The fourth proposed application for future networks of mobile is Wireless Regional Area Network. In sparsely populated regions, where usage of mobile is low, it's unfeasible economically to specify licensed frequencies for the mobile working area. As a result, the Wireless Regional Area Network technology aims to address this issue by making use of unoccupied spaces of the channel like unused TV bands, gained spaces due to improved BW efficiency, and the possible bands of channel reallocation. Considering the main limitations of the CP-OFDM, it's hard to believe that current waveform with no filtration process can still be able to mitigate efficiently the impact of spectrum emission due to high OOB emission. In addition, the occupied band protection of the cyclic prefix can cause extra waste in the BW. As such, CP-OFDM cannot consider as a probable solution for the Wireless Regional Area Network application due to the inability of offering new spaces.

On the other hand, the GFDM that is considered as a suitable waveform for the modern applications tends to manipulate this problem efficiently by utilizing developed features can

participate in supplying new bands to the wireless channel. As such, the lower OOB due to filtration technique, efficient use of the cyclic prefix and the flexibility in reallocating spectrum can play a big role in accommodating the required bands (Towliat, Mohammad and Asgari, 2018). Hence, because of the small OOB emissions, manageable cyclic prefix, and other related important facilities of the GFDM, offered spectrum which is technically allocated to other purposes can be effectively used without causing any improper interference. Despite that, some of the available TV channels stay unused providing suitable guard intervals between the occupied channels. Thus, it is necessary also to keep some vacant channels to prevent any probable interference (Agiwal, Roy and Saxena, 2016). Depending on the significant features of the GFDM, the main requirements of the 5G scenarios can be tackled appropriately.

# **Chapter 3: Processing Levels of OGFDM Waveform**

## **3.1 Filtration Level**

### **3.1.1 Introduction**

The “data-hungry” applications of future lifestyle technology can play a significant role in developing a high channel capacity for modern communication networks. (Prabu *et al.*, 2016). This, as a result, make the present research concentration of wireless communications is dedicating mainly on improving the maximum transmission bit-rate. In this context, the future mobile networks tend to support vital scenarios like Bit pipe Communication (Prabu *et al.*, 2016), Tactile Internet (Aijaz, 2016), Wireless Regional Area Network (Agiwal, Roy and Saxena, 2016), and Machine Type Communication (Li *et al.*, 2017).

Presently, the CP-OFDM is the most commonly applied waveform since its powerful ability in treating the multipath phenomena and relatively simple execution employing the FFT (Stern and Fischer, 2014). However, the emerging requirements of upcoming networks state a big challenge for the current air interface (CP-OFDM) which principally suffers from several limitations in tackling the new technical issues. Therefore, offering high BW efficiency for the Bit-pipe Communication, low transmission latency for the Tactile Internet, low consumption power for the Machine Type Communications, occupy a high priority in the forthcoming network. Due to key downsides of the applied CP-OFDM like the high OOB emissions, wasted BW spaces (cyclic prefix) and restriction of the frequency offset, the *“OFDM is not the most promising waveform for the next generation networks”* (Michailow *et al.*, 2014) (Wunder *et al.*, 2014) (Agiwal, Roy and Saxena, 2016) (Hazareena, 2018).

To manage this challenge, alternative waveform systems are investigated by the research community supporting the innovative wireless communication systems. The FBMC, where each frequency subcarrier is filtered individually to mitigate the OOB emissions, is one of the nominated multi-carrier systems for the next mobile applications. Unfortunately, this cannot be applicable for all predicated scenarios of the modern network, particularly, that needs low latency transmission. Thus, unless using it for long burst applications, the narrow subcarrier spacing expands the response length of the transmitted symbol causing poor BW efficiency. This, as a result, makes it not mostly recommended as a reasonable addressing for the upcoming network design. (Kim and Rautio, 2016).

The UFMC is another explored waveform, where each fixed set of frequency subcarriers are filtered reducing the OOB emissions. In contrast to the previous one, this technique can support more short response applications than the long response transmission. Hence, a good BW efficiency is achieved especially with a short burst transmission. However, this waveform still has high sensitivity towards time misalignment issues. This, as such, makes the UFMC not suitable for some modern mobile applications where the time synchronization is sacrificed to keep the energy (Naga Rani and Santhi Rani, 2017).

The F-OFDM, which is principally stated as a similar waveform to the UFMC but with higher flexibility in dealing with the filtration process, is also studied. Nonetheless, the key disadvantages of the formerly mentioned UFMC are partially attending at this technique. (Weitkemper *et al.*, 2016).

The GFDM, that is proposed currently as the 5G waveform due to its ability in addressing the majority of the modern telecommunication requirements, is researched too (Demel, Bockelmann and Dekorsy, 2017). The presented waveform improves the BW efficiency and the time synchronization for the future transmission by employing a small overhead cyclic prefix for each GFDM block. In addition, each frequency subcarrier of the GFDM is filtered separately reducing the OOB emissions. Moreover, both the short-latency and long-latency applications can be accommodated by this flexible air interface. As a result, the GFDM can be considered as a promising solution for the physical layer of future wireless networks. Nevertheless, the applied filtering process of this waveform can impact mainly the criteria of the orthogonality. Hence, destroying the BW efficiency between the utilized frequency subcarriers. (Han, Sung and Lee, 2017).

In this part (filtration level), the first experiment for producing a new technique of the transmission waveform is introduced, the developed design which is termed as OGFDM is mainly obtained herein for a single carrier of transmission with adopting a new scheme of filtration. In addition, the OGFDM system model highlighting the filtration level of processing is explored. Moreover, the promoted design is experimentally demonstrated showing the impact of utilizing the advanced filters on the BW efficiency which in turn can highly influence the transmission performance (channel capacity and BER). Regarding the simulation tools, the MATLAB and Visio software applications are utilized to validate and demonstrate graphically the achieved results.

The rest of the part is ordered as follows: Section 3.1.2 explores theoretically the key aspects of the proposed system model. Section 3.1.3 evaluates the OGFDM transceiver performance in terms of the channel capacity and BER using computer simulation.

### 3.1.2 System Model

In this section, the system model of the developed single carrier OGFDM is presented. The improved design can increase the system performance in terms of channel capacity yet keeping the calculated BER at an acceptable level. This is principally achieved by employing a durable kind of filtering operation capable to accommodate the downsides of the conventional GFDM filtration.

As is clear in Figure 3.1.1, at the transmitter side, the primary input stream of bits is fundamentally converted from the binary form to the complex number scheme using an appropriate format of the modulation. Thereafter, using the IFFT, the output of the modulation formats is transferred from the frequency domain to the time domain. Subsequently, by inserting  $K-1$  zero samples between adjacent original samples, the transmitted signal is up-sampled by a factor of  $K$ , which is represented here as  $(K\uparrow)$ . Then, the up-sampled subcarrier of a single frequency centre is passed over the developed Hilbert filters where a sine or cosine filter is utilized for the shaping process. This, as a result, comes up with generating the convoluted frequency subcarrier of the OGFDM waveform that in turn is multiplexed with the second manipulated subcarrier of each frequency centre. Worth noting that the created pair of the filtered frequency subcarriers, that functions at the same frequency centre but with the orthogonal difference in the phase is named as a “chunk”. In addition, all applied steps of the chunk management that start with receiving the un-convoluted frequency subcarrier and ends up with the filtered frequency subcarrier including the digital combination at the synthesis stage is referred to as the “Digital Chunk Processing” (DCP) of the transmitter. Later, the DCP level output is passed through a suitable DAC preparing it for transmission. In the analog domain, the converted signal that is exponentially represented as  $(e^{j2\pi f t})$  is transmitted by the antenna.

As is seen in Figure 3.1.2, at the receiver side, the detected signal by the antenna is transferred from the analog to the digital domain using an equivalent ADC. After that, in the DCP level of the receiver, where a reverse treatment is applied to the chunk, the received signal is decomposed into two filtered frequency subcarriers that are allocated for a single frequency

centre. In this context, the processed chunk is de-multiplexed by either a sine or cosine matching filter of the Hilbert, achieving the corresponding frequency subcarrier. Subsequently, the released subcarriers that output from the DCP level are down-sampled by a  $K$  factor that is referred to as ( $K\downarrow$ ), where  $K-1$  zeroes between every two adjacent samples are removed. Using a comparable FFT, the down-sampled frequency subcarriers are transformed back to the frequency domain. Ultimately, the complex numbers are converted to the binary numbers by applying a compatible demodulation format.

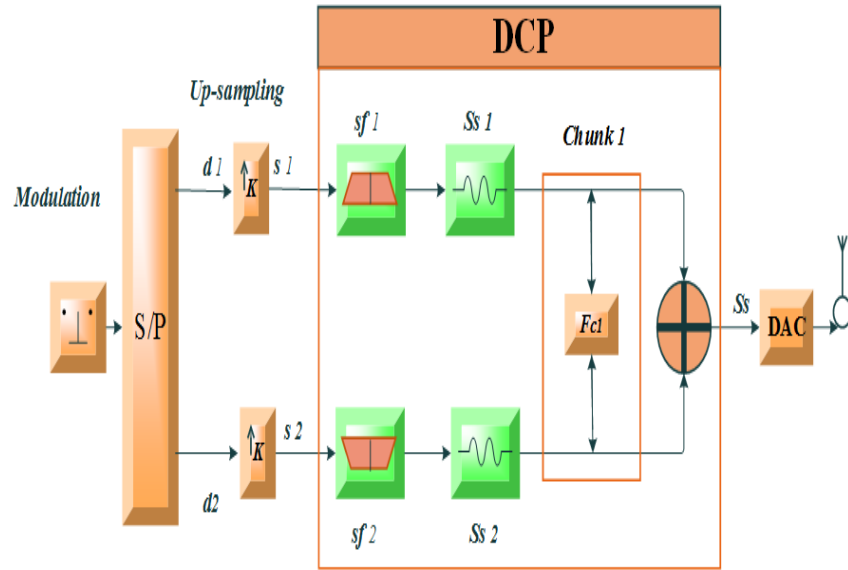


Figure 3.1.1: Block diagram of single carrier OGFDM transmitter (Kadhum *et al.*, 2018).

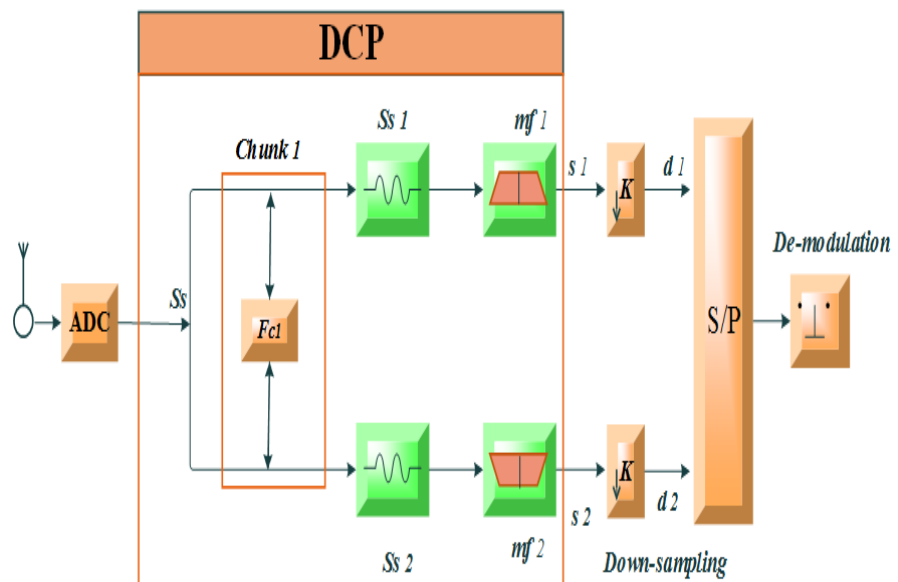


Figure 3.1.2: Block diagram of single carrier OGFDM receiver (Kadhum *et al.*, 2018).

The key feature that is highlighted in this single frequency carrier system is utilizing the Hilbert filters for orthogonally combining and separating every two of frequency subcarriers.

According to the Hilbert transform, the orthogonality ( $90^0$  change in phase) can be achieved between the shaping and matching filters. Therefore, in this presented design the first filter (cosine/sine) operates in an opposite phase to its Hilbert transform (sine/cosine).

To clarify more about this kind of filters correlation, the Hilbert transforms  $\hat{w}(t)$  of a signal  $w(t)$  is defined as following (Alexander and Poullarikas, 1999):

$$\hat{w}(t) = w(t) \otimes \frac{1}{\pi t} = \frac{1}{\pi} \int_{-\infty}^{\infty} \frac{w(t - \tau)}{\tau} d\tau \quad (1)$$

where  $\otimes$  represents the convolution operation between  $w(t)$  and the signal  $1/\pi t$  in time domain.

In Fourier transform the signal  $1/\pi t$  can be represented as  $-sgn(f)$  (Alexander and Poullarikas, 1999):

$$-sgn(f) = \begin{cases} -j, & \text{if } f > 0 \\ 0, & \text{if } f = 0 \\ j, & \text{if } f < 0 \end{cases} \quad (2)$$

“As such, if Fourier transform of  $w(t) = W(f)$ , then  $\hat{w}(t)$  has Fourier transform  $\hat{W}(f)$  which is equivalent to  $-sgn(f)W(f)$ . Consequently, the positive frequencies are multiplied by  $-j$  while negative frequencies are multiplied by  $j$  which are corresponding to phase change of  $-\pi/2$  and  $\pi/2$  respectively” (Kadhum *et al.*, 2018). That’s means, employing the Hilbert transform, the amplitude of the signal in the frequency domain is not changed, only the phase is perpendicularly altered, where the real and imaginary parts of each complex number are switched during the phase alteration process. This, as a result, makes the implementation of the Hilbert transformation in the frequency domain is easier than in the time domain

The central idea of the Hilbert transformation is, if  $w(t)$  is a signal, then it is orthogonal to its Hilbert transform  $\hat{w}(t)$  since the integration between them equals to zero (no interference) as following (Alexander and Poullarikas, 1999):

$$\int_{-\infty}^{\infty} w(t) \hat{w}(t) dt = 0 \quad (3)$$

Accordingly, the relationship between the introduced pair of the Hilbert filters (cosine and sine) can be considered as an orthogonal since  $\cos(t)$  represents the Hilbert transform of  $\sin(t)$ . Worth noting that applying the orthogonality between adjacent filters lets them capable to participate in the same frequency centre. Thus, with such kind of filtration, the frequency centre of the filter can be reused twice yet keeping the same number of the utilized filters. Since the computational complexity of output point can be calculated depending on the overall number of multiplications (Ingle and Proakis, 2012). In this context, employing the developed Hilbert filters with the OGFDM does not increase the computational complexity if a similar number of applied filters (multiplication operations) is adopted in both the OGFDM and GFDM filtering operation.

To retrieve the main signal from its Hilbert transform, a reverse transform of the Hilbert is applied, therefore,  $w(t)$  is recovered from  $\hat{w}(t)$  by performing another Hilbert transformation followed by inverting the achieved result as following (Alexander and Poullarikas, 1999):

$$w(t) = -\hat{w}(\hat{w}(t)) \quad (4)$$

From the filtration level perspective, the transmitter side of the single carrier OGFDM includes two perpendicular shaping filters that are mainly recognized by their finite impulse responses  $Sf_I^I(t)$  and  $Sf_I^Q(t)$ , where the superscripts  $I$  and  $Q$  specifies the in-phase and out-phase respectively. In the digital domain, the transmitted signal that is generated by summating those two convoluted frequency subcarriers can be expressed as following (Tao *et al.*, 2013):

$$St(t) = \sum_{k=1}^2 S_k(t) \otimes Sf_1^{(I/Q)}(t) \quad (5)$$

where  $St(t)$  refers to a combination of the convoluted frequency subcarriers  $S_k(t)$  with their impulse responses  $Sf_I^I(t)$  and  $Sf_I^Q(t)$  that are counted for transmitting two of frequency subcarriers. In the wireless system, the multiplexed signal  $Ss(t)$  is then passed over the DAC for transmission.

At the receiver side of the single carrier, two corresponding matching filters are used that are principally identified by their impulse responses  $Mf_1^{(I)}$  and  $Mf_1^{(Q)}$ . The extracted frequency subcarriers after performing the matching operations can be expressed as following (Tao *et al.*, 2013):

$$Sr(t) = \left[ \sum_{k=1}^2 S_k(t) \otimes Sf_1^{(I/Q)}(t) \right] \otimes Mf_1^{(I/Q)} \quad (6)$$

It's worth pointing that, the intended frequency subcarrier  $S_r(t)$  can be retrieved only for the same order convolution between the shaping and matching filters. As such, the impulse response of the convolution for the same phase filters ( $C = D$ ) represents as following (Tao *et al.*, 2013):

$$Sf_1^C(t) \otimes Mf_1^D(t) = \delta(t - t_0) \quad (7)$$

where the superscripts  $C$  and  $D$  indicates either the in-phase or out-phase and  $t_0$  denote to the possible delay of transmission for each frequency subcarrier.

On the other hand, with different phase filters  $C \neq D$ , the output frequency subcarrier tests high interference making it unrecognized, the impulse response of such type of convolution is expressed as follows (Tao *et al.*, 2013):

$$Sf_1^C(t) \otimes Mf_1^D(t) = 0 \quad (8)$$

The impulse responses of the utilized shaping filters for the Hilbert pair (cosine and sine) are expressed as the follow (Tao *et al.*, 2013):

$$Sf_1^I(t) = g(t) \cos(2\pi f_{c1} t) \quad (9)$$

$$Sf_1^Q(t) = g(t) \sin(2\pi f_{c1} t)$$

where  $f_{c1}$  refers to is the single frequency centre of the applied filter and  $g(t)$  signifies the baseband pulse that has a square-root raised cosine form expressed as following (Tao *et al.*, 2013):

$$g(t) = \frac{\sin[\pi(1 - \alpha)\gamma] + 4\alpha\gamma \cos[\pi(1 + \alpha)\gamma]}{\pi\gamma [1 - (4\alpha\gamma)^2]} \quad (10)$$

where  $\gamma = t/\Delta t$ ,  $\alpha$  expresses the BW limits of the filter and  $\Delta t$  is the sampling time.

The equivalent Hilbert filters for the matching process are expressed as following (Tao *et al.*, 2013):

$$\begin{aligned} Mf_l^I(t) &= Sf_l^I(-t) \\ Mf_l^Q(t) &= Sf_l^Q(-t) \end{aligned} \quad (11)$$

In terms of the BW access of the filtered subcarrier, the filter limits should be verified perfectly to avoid the influence of any probable aliasing. Since the roll-off factor range fluctuates between 0 and 1, the frequency response of the baseband pulse alters from a uniform to a pure square-root raised-cosine according to the impact of the rolling. Moreover, to reasonably decrease the digital filter complexity yet achieving an acceptable system BER, the number the filter coefficients should optimally be selected (Tao *et al.*, 2013).

From digital signal processing perspective, the obtained sequence of data (discrete signal) comes from equivalently sampling the continuous signal in both the input and output sides of the transmission system at  $\Delta t$  sampling interval. In addition, the total period that is needed for transmitting one OGFDM symbol composes of  $K$  samples is equivalent to  $K \Delta t$ . Moreover, the transmission speed of the transceiver is chiefly decided according to the converter sampling rate ( $F_{DAC/ADC}$ ). Furthermore, the sampling rate of both the shaping and matching filters that are originally resulted from dividing the  $F_{DAC/ADC}$  on the applied number of frequency subcarriers must be manipulated to be compatible with the utilized  $F_{DAC/ADC}$ .

The overall bit-rate of transmission can be produced by gathering bit-rates of all frequency subcarriers in one time period. Therefore, depending on Shannon theorem, the channel capacity that represents the maximum number of bits for one iteration of transmission with an acceptable possibility of errors is defined as following (Im *et al.*, 1995):

$$Capacity = BW * \log_2(1 + SNR) \quad (12)$$

where SNR refers to the signal to noise ratio that is changed mainly due to the induced interference among frequency subcarriers. It's worth noting that the used modulation format can play a big role in affecting the SNR, hence, if the modulation scheme is promoted the required SNR is elevated to optimally recoup the required signal. Thus, without improving the SNR, space between adjacent samples on the constellation map is reduced causing in difficulty in deciding the right places of the intended complex numbers at the receiver side.

As such, with a specified power of transmission for each modulation shape, there is an equivalent SNR that in return controls the transmission performance in terms of the channel capacity and BER. With respect to the influence of the channel mode, in this system, a Gaussian channel is supposed in the presence of the AWGN where the noise power is distributed uniformly over the BW frequencies of the wireless transmission channel.

To demonstrate key variances between the conventional RRC and the developed Hilbert filters, the following two cases can explain the effect of utilizing the orthogonal filters in the wireless system comparing to the non-orthogonal RRC filter.

Case-1 (Symmetric BW): In this case, as is seen in Figure 3.1.3, where the BW size, with both the RRC and the Hilbert, is similar, a one frequency carrier is applied to explore the impact of both filters (RRC & Hilbert) on the system performance. As such, investigating the feasibility of replacing the currently employed filters by the advanced Hilbert filters in terms of the channel capacity, BW size, transmission duration, and computational complexity.

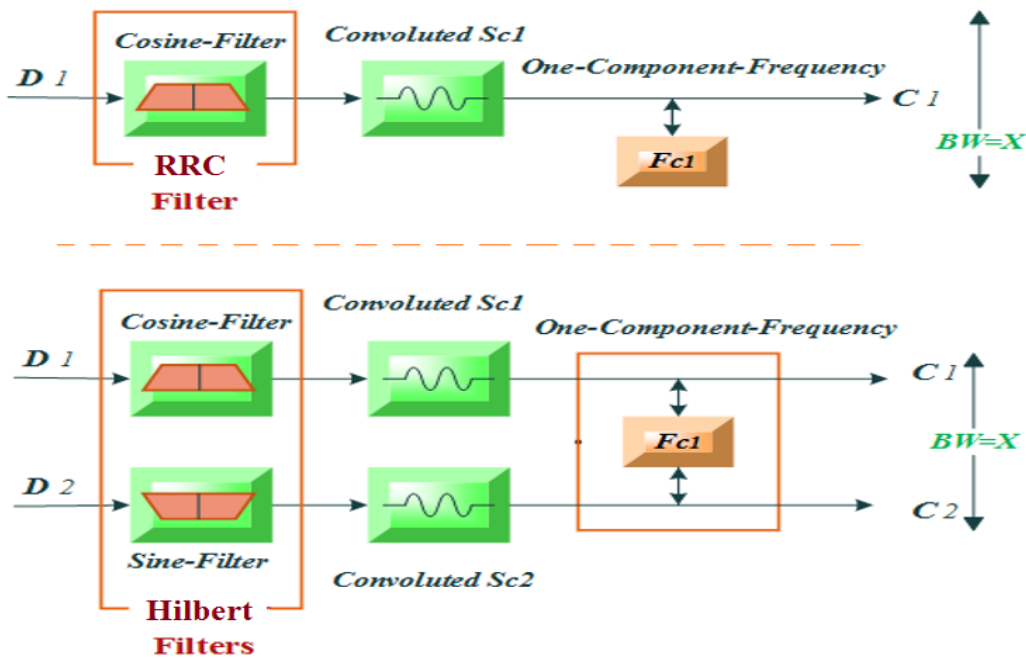


Figure 3.1.3: Bandwidth efficiency with both RRC and Hilbert filters (1<sup>st</sup> case).

Concerning the capacity of the channel, the ability to carry two magnitudes of data instead of only one leads to double the carried information for each used frequency carrier. Thus, by depending the orthogonal filtering (cosine and sine) a double amount of transmitted data can

be achieved comparing to the non-orthogonal filter (RRC), where  $\text{Capacity\_Hilbert} = 2 * \text{Capacity\_RRC}(r)$ .

With reference to the size of the BW, the required BW with the Hilbert will not be doubled in parallel with the doubled capacity of the channel, where  $\text{BW\_Hilbert} = \text{BW\_RRC}$ . Thus, in comparison to the RRC, no extra cost is requested for employed resources with the supportive filters (Hilbert).

As is shown in Figure 3.1.4, on the topic of the transmission duration, despite achieving a doubled bit-rate with the advanced Hilbert filters, the level of consumed time will not be doubled in relative to the RRC. Hence, since both sides of Hilbert (cosine & sine) work simultaneously, the required time for transmission by them is yet like the time with RRC.

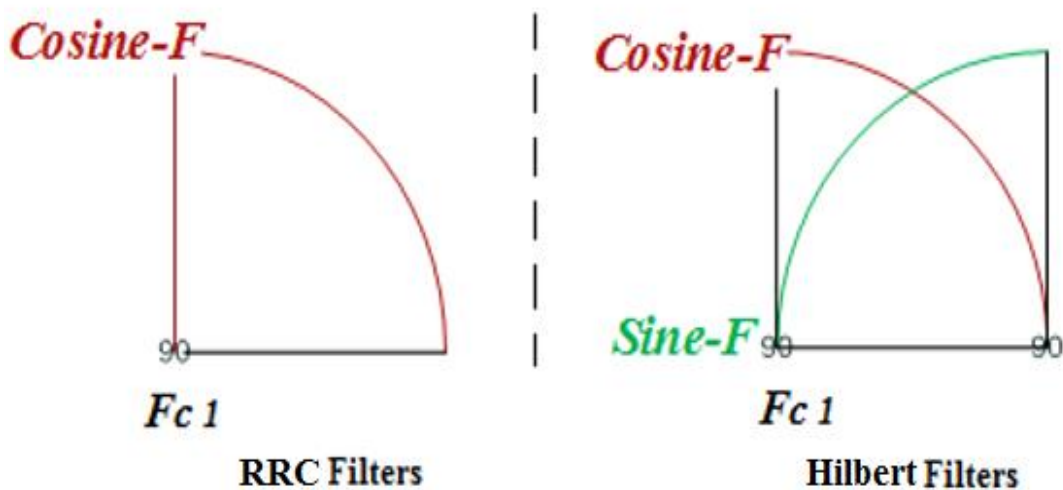


Figure 3.1.4: Orthogonal Hilbert filters vs non-orthogonal RRC filter (1st case).

The computational complexity of the transmission system is doubled in accordance with the double number of applied filters. This is essentially due to the increased number of multiplication operations that are required for each used frequency centre. As such, as is clear in Figure 3.1.3, a twice number of filters that are used with the Hilbert increases the complexity of transceiver operation in comparing to the RRC. Nevertheless, modern signal processors are fully capable of filtering more than one input signals per time without the need for additional hardware resources, particularly, when processed operations are independent (Jiang and Mao, 2015). As a result, today's technology can be considered as a quite supportive tool for Hilbert filters.

Case-2 (Asymmetric BW): As it is seen in Figure 3.1.5, where the applied BW size with the RRC is larger than the Hilbert filters by twice, two frequency carriers for the conventional RRC and one frequency carrier for the advanced Hilbert are employed to demonstrate the impact of both filters (RRC & Hilbert) on the system performance. Thus, explore from a different perspective the benefit of switching from the RRC filters to the Hilbert filters considering key factor determinations like the capacity of the channel, size of the BW, transmission duration, and computational complexity.

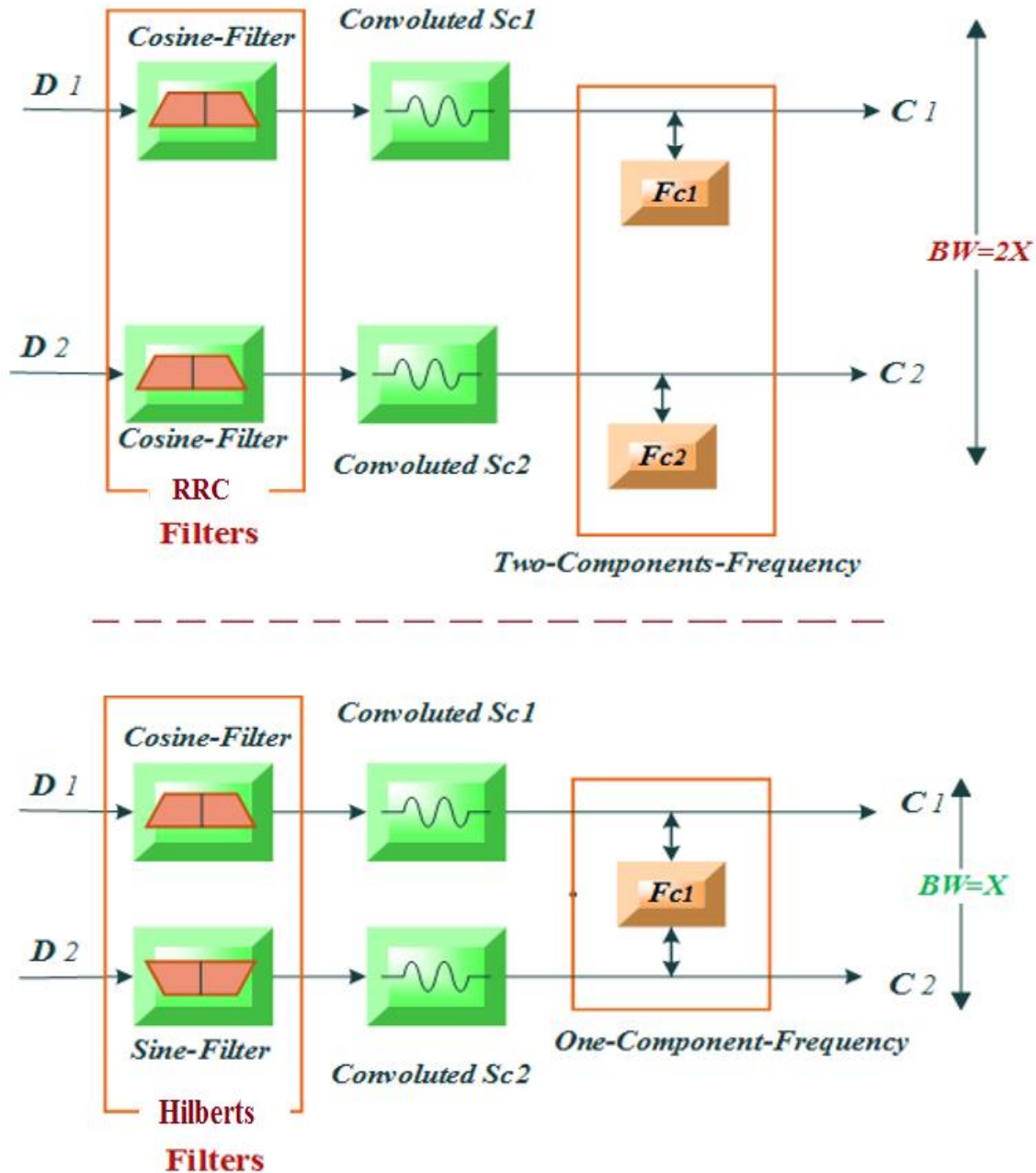


Figure 3.1.5: Bandwidth efficiency with both RRC and Hilbert filters (2<sup>nd</sup> case).

With respect to the capacity of the channel, the advantage of getting a double channel capacity is not achieved here since the RRC tends to work with doubling its BW size to have a similar Hilbert channel capacity, where  $\text{Capacity}_{\text{RRC}} = \text{Capacity}_{\text{Hilbert}}$ . On the topic of the BW size that introduced for Hilbert filters, it will be halved herein obtaining a similar channel capacity to the RRC, where  $\text{BW}_{\text{Hilbert}} = 1/2 * \text{BW}_{\text{RRC}}$ . Hence, by employing the orthogonal feature of the Hilbert a similar channel capacity to the RRC is achieved reducing the cost of required resources.

In relation to the transmission duration, compared to the consumed time by the RRC, the required level of time duration for the Hilbert will be reduced to the half in parallel with achieving the same channel capacity for both the RRC and Hilbert filters, hence,  $\text{transmission duration}_{\text{Hilbert}} = 1/2 * \text{transmission duration}_{\text{RRC}}$ .

Finally, as is clear from Figure 3.1.6, the computational complexity that resulted from using Hilbert filters in this wireless system will not be increased since no extra filters are added in comparison to the RRC case. Thus, the number of applied filters with Hilbert is equivalent to that one with RRC, where  $\text{No. Filters}_{\text{RRC}} = \text{No. Filters}_{\text{Hilbert}}$ .

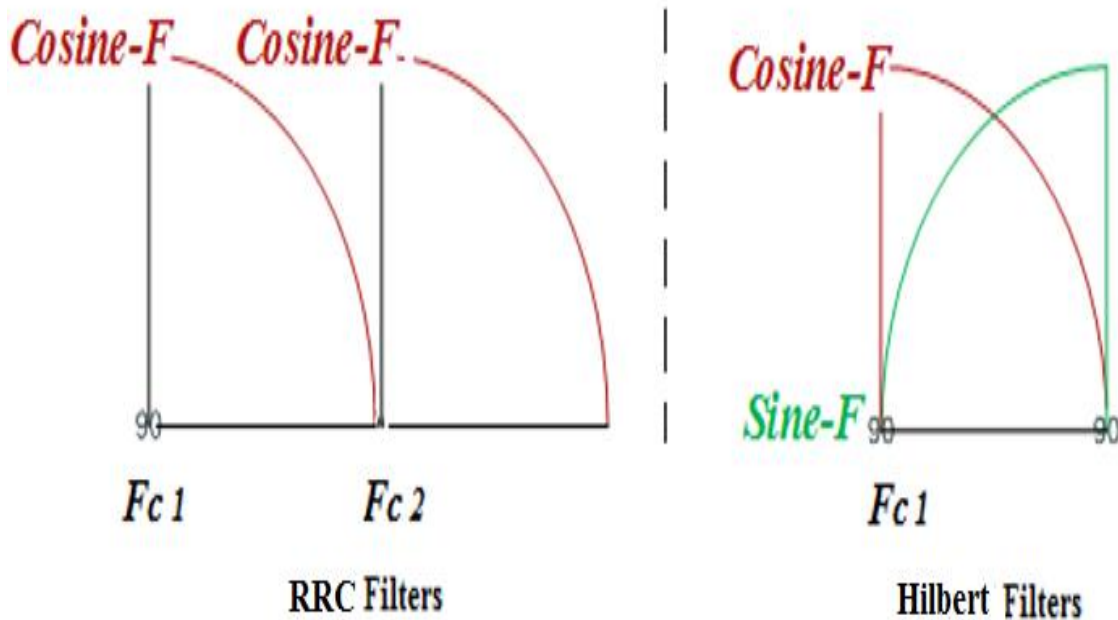


Figure 3.1.6: Orthogonal Hilbert filters vs non-orthogonal RRC filter (2<sup>nd</sup> case).

### **3.1.3 Experimental Results**

In this demonstration, the introduced single carrier OGFDM is numerically simulated. The experimented system is considered for two of frequency subcarriers that are fundamentally based on employing the orthogonality of the developed Hilbert filters on a single frequency centre working with a diverse range of modulation formats.

Since the digital Hilbert filters are the core of the OGFDM system, the key restrictions of the functional filters at this experiment are optimally adjusted to be compatible with the highest limit of transmission bit-rate at an acceptable level of errors. The maximum capacity of the channel that is undertaken with optimum filter parameters is basically achieved in an electrical back-to-back wireless system. The transceiver system performance, in terms of the channel capacity and BER, is tested under the circumstances that are stated in Table 3.1.1.

Regarding the simulation tools, the MATLAB is utilized to validate and demonstrate graphically the achieved results. The MATLAB software environment that helps telecommunication engineers to simulate transmission systems with higher processing speed and accuracy is employed to implement the required communication system models. Hence, the MATLAB application is used to support proficiently digital signal processing and simulate easily many elements of wireless communication systems. For example, to convert from the frequency domain to the time domain and vice versa, the IFFT (x) and FFT (x) functions are used. Besides, REAL (x) and IMAG (x) functions are employed to extract the real and imaginary parts of the obtained complex numbers. In addition, depending on the ANGLE (x) and ABS (x) functions, the phase and amplitude of each transmitted complex number are calculated. Moreover, to prepare the required conjugates of the processed complex numbers, the CONJ (x) function is utilized. Also, to shift the zero-frequency component to the spectrum centre, the FFTSHIFT (x) function is applied. Furthermore, to add additive white Gaussian noise to a transmission signal, the AWGN (x) function is used. It's worth noting that the Visio software environment that supplies special symbols of electrical and telecommunication equipment, lines, etc was also utilized to draw the designed system models in a fast and effective way. For instance, to draw clear and simple transmission diagrams, the Shapes toolbox of the Visio is used to select shapes related to the electrical engineering field where a set of template options like Analog Digital Logic, Telecom Switches Peripheral Equipment, Transmission Paths, etc., are supplied.

Table 3.1.1: System parameters for the single carrier OGFDM

Parameter	Value
No. of frequency centres	1
$F_{DAC/ADC}$	2 GHz
Roll-off	0.1
System mode	Single carrier
Number of subcarriers	2
Filter length	32
OGFDM symbols	2000
Filter type	Hilbert filter

Considering the first important factor of the applied filter (coefficients), it is seen from Figure 3.1.7 that by increasing the number of the used coefficients, the system performance of the BER can be improved gradually achieving the acceptable limits of the errors ( $10^{-3}$ ) with 32 taps. As such, due to professionally decreasing amplitude variance between adjacent taps, enhanced stages of errors are orderly recorded. Worth noting that by continuing with increase the coefficients, the BER is extra improved exceeding the required standards of errors. This, however, comes up with escalating the level of the computational complexity according to the expanded range of the coefficients at the applied filter.

With reference to the second significant factor of the used filter (roll-off), it is clear from Figure 3.1.8, the optimum level of rolling can be achieved with roll-off equals to 0.1. It's worth pointing that, the BER values for roll-off higher than 0.2 are affected severely due to destroying the portion of the convoluted filter that excesses the Nyquist rate boundary. On the other hand, the roll-off value equals to zero testes a high level of errors as well due to expanding the variance between adjunct taps of the utilized filter. Therefore, for the employed pair of the Hilbert filters that are working on the single frequency centre, the roll-off factor can mainly impact the optimized limit of the filter BW access. As a result, in terms of channel capacity and the BER, both filter parameters (coefficients number and roll-off factor) can crucially influence the overall system performance.

In this context, as is seen in Figure 3.1.9, the frequency responses of the passband ripples for the applied filters are randomly different reflecting obviously the oscillatory construction of both the cosine and sine filters in the frequency domain. Consequently, unless such kind of

fluctuation is managed well, the filtering operation of the convoluted frequency subcarrier can be principally attenuated by the frequency responses of the utilized filters.

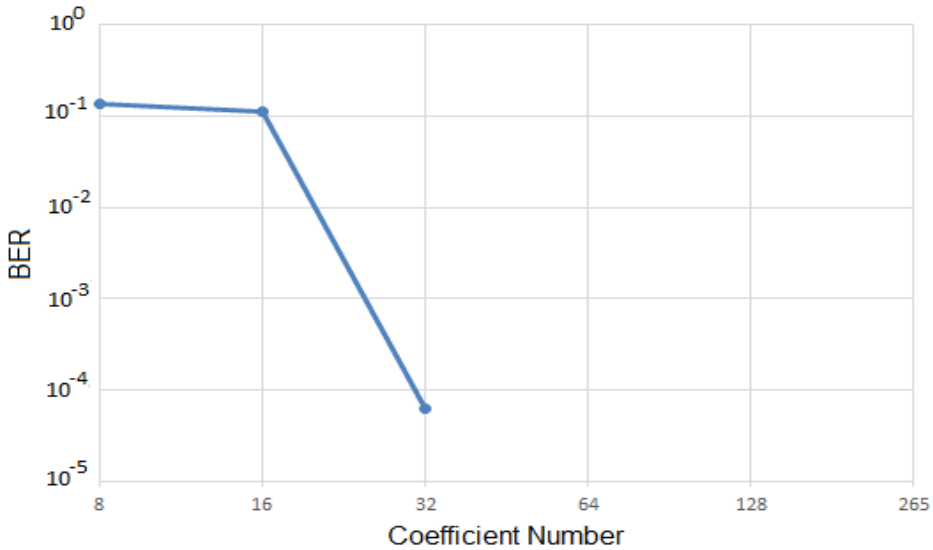


Figure 3.7: Effect of the filter coefficients on the BER system performance (Kadhum *et al.*, 2018).

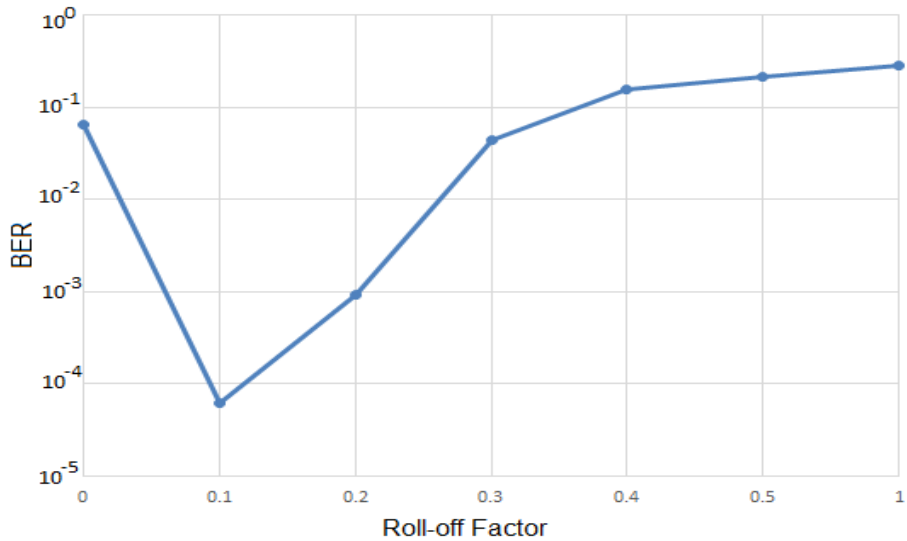


Figure 3.1.8: Roll-off effect on BER system performance (Kadhum *et al.*, 2018).

To minimize the wobbling behaviour of the frequency response, the number of filter coefficients is increased obtaining a better estimation for the convoluted taps in the frequency domain than the previous case. Nevertheless, as formerly mentioned, the increased number of the taps causes in elevating the computational complexity at the functional filter. Thus, the coefficient number can be considered as a critical issue should be treated precisely at the acceptable limits of BER.

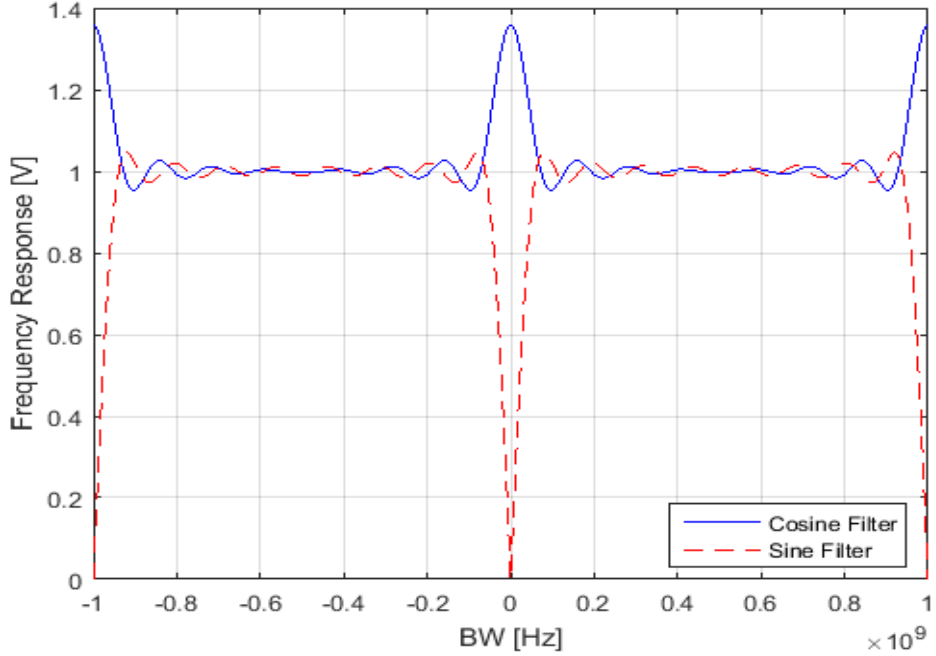


Figure 3.1.9: Combination of cosine and sine filter responses in the frequency domain (Kadhum *et al.*, 2018).

As is shown in Figure 3.1.10, in terms of the channel capacity, better system performance is recorded for the proposed single carrier of the OGFDM than the conventional GFDM. Therefore, due to the orthogonal feature of the utilized filters, the advanced design of the OGFDM can relatively double the transmission bit-rate of each employed frequency centre. This, as a result, makes a single frequency carrier of the OGFDM carries a double amount of transmitted data in comparison with the traditional GFDM that needs two frequency carriers to achieve this. As such, a stable 2 dB gain is attained between channel capacities of the single carrier OGFDM and GFDM with diverse formats of the modulation. The extra increment of the channel capacity results from the perpendicular difference in the phase between the developed Hilbert filters that are related to one frequency centre of the OGFDM.

As is clear in Figure 3.1.11, in terms of the BER performance, the required SNR of both the single carrier OGFDM and GFDM is calculated herein in presence of the AWGN effect reflecting the impact of the ideal noise on the filtered subcarriers. It's worth pointing that, a similar level of the SNR is required for both the OGFDM and GFDM demonstrating that the proposed OGFDM can reach a double capacity of the channel with an equivalent degree of the acceptable BER to the GFDM. Eventually, considering the same conditions of the transmission, the gained results of this experimental work presents that the system performance of the channel capacity and BER for the single carrier OGFDM far outweigh the conventional GFDM performance.

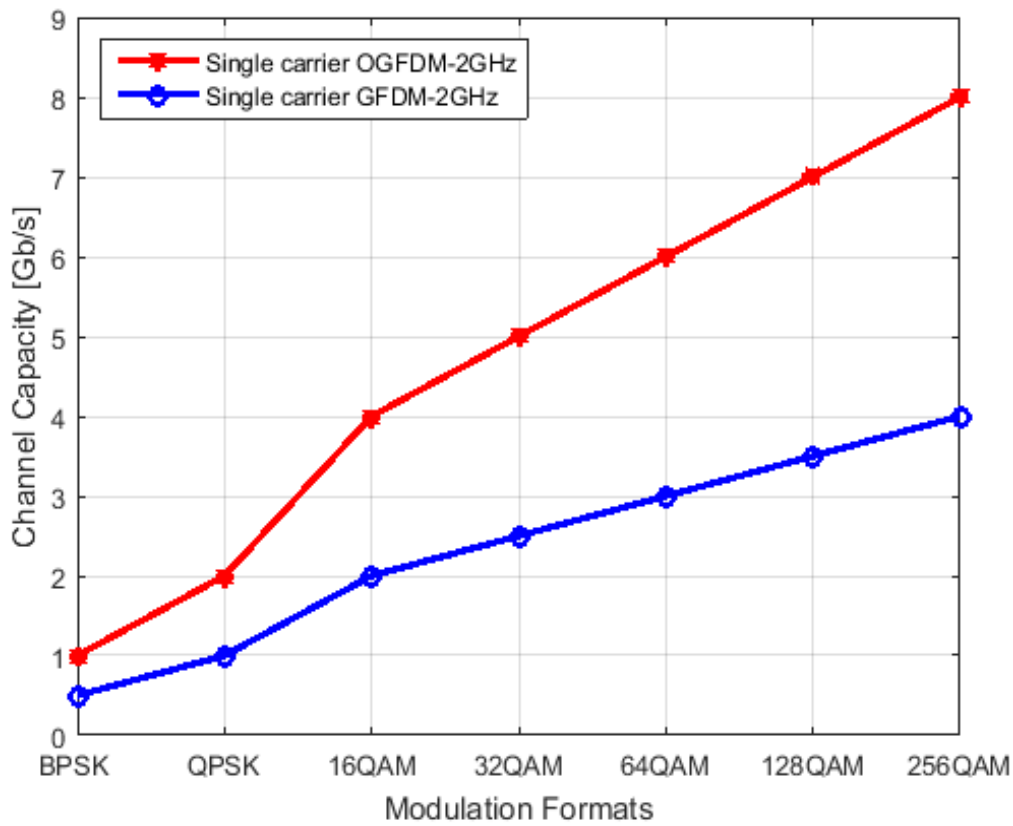


Figure 3.1.10: Higher (double) channel capacity of single carrier OGFDM than the GFDM (Kadhum *et al.*, 2018).

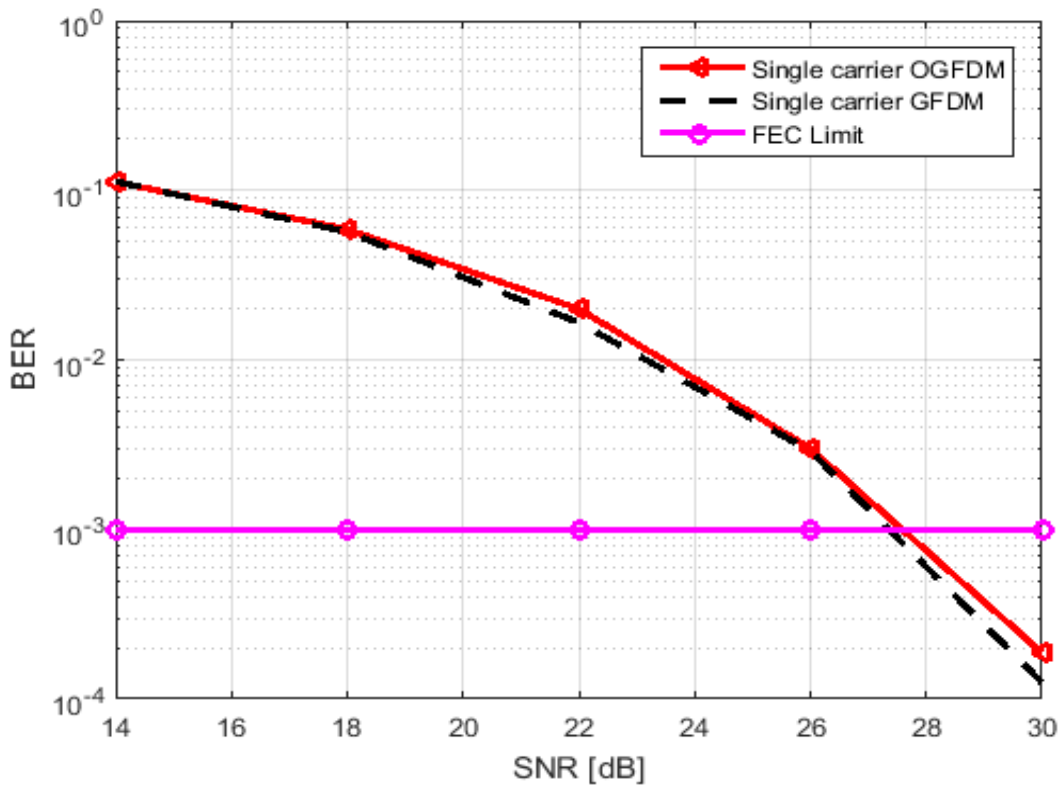


Figure 3.1.11: Similar SNR for both single carrier OGFDM and GFDM (Kadhum *et al.*, 2018).

## 3.2 Oversampling Level

### 3.2.1 Introduction

Due to the high restriction of the present mobile waveform and the revolutionary evolution of the upcoming cellular networks, mobile communication developers have been exploring advanced transmission techniques that can highly improve the capacity of the channel and deliver better transmission reliability than the currently applied (Habibi *et al.*, 2019). Therefore, since the CP-OFDM has severe drawbacks (Schaich *et al.*, 2014), new alternative waveforms like the FBMC (Gaohui, 2018), the UFMC (Wen, Hua and Lu, 2018), the F-OFDM (Jayan and Nair, 2018), and the GFDM (Hilario-tacuri, Fortes and Sampaio-neto, 2018) are proposed for the upcoming scenarios of the mobile network.

Novel waveform called OGFDM (Kadhum *et al.*, 2018) was introduced with a single frequency carrier to extra support the wireless channel capacity of the future mobile communication. Consequently, yet keeping a similar error level relative to the GFDM waveform, the recently offered OGFDM waveform can realize a double transmission bit-rate. It's worth pointing that, the need for a better BW efficiency than the previous one (single) which in turn improves the achieved channel capacity pushes the waveform developers to increase the employed number of frequency subcarriers. This, however, can cause in raising the interference level of the adjacent frequency subcarriers, particularly, at the bad conditions of the transmission (Gaspar *et al.*, 2014). Since, the expected scenarios of the modern mobile generations (5G and beyond), that are related mainly to the high channel capacity, need for an improved BW usage, the traditional treatment of the induced interference is no longer applicable for the wireless networks (Chiumento *et al.*, 2014). Therefore, addressing the interference of the influenced frequency subcarriers by the conventional approach can result in wasting the BW efficiency, hence, decreasing the amount of the delivered channel capacity (Sacchi *et al.*, 2017).

This, as a result, makes the developed design of the OGFDM waveform, where a couple of frequency carriers are applied instead of one, is highly requiring for an advanced interference management to be compatible with the predicated demands of the forthcoming mobile communications. Accordingly, a new approach named intra-channel interference avoidance (ICIA) is presented herein. The introduced ICIA utilizes the features of the oversampling operation by moving from normal to double oversampling to eliminate potential interference

that might be occurred between the adjacent filters of the OGFDM subcarriers. Therefore, the proposed management tends principally to utilize the oversampling process for effectively removing the bad roll-off behaviour of the employed filters. As such, controlling perfectly the oversampling factor that is precisely setting guard intervals between the filtered subcarriers can accommodate entirely the expanded statuses of the roll-off factor.

By optimally fixing the created distances between the filter frequency centres, all Nyquist intervals of filtered frequency subcarriers can be secured. Therefore, depending on a similar allocation process with different frequency centres, the transmitted signal can be carried by variant frequency centres and received subsequently by their counterparts (Prommee, Thongdit and Angkeaw, 2017).

To gain a high bit-rate for all transmission situations, the assigned value of the oversampling is managed relative to the situation of the filter roll-off factor. Thus, due to the unstable transmission conditions, the obtainable degree of power attenuation that varies between the acceptable and severe rolling can fundamentally stimulate the best mode of the oversampling. It's worth noting that, the possibility of the interference that occurs between the applied filters is enlarged if the filter rolling expansion is increased due to the reduced average power of the transceiver (Han, Sung and Lee, 2017). The most favorable filter layout is identified by the trade-off relationship between the aggregate channel capacity and the filter rolling under diverse transmission states.

The rest of this part (oversampling level) is organized as follows: Section 3.2.2 discusses theoretically the main advantages and disadvantages of the proposed system. Section 3.2.3 evaluates the transmission performance (channel capacity and BER) of the OGFDM transceiver in an electrical back-to-back wireless mobile system utilizing a computer simulation.

### **3.2.2 System Model**

As is seen in Figure 3.2.1, on the transmission process, each OGFDM frequency subcarrier is firstly encoded. At that point, by applying one of the most common modulation shapes as QPSK, 16 QAM, 128 QAM, etc. on the digital stream, the complex numbers are generated. Each modulated frequency subcarrier is dynamically up-sampled by either K or 2K factor

according to the adopted system (normal/double). Thus, between every two successive samples, a set of nulls (zeros) equals to the employed oversampling factor is inserted. It's worth noting that, all significant manipulations that directly relate to the oversampling stage are realized in the ICIA level of the system.

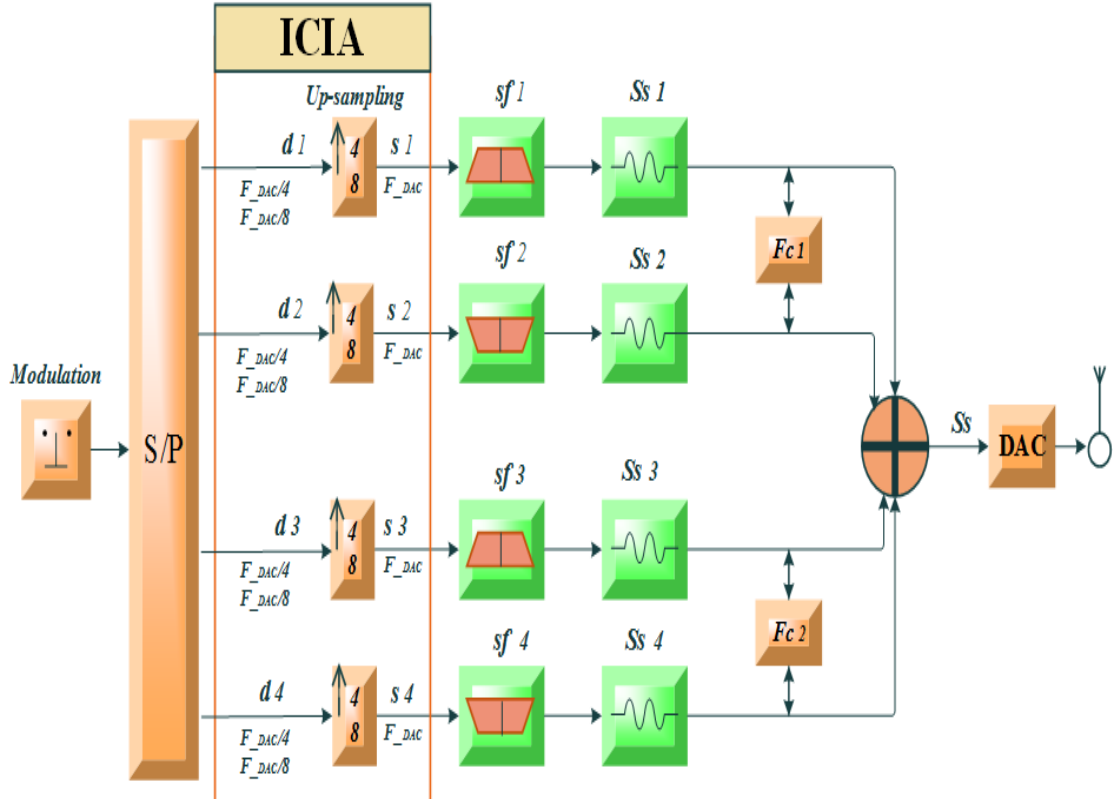


Figure 3.2.1: Transmitter of the couple carriers OGFDM with ICIA (Kadhum, Kanakis and Crockett, 2019b).

Afterwards, the up-sampled frequency subcarriers are convoluted by the applied Hilbert filters (shaping pair). Consequently, in a sequential way, every couple of close frequency subcarriers are allocated orthogonally to a similar filter frequency centre. As such, simultaneously, each single frequency centre is shared between two various frequency subcarriers. This, as a result, comes up with accommodating a further number of the filtered frequency subcarriers where the same BW is used in a double way. To ensure optimum filtration process for the system performance in the physical layer, important parameters of shaping filter like the filter taps are adjusted accurately. Having been digitally convoluted, the filtered frequency subcarriers of different frequency centres are then collected employing an electrical adder. The combined data sequence is passed through the DAC producing the analog domain signal that is ultimately propagated by the antenna.

As is shown in Figure 3.2.2, on the reception process, the analog signal is digitized using the ADC. Subsequently, the data stream of each frequency subcarrier is de-multiplexed utilizing corresponding filters (matching pair). Besides, the matching filter taps are adjusted in a similar way to their equivalent shaping coefficients achieving an effective filtration operation. At the oversampling manipulation (ICIA level), the up-sampled frequency subcarriers that were matched and de-multiplexed through the digital filters are down-sampled by removing all formerly stuffed zeros. Eventually, the original stream of data is mostly recovered at the de-modulation stage where the previously adopted format of the modulation process is considered.

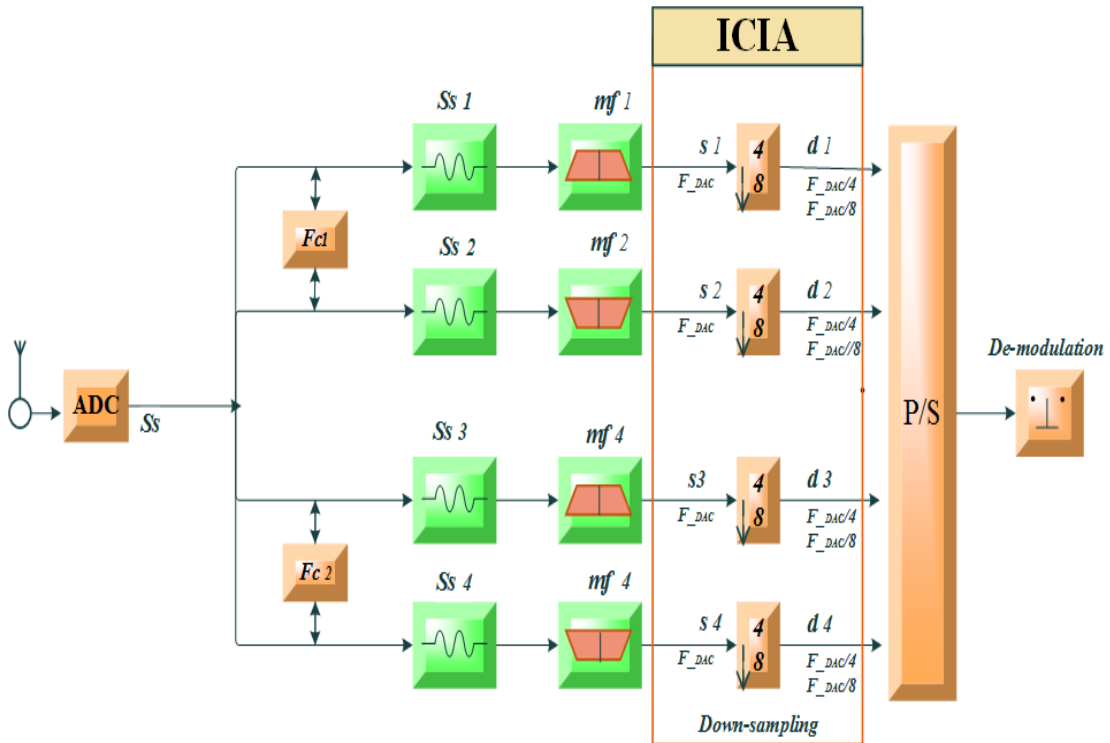


Figure 3.2.2: Receiver of the couple carriers OGFDM with the ICIA (Kadhum, Kanakis and Crockett, 2019b).

“Mathematically speaking, the key required operations of the proposed transceiver system are demonstrated. Thus, on the transmitter side, the impulse responses of the  $h^{th}$  shaping pairs of Hilbert filters are written as follows” (Kadhum, Kanakis and Crockett, 2019b) (Tao *et al.*, 2013):

$$\begin{aligned} Sf_h^A(t) &= g(t) \cos(2\pi f c_h t) \\ Sf_h^B(t) &= g(t) \sin(2\pi f c_h t) \end{aligned} \quad (1)$$

where  $f_{ch}$  represents the centre frequency of the  $h^{th}$  Hilbert filters pairs, ( $1 \leq h \leq 2$ ), and  $g(t)$  is the baseband pulse which is expressed as follows (Tao *et al.*, 2013):

$$g(t) = \frac{\sin[\pi(1 - \alpha)\Upsilon] + 4\alpha\Upsilon \cos[\pi(1 + \alpha)\Upsilon]}{\pi\Upsilon[1 - (4\alpha\Upsilon)^2]}, \quad \Upsilon = t/\Delta t, \quad (2)$$

“In addition, the in-phase and quadrature-phase of the Hilbert filter pair components are denoted by the superscripts  $A$  and  $B$  respectively. It’s worth noting that each of those components is utilized independently to convolute the frequency subcarrier. Moreover, on the receiver side, a version of impulse responses of matched filters for the corresponding shaping filters of Hilbert-pair are written as follows” (Kadhum, Kanakis and Crockett, 2019b) (Tao *et al.*, 2013):

$$\begin{aligned} Mf_h^A(t) &= Sf_h^A(-t) \\ Mf_h^B(t) &= Sf_h^B(-t) \end{aligned} \quad (3)$$

To recover the signal at the receiver side, convolution applied between shaping and matching filters achieves the following (Tao *et al.*, 2013):

$$Mf_j^C(t) \otimes Sf_i^D(t) = \begin{cases} \delta(t - t_0), & \text{if } C = D \text{ and } j = i \\ 0, & \text{if } C \neq D \text{ or } j \neq i \end{cases} \quad (4)$$

where the superscripts  $C$  and  $D$  indicate either in-phase or quadrature-phase level, and the subscripts  $i$  and  $j$  refer to the position of the frequency centre.

It is clear from Figure 3.2.3 that with the normal oversampling, the oversampling factor (OV) is set in equivalent to the overall number of the frequency subcarriers (OV = 4) where four compatible copies of each original subcarrier BW are generated to support four frequency subcarriers.

Moreover, assuming an identical frequency sampling speed at both the transmitter (DAC) and the receiver (ADC), the central frequency allocation of each Hilbert filter pair is precisely determined. Furthermore, considering the two phases of each assigned frequency centre, the frequency responses of the filters are distributed optimally through the spectral area of the

available frequency sampling. This, as a result, makes the accommodation process of every applied filter is achieved orthogonally and sequentially.

From the Hilbert filtering perspective, each orthogonal filter pair operates on two oversampled copies of the applied frequency subcarrier. Consequently, for a filter pair with a specific frequency centre, the first oversampled copy of the first frequency subcarrier is convoluted by the cosine filter while the second oversampled copy of the second frequency subcarrier is convoluted by the sine filter. As such, utilizing the in-phase and out-phase of the orthogonal filters, the odd and even frequency subcarriers can be convoluted perpendicularly. It's worth noting that two crucial parameters can be employed to decide the assigned extension of the applied filters ( $F_m$ ).

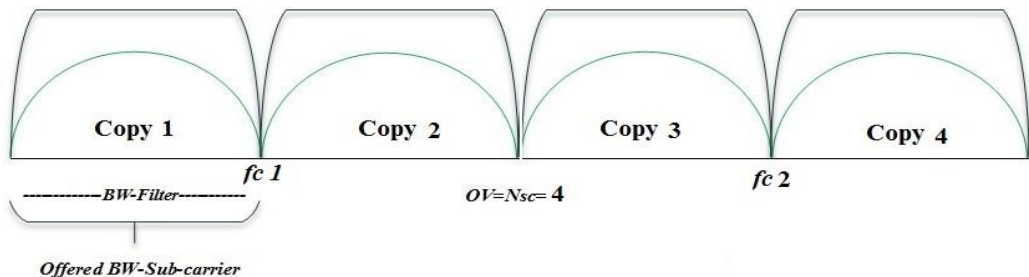


Figure 3.2.3: Normal oversampling for 4 filtered subcarriers (Kadhum, Kanakis and Crockett, 2019b).

The first one related to the given sampling rate of the utilized copy that refers to the filter BW size (Subs) whereas the second one associated with the BW excess limit of the filter rolling factor.

Concerning the first parameter (filter BW), according to the variant size of the oversampled copy at each individual subcarrier, the filter expansion is accurately decided. The key reasons beyond the filter BW variation are the oversampling configuration change and the alteration in the speed of frequency sampling. Therefore, assuming unchanged  $F_{DAC}$ , the decreased filter BW is recorded for the increased OV value and vice-versa, where  $Subs = F_{DAC}/OV$ .

With respect to the second parameter (roll-off factor), different rolling values between 0 and 1 can be assigned for each applied filter. For instance, with a roll-off factor equals to zero, the filter BW extension is equivalent to the sampling rate of the utilized copy. This, as a result, introduces a brick wall filter without interference at both the in-phase and out-phase levels (Kawamura *et al.*, 2006).

On the other hand, a doubled expansion of the filter is created by increasing the roll-off factor to one, that in turn, elevates the interference between adjacent filters to its maximum level, particularly, with a normal oversampling mode (Mukumoto and Wada, 2014). Thus, since the roll-off ( $\alpha$ ) factor represents the BW excess measurement of each filtered subcarrier, the increasing  $\alpha$  value causes in dropping the filter amplitude that in turn escalates the level of interference between adjacent filters. The correlation between these two important factors and the maximum filter expansion is expressed as following (Im *et al.*, 1995):

$$F_m = Sub_S * (1 + \alpha). \quad (5)$$

where  $0 \leq \alpha \leq 1$ .

As is seen in Figure 3.2.4, with a double oversampling, the OV is equivalent to a double number of the frequency subcarriers ( $OV = 8$ ) where eight well-matched copies of the subcarrier BW are established to assist four frequency subcarriers. Correspondingly, the specified BW of each oversampled copy at the double mode is reduced by a half in comparison with the previously assigned BW in the normal mode.

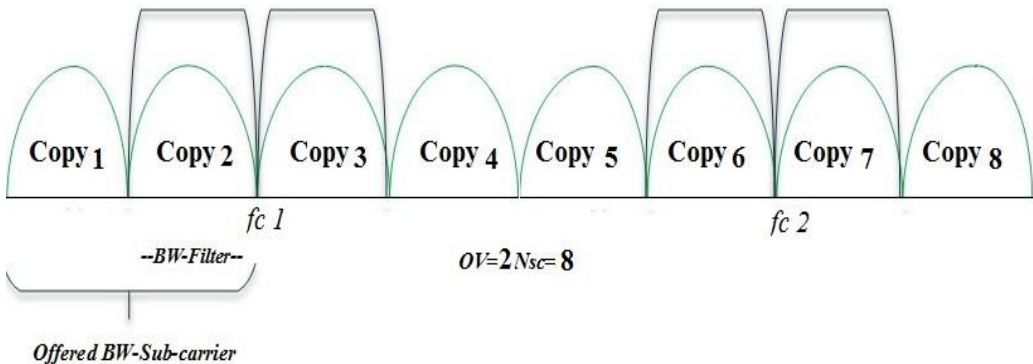


Figure 3.2.4: Double oversampling for 4 filtered subcarriers (Kadhum, Kanakis and Crockett, 2019b).

This, as a result, introduces new free spaces between the adjacent filters. However, with a similar frequency centre to the normal oversampling mode, the overall channel capacity of the double oversampling mode is impacted badly. That's mean, comparing to the obtained filter BW at the normal mode ( $Sub_S = F_{DAC}/4$ ), the generated BW of each filter at the double-mode is dropped half ( $Sub_S = F_{DAC}/8$ ). As such, the aggregated channel capacity according to Shannon theorem is calculated as following (Im *et al.*, 1995):

$$Cap_{Double} = BW/2 * \log_2(1 + SNR) \quad (6)$$

From the time-domain perspective, the transmission time that is stated for every OGFDM symbol iteration is not affected by the adaptable process of the oversampling operation (Wang *et al.*, 2012). As such, since the interval time between every two adjacent samples can be divided by OV, the increased number of samples due to multiplication by OV cannot rise the total delay of the symbol time. For instance, the recorded time T1 for transmitting N samples through one OGFDM symbol in a normal sampling process is,  $T1 = N * dt$ . On the other hand, after oversampling the system by OV, the required time for transmission T2 can be achieved by multiplying the oversampled samples by the rearranged time interval ( $T2 = N*OV * dt/OV$ ), which in turn equals to T1, where dt signifies the specified duration between two neighbouring samples. It's worth pointing that, a perfect convolution can be obtained between the identical frequencies of both the utilized filter and the oversampled subcarrier (Yli-kaakinen *et al.*, 2017). Thus, in the convolution process, the frequency that is assigned for a selected sample ( $f_i$ ) is accurately decided as a first input whereas the second input belongs to the corresponding sample of the employed filter ( $f_j$ ). If the allocated frequencies for the convoluted samples of both the applied filter and oversampled subcarrier are compatible ( $f_i = f_j$ ), then the convolution is accomplished effectively.

Occasionally, the difference between the two adjacent coefficients of the functional filter is relatively large. This, nevertheless, can be mitigated by increasing the taps number of the applied filter. The predicated frequency of the added coefficient between the two adjacent frequencies ( $f_j, f_{j+1}$ ) of the employed filter is convoluted with its equivalent frequency of the utilized sample of the subcarrier. In this context, such a kind of convolution can improve the BER performance of the transmission system since the elevated resolution of the filter can play a big role in recognizing additional in-between frequencies for the OGFDM samples. However, high filter resolution comes with raising the computational complexity of the applied filter due to increasing the required number of the multiplication processes in the filtration stage. On the other hand, considering the positive impact of enlarging the roll-off factor with the double OV mode, the variance between filter coefficients is addressed optimally. As such, if the value of assigned rolling is increased, the filter passband ripple is reduced and vice-versa.

This, though, cannot be fit for the normal scenario of the oversampling ( $OV = K$ ) where the increased value of the roll-off can cause a side effect. Hence, the enlarged roll-off factor with

the normal oversampling can enhance the error level of the filter passband ripples but cause a further interference between the utilized filters.

### 3.2.3 Experimental Results

In this experiment, a numerical simulation is principally undertaken in the physical layer of an electrical back-to-back wireless transmission system exploring the main characteristics of employing the proposed ICIA on the OGFDM system performance in terms of the BER and channel capacity.

With reference to the key system parameters, variant range of the modulation formats, that alters from the low schemes like the BPSK to the higher formats as the 256 QAM, is used for the applied frequency subcarriers. In addition, according to the adopted manipulation for the induced interference, the oversampling value is fundamentally compatible with either an equivalent number of the frequency subcarriers ( $OV = K$ ) or a double number of the frequency subcarriers ( $OV = 2K$ ). Moreover, the shaping and matching operations that were already applied for two of the filtered subcarriers (Kadhum *et al.*, 2018) are expanded for four convoluted frequency subcarriers. Thus, two frequency centres are considered herein instead of only one as in the DCP scheme. The utilized subcarriers are digitally sampled with a convertor speed ( $F_{DAC/ADC}$ ) equals to 2 GHz.

The vital guidelines of the most favorable filter design where the maximum bit-rate is achieved at the acceptable limit of BER are decided by the trade-off relationship between the overall channel capacity and the flexibility feature of the filter. Therefore, despite that the BW access of the filter can engage with a dynamic range of values between 0 and 1, the initial one is assigned essentially for the roll-off factor that can achieve a maximum bit-rate ( $\alpha = 0.1$ ). The co-existence between the amended passband ripples of the filter frequency response and the roll-off factor of the overlapped filters can also participate in obtaining the best value of rolling that corresponds to maximum channel capacity.

The main constraints of this experimental work are shown in Table 3.2.1. Besides, MATLAB tools that were mentioned in section 3.1.3 are utilized herein to represent the obtained results graphically.

Table 3.2.1: System parameters for the couple carriers OGFDM

Parameter	Value
No. of frequency centres	2
Number of subcarriers	4
System mode	Couple carriers
$F_{DAC/ADC}$	2 GHz
SNR	23
Roll-off	0 - 1
Filter length	32
Spectral efficiency	1Hz
Oversampling	Normal - Double
Modulation format	BPSK - 256 QAM
OGFDM symbols	2000
Filter type	Hilbert filter

As is seen in Figure 3.2.5, the correlation between the aggregated channel capacity and the roll-off level of the utilized filter is investigated with two different modes of the oversampling. Thus, considering the changeable value of the rolling factor, the impact of employing a normal oversampling ( $OV = 4$ ) and a double oversampling ( $OV = 8$ ) on the interference handling is explored in terms of the maximum achieved bit-rate of the channel. In this context, the channel capacity of the normal oversampling, which fluctuates relative to the steady bit-rate of the double oversampling, can be divided herein into three key regions.

With respect to the first region that is termed as the ‘Green Zone’ (GZ), the calculated channel capacities in this area are higher than the stable level of the double oversampling channel capacities. As such, GZ channel capacities that relate to the roll-off values between 0 and 0.3 ( $0 \leq \alpha \leq 0.3$ ) at the normal oversampling mode are better than the gained channel capacities of the double oversampling.

Concerning the second region that is named as the ‘Yellow Zone’ (YZ), the obtained channel capacities of the normal oversampling are identical to the double oversampling in this neutral area where the roll-off of the filter is equivalent to 0.4. From the oversampling standpoint, two logical situations (alarm and safe) are realized in the YZ. That’s means, the YZ with the normal oversampling mode takes the system down to the alarm state, whereas the double

oversampling mode with the YZ sets the system up to the safe state. As such, to avoid unwanted increment in the roll-off factor of the normal oversampling mode, the alarm system of the YZ is ringing when the accepted limits of the GZ is exceeded.

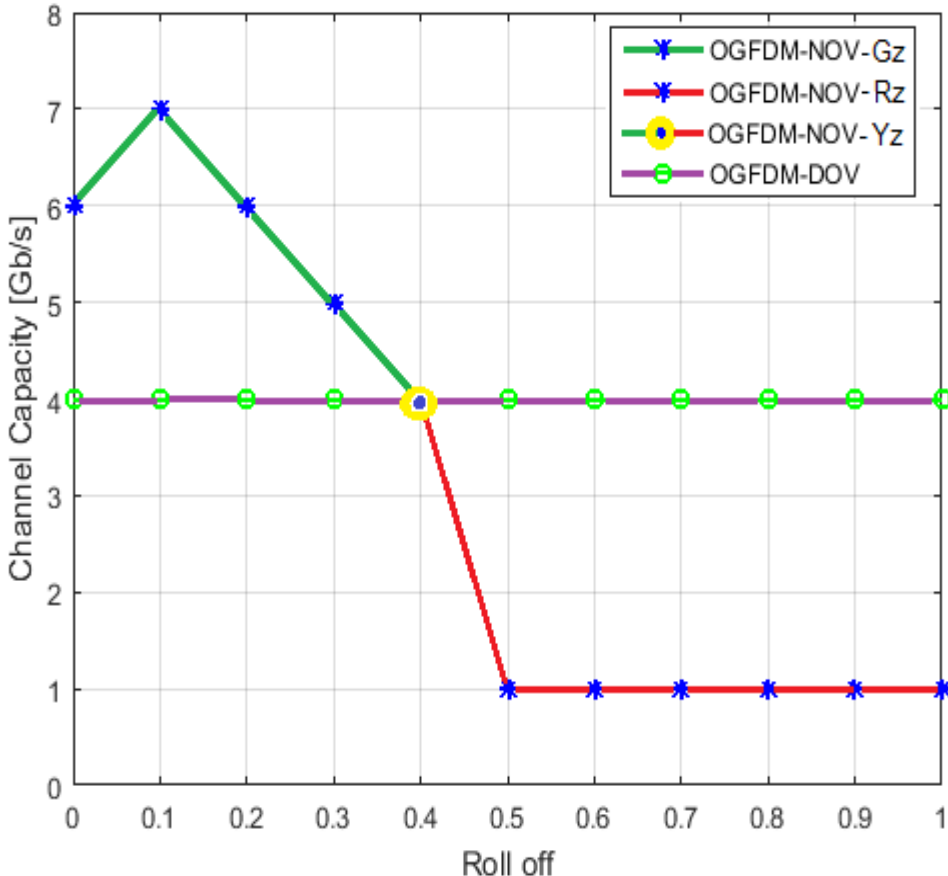


Figure 3.2.5: Channel capacity vs roll-off factor of OGFDM with normal /double oversampling (Kadhum, Kanakis and Crockett, 2019b).

With respect to the third region that is called the ‘Red Zone’ (RZ), the maximum bit-rate in this area is calculated for the roll-off values between 0.5 and 1 ( $0.5 \leq \alpha \leq 1$ ). It’s worth noting that, in contrast with the employed double oversampling, the recorded channel capacities of the normal oversampling, which is presented below the steady line of the double oversampling, suffers from a sharp reduction.

As a result, the transmission system is switched to the alternate mode (double oversampling) to stop decreasing in the channel capacity despite continuous increasing in the rolling-off ( $\alpha \leq 1$ ). Hence, in this case (RZ), it is quite necessary to exchange the conventionally utilized system (normal oversampling) with the enhanced double oversampling achieving a transmission bit-rate comparable to the YZ.

In terms of the system performance, particularly, the gained channel capacity, the maximum bit-rate of the normal oversampling can be obtained at the optimum value of the roll-off ( $\alpha=0.1$ ). Besides, according to the best-achieved channel capacity, the other ratios of both the normal and double oversampling channel capacities are calculated.

For instance, the recorded proportions of the highest channel capacities in the GZ can reach 85.7%, 85.7%, and 71.4% for roll-off values equals to 0, 0.2 and 0.3 respectively. In addition, at the YZ, the medium ratio of the channel capacity for a roll-off value approaches 0.4, is dropped to 57.1%.

On the other hand, at the RZ with roll-off values between 0.5 and 1, about 14.4% is registered as the lowest ratio of the channel capacity. Nevertheless, this case can be enhanced by employing the double oversampling that is capable to cease the bad impact of the expanded roll-off values greater than 0.4. It's worth pointing that, utilizing the double oversampling, the average ratio of the maximum bit-rate for all roll-off values between 0 and 1 can be stabled at 57.1%. This, however, results in reducing the recorded proportions of the channel capacities at the double oversampling mode for the roll-off values between 0 and 0.3 compared to the corresponding ratios of the normal oversampling (85.7%, 71.4%,). As such, the double oversampling utilization is more appropriate for the RZ than the GZ where the ratio of the channel capacity is improved from 14.1% with the normal oversampling to 57.1% with the double oversampling, presenting 4 times gain between the two investigated modes.

To address this kind of issue, the hybrid manipulation is suggested where the features of both the double oversampling and normal oversampling are employed in one strong transmission system. The hybrid system can assign the normal oversampling mode for the roll-off values between 0 and 0.4 whereas allocating the double oversampling mode for the roll-off values between 0.5 and 1. In such robust treatment, the minimum limit of the capacity ratio can be fixed at 57.1% at the bad transmission circumstance, while, at the optimum condition of the rolling, the maximum ratio can even gain 100%.

Consequently, depending on the hybrid processing, better channel capacity and transmission reliability can be offered together through the introduced system that is principally able to sustain the maximum bit-rate of the roll-off values between 0 and 0.4 and remove the serious effect of roll-off values between 0.5 and 1.

As is shown in Figure 3.2.6, in terms of the BW efficiency, different levels of the filter rolling are considered for both the normal oversampling and double oversampling exploring the impact of the oversampling manipulation on the BW usage. Within this framework, the optimum value of the roll-off ( $\alpha=0.1$ ) is firstly taken with the normal oversampling mode achieving best BW efficiencies for variant SNR thresholds. The gradually dropped levels of the SNR which in turn come up with lower peaks of BW efficiencies result from the enlarged interference between adjacent samples in the constellation map.

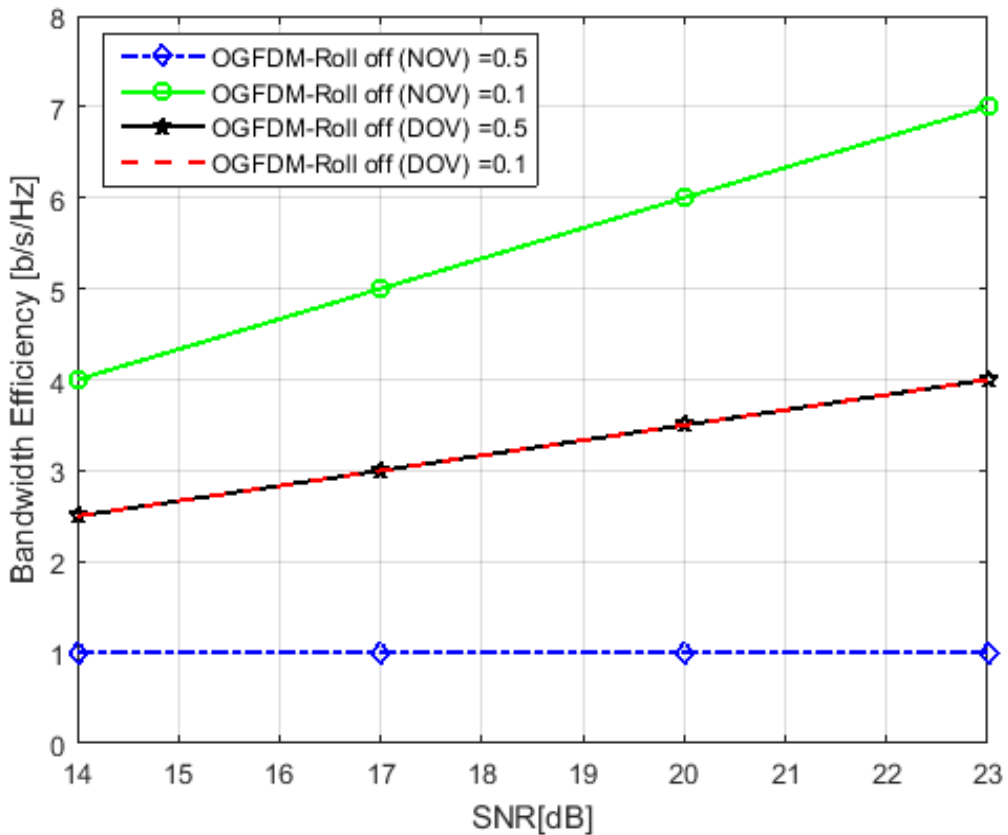


Figure 3.2.6. BW efficiency of the OGFDM with normal /double oversampling vs the SNR (Kadhum, Kanakis and Crockett, 2019b).

On the other side, the transmission system can show a severe reduction in the BW efficiency with the normal oversampling that adopts expanded levels of the roll-off ( $0.5 \leq \alpha \leq 1$ ). This sharp fluctuation in the efficiency of the BW is due to increasing the induced interference between the filtered subcarriers inside the channel. However, in the OGFDM system, such an issue can be accommodated by employing the double oversampling mode where a steady acceptable level of the BW efficiency is demonstrated for all possible values of the roll-off ( $0 \leq \alpha \leq 1$ ). It's worth noting that, even with halving the obtainable BW in the double oversampling process, the BW efficiency rates for a diverse range of the roll-off values (good

and bad) are decreased by around 40% rather than 50%. This is mainly achieved due to the cancelled interference between contiguous filters, which in turn, increase the achieved BW efficiency from 50% to about 60% for the same SNR limit. Therefore, as the efficiency of the BW is principally depending on two significant parameters (BW and SNR), about 10% additional enhancement is realized due to the SNR improvement.

Comparing with the normal oversampling where the rates of the BW efficiency are reduced by around 85% at worst filter conditions, the introduced double oversampling can come up a better BW employment, particularly, for the roll-off value between 0.5 and 1. This fundamentally occurs because of the double oversampling that can challenge the overstated interference between neighbouring filters in the bad transmission conditions.

In this wireless transmission system, the recorded rates of the BW efficiency for both the double and normal oversampling are calculated relative to the best BW efficiency of the normal oversampling where SNR equals 23 dB and the roll-off factor is equivalent to 0.1. Besides, the terms NOV and DOV are used in the figures to indicate the normal and double oversampling respectively.

### **3.3 Modulation Level**

#### **3.3.1 Introduction**

Increased demand for the high transmission rate in the future mobile applications makes researchers concentrate mostly on evolving the efficiency of the offered BW. As such, to cope with the speedy alteration of the traffic pattern services, the mobile communications performance, particularly, the channel capacity, must be developed in the next wireless access networks (Liu and Jiang, 2016). Despite the rapid evolution in the digital signal processing domain, the optimization problem of the transmission techniques, especially, that are related fundamentally to the waveform performance is yet in a progress (Hazareena, 2018). Thus, considering the CP-OFDM downsides (Schaich *et al.*, 2014), alternative waveforms as the FBMC (Kim *et al.*, 2018), the UFMC (Saad, Al-ghouwayel and Hijazi, 2018), the F-OFDM (Shuqi, Xin and Yongqiang, 2018), and the GFDM (Jorswieck, 2018) were introduced for investigation by the 5G air interface experts. Recently, a new introduced waveform termed OGFDM (Kadhum *et al.*, 2018), (Kadhum, Kanakis and Crockett, 2019b) was introduced with a single and couple frequency carriers offering additional sustenance to the channel capacity

of the future mobile communications. The developed OGFDM has supported the transmission bit-rate on both the filtration and oversampling stages.

To extra improve the BW efficiency on the modulation stage, an advanced approach called dynamic bit loading (DBL) is presented herein for quadrable frequency carriers of the OGFDM. The introduced handling aims mainly to employ the flexible modulation instead of the fixed one, hence, apply a hybrid modulation scheme can merge various types of formats in one normalized modulation process. Accordingly, diverse shapes of the modulation can be adaptively assigned for different frequency subcarriers, which in turn, switch the modulation process from the static case towards a scalable, and dynamic state (Yu, 2011).

Depending on this kind of the modulation, each frequency subcarrier is variously reassigned by allocating dynamically different schemes of the modulation to be compatible with the transmission circumstances (Junhui, Guan and Gong, 2011). That's means, for a diverse range of the transmission situations (good & bad), a suitable modulation shape is adaptively allocated for maintaining a maximum bit-rate with the applied waveform. By exploiting the subcarrier power variance, different levels of transmission boost can be obtained in the frequency domain, which in turns, can optimally update the propagation system performance of the DBL system (Hao, Hongwen and Jun, 2012).

The adaptive modulation is principally utilized with the future networks, since the fixed modulation that is used with the traditional communication system, is not perfectly suitable to the progressive applications where bit-rate needs always to be maximized (Hazareena, 2018). Therefore, with the uniform modulation, the system performance in terms of the channel capacity is entirely restricted to the worse propagation case while only the BER is improved with the enhanced channel circumstance (Tarchi, Corazza and Vanelli-coralli, 2013). Hence, the upcoming mobile generation tends fundamentally to employ the resilient modulation due to its ability to bend with the realistic conditions rather than the specific modulation that is basically assigned just for the worst spread situation (Al-mawali *et al.*, 2011).

With the DBL system, the high modulation format is specified for the powerful frequency subcarrier which physically has a higher ability to carry extra bits than others (Torrea-duran *et al.*, 2012). Therefore, assuming the propagation states of all subscribers are known by the base station, the employed wireless air interface with the DBL system can efficiently decide the sample size of each used frequency subcarrier. Subsequently, the maximum channel

capacity at the acceptable BER limit can be gained with the best condition carrier where the highest modulation format is supplied in accordance with the signal strength (Ding, Wang and Yang, 2016). As a result, the newly introduced DBL can be exploited for enhancing the channel capacity of future mobile technology where a more accurate bit loading scheme and a better BW usage than the traditional way are required. However, the irregular modulation system causes in the constellation map power diversity, this, nevertheless, can be addressed by utilizing the normalization process (Kim *et al.*, 2014).

Regarding the simulation tools, the MATLAB and Visio software applications are utilized to validate and demonstrate graphically the achieved results. The rest of this part (modulation level) is organized as follows: Section 3.3.2 demonstrates the DBL system model of the OGFDM transceiver. Section 3.3.3 for the simulation work including the results and discussion.

### **3.3.2 System Model**

To mitigate the key downside of the traditional bit loading scheme at variant channel conditions, the dynamic bit loading is alternatively utilized with the OGFDM system where the adaptive handling can increase the aggregated channel capacity at the acceptable error limit.

As is clear in Figure 3.3.1, on the transmitter side, the multi-level modulation system is introduced as a replacement for the flat one. By accommodating different sample sizes for each applied frequency subcarrier, various constellation tables can be presented. As such, a varied range of modulation formats is offered adaptively for every employed frequency subcarrier. Consequently, with flexible modulation, the specified number of bits can potentially be increased for each complex number in the frequency domain. Due to improving the freedom level of the modulation, a better BW efficiency can be achieved which in turn, can improve the overall transmission bit-rate in accordance with the adaptable modulation format. This, nevertheless, can cause an irregular constellation table power, hence, differ limits of power average are assigned for each dynamic Gray mapping. However, by exploiting the normalization operation, the average energy of the collective mapping is unified to one. It's worth pointing that, all bit loading managements for both the transmitter and receiver are combined in the DBL level of the OGFDM where a generated complex number is

corresponding to a sample and a set of samples with a determined length is equivalent to one symbol in the time domain.

Subsequently, by adopting an appropriate factor of oversampling ( $OV = K$  or  $2K$ ) the normalized frequency subcarrier is up-sampled via inserting ( $OV - 1$ ) null samples (zeroes) between every two successive original samples. The up-sampled frequency subcarrier is then convoluted by utilizing one of cosine/sine shaping filters (Hilbert pair) constructing orthogonally a filtered frequency subcarrier. Hence, the shaped frequency subcarriers are multiplexed together into the available BW depending on the employed digital filters. By using the electrical adder, the passed samples of the utilized frequency subcarriers are combined in one data stream (digital signal). Ultimately, the DAC is used outputting the analog signal in the transmission mode. The obtained signal that is exponentially represented as  $(e^{j2\pi fct})$  is spread by the supplied antenna.

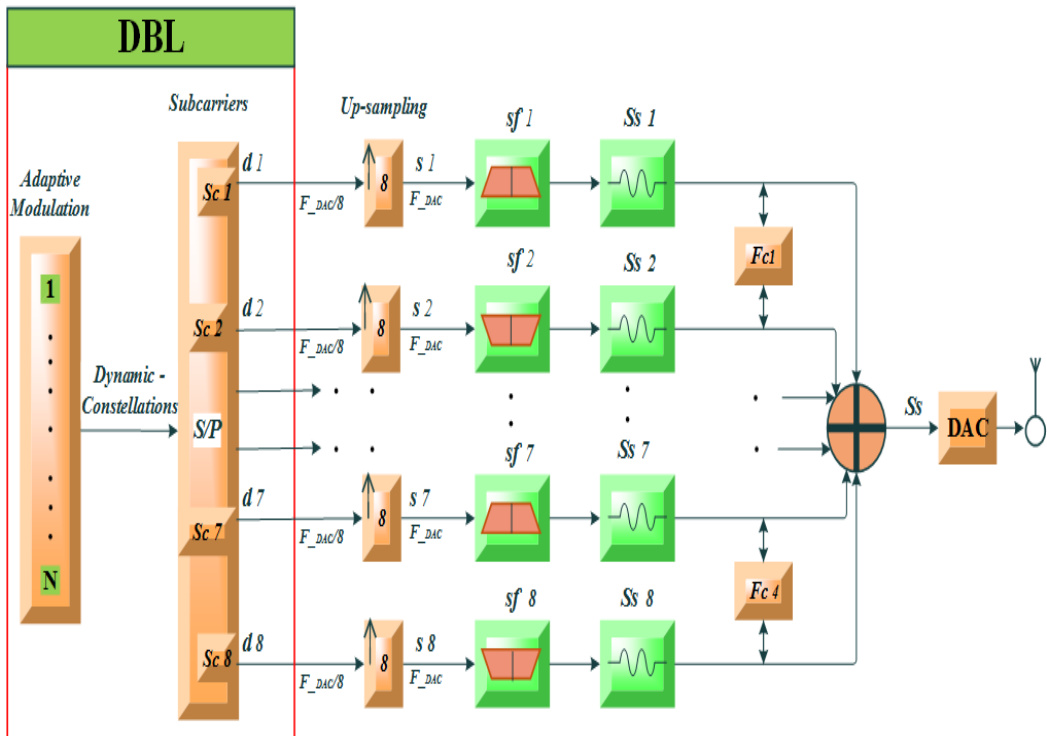


Figure 3.3.1: DBL system for the transmitter side of the quadruple carriers OGFDM (Kadhum, Kanakis and Crockett, 2019a).

As is seen in Figure 3.3.2, on the receiver side, the sensed signal at the antenna side is dispatched to the ADC. Consequently, to retrieve the original data of the transmission, inverse processing is perfectly applied. By distributing the digital signal into different frequency subcarriers, each pair of the orthogonal frequency subcarriers are distinguished via its identical

frequency centre. Then, exploiting the key features of matching filters (Hilbert pairs), the previously convoluted frequency subcarriers are extracted, where each matching process should be compatible with its corresponding shaping process. The de-multiplexed frequency subcarriers are subsequently down-sampled by a factor of oversampling ( $OV = K$  or  $2K$ ), which in turn eliminates the formerly added ( $OV - 1$ ) zero samples between every two neighbouring samples. It's worth noting that each received sample is represented as a complex number in the frequency domain.

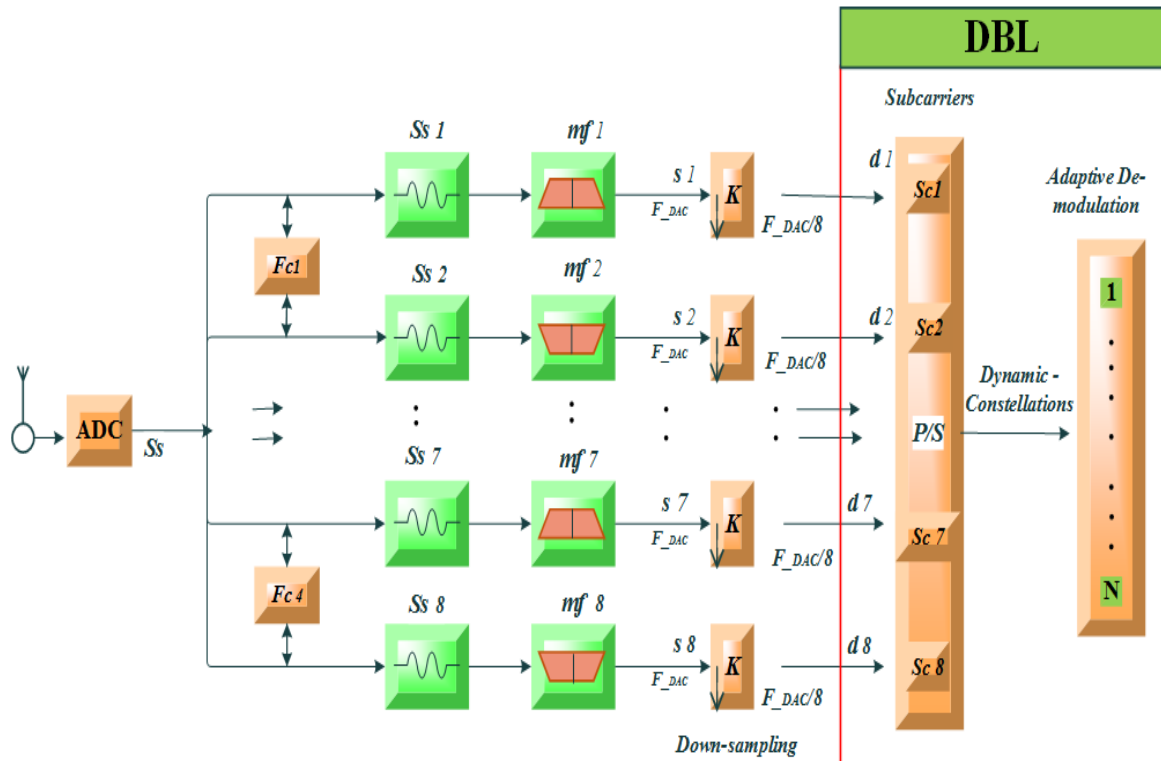


Figure 3.3.2: DBL system for the receiver side of the quadruple carriers OGFDM (Kadhum, Kanakis and Crockett, 2019a).

Since the introduced design of the OGFDM comes up with adopting the DBL scheme at the modulation stage, a resilient de-modulation system is utilized to adaptively transform the obtained complex numbers into binary digits. As such, by following the transmission conditions, the most common de-modulation formats can be used dynamically with functional frequency subcarriers. Hence, multi-levels of the de-modulation operation can be realized relative to the diversity circumstance of frequency subcarriers. However, due to different levels of power consumption with the frequency subcarriers at variant channel state, unstable average power can be recorded for the receiver constellation tables. Nevertheless, by adopting the normalization process, a uniform level of the Gray mapping power can be achieved. At

the end of this hybrid de-modulation format, every complex number is converted dynamically back to the binary digit domain, where bit token size (N) can mainly identify the order of the applied modulation/de-modulation shape for the received frequency subcarrier. The principal idea of this improved system is employing the DBL scheme at the modulation /de-modulation process where different kinds of the modulation formats are combined adaptively.

Consequently, the main mathematical operations that are directly related to the modulation level, are considered herein. Through the modulation stage, each fixed-size stream of the binary digits is transformed into a compatible form of the complex number that can be described in the Cartesian domain as following (Barry, Lee and Messerschmitt, 2004):

$$C_i = I_i + jQ_i \quad (1)$$

where  $I_i$  and  $Q_i$  signifies the real and imaginary components of the  $i^{th}$  complex number, and  $j = \sqrt{-1}$ .

Accordingly, the amplitude value ( $M$ ) of each employed complex number is expressed as following (Alexander and Pouliakas, 1999):

$$M_i = \sqrt{I_i^2 + Q_i^2} \quad (2)$$

In addition, the applied phase / theta ( $\Theta$ ) of the transmitted complex number that resulted from employing the imaginary component ( $Q_i$ ) and the real component ( $I_i$ ) is obtained as following (Alexander and Pouliakas, 1999):

$$\Theta_i = \tan^{-1} = \frac{Q_i}{I_i} \quad (3)$$

Despite that both the amplitude and phase are calculated depending on the Cartesian formula of the complex number, other mathematical operations like multiplication and division of the complex number are still hardly achieved by this kind of representation. To solve this issue, another form can be used (Polar form) to attain easily both the multiplication and division of the complex number. The applied formula of the complex number in the Polar domain is expressed as following (Barry, Lee and Messerschmitt, 2004):

$$C = Ae^{j\Theta} \quad (4)$$

At the acceptable limit of the BER, the transmission system performance in terms of the maximum bit-rate ( $Br$ ), is obtained as following (Im *et al.*, 1995):

$$Br = BW * \log_2(1 + SNR). \quad (5)$$

The relation between the power the received signal ( $P_R$ ) to the noise power of the undesirable signal ( $P_N$ ) is expressed as following (Im *et al.*, 1995):

$$SNR = P_R/P_N \quad (6)$$

As a result, in terms of improved channel capacity, the DBL system, particularly with the enhancement power cases, can be more suitable to the dynamic SNR range than the fixed modulation formats that are mainly applied for the worst channel condition with a static SNR case. The signal at the receiver side  $R$  which is composed of the signal of transmitter  $T$  multiplied by the channel response  $E=1$  and added to  $N$  that indicates the AWGN, is expressed as following (Ghogho *et al.*, 2005):

$$R = ET + N \quad (7)$$

It's worth noting that, the performance of the transmission can be basically regulated employing the relationship between the power constriction and normalized signal power as following (Ghogho *et al.*, 2005):

$$\frac{1}{L} \sum_{i=1}^L M_i^2 \leq P_R \quad (8)$$

where  $P_R$  refers to the maximum assigned power for  $L$  transmitted samples at the receiver.

In presence of the channel response  $E \neq 1$ , wireless channel frequency response shows changes in phase and amplitude of frequency subcarriers. Hence, the received frequency subcarriers are no longer good representatives of the transmitted frequency subcarriers unless further actions are applied. To manipulate these issues two important steps should be taken into consideration. Firstly, using the inverse of the channel response to eliminate the effect of the channel. Secondly, by averaging the received pilots over  $m$  transmitted samples per each frequency subcarrier to reduce the noise of signal and then to recover the signal itself. For channel response elimination, the response in the receiver has to be inverted (Ghogho *et al.*,

2005). This is usually known as a zero forcing equalization which can be achieved by estimating Channel Transfer Function (CTF). To perform the equalization per frequency subcarrier in a simple way, the CTF, amplitude and phase of each frequency subcarrier at the corresponding frequency need to be known. To calculate the CTF of each frequency subcarrier in the frequency domain, training samples  $T_i$  are transmitted periodically with recognized magnitude and phase as following (Yang *et al.*, 2009):

$$T_i = I_i * e^{j\phi_i} \quad (9)$$

where  $I_i$  and  $\phi_i$  represents the amplitude and phase of the  $i^{\text{th}}$  transmitted sample respectively. The equivalent received training samples  $R_i$  is expressed as following (Yang *et al.*, 2009):

$$R_i = J_i * e^{j\bar{\phi}_i} + N_i \quad (10)$$

where  $J_i$  and  $\bar{\phi}_i$  represent the amplitude and phase of the  $i^{\text{th}}$  received sample respectively and  $N_i$  is the  $i^{\text{th}}$  sample noise.

By making use of the identified transmitted training samples and the received training samples, the CTF in frequency domain  $E_i$  can be determined as following (Yang *et al.*, 2009):

$$E_i = \frac{R_i - N_i}{T_i} \quad (11)$$

Thus, the estimated CTF can be explained as following:

$$\hat{E}_i = \frac{R_i}{T_i} = E_i + \frac{N_i}{T_i} \quad (12)$$

According to equation (12), large magnitudes of the transmitted training samples can reduce the influence of the overall signal noise power in the channel, thus, good amplifiers at the transmitter side help protect training samples from distortion by distance. For more signal noise reduction, the average of the predictable CTF can be calculated over number of training samples to get static changes in amplitude and phase for the corresponding samples. Each complex value of the  $i^{\text{th}}$  received sample in frequency domain  $V'_i$  is equalized via multiplying by the inverse of the estimated CTF,  $\hat{E}_i^{-1}$  (Yang *et al.*, 2009):

$$V''_i = \hat{E}_i^{-1} * V'_i \quad (13)$$

### 3.3.3 Experimental Results

In this experimental work, a numerical simulation is mainly applied in the physical layer of an electrical back-to-back wireless system to highlight the key impact of utilizing the proposed DBL on the transmission performance of both the channel capacity and BER of the OGFDM. The transmission performance (channel capacity & BER) of the presented system is studied under the specified condition of Table 3.3.1. Besides, MATLAB tools that were mentioned in section 3.1.3 are utilized to represent the obtained results graphically.

Table 3.3.1: System parameters for the quadruple carriers OGFDM

Parameter	Value
No. of frequency centres	4
Number of subcarriers	8
System mode	Quadruple carriers
$F_{DAC/ADC}$	2 GHz
SNR	Static & Dynamic
Modulation format	Fixed & Adaptive
Filter type	Hilbert filter

As is seen in Figure 3.3.3, the possibly enhanced SNR that essentially comes from the improved case of the transmission channel can be optimally exploited in the DBL system. Consequently, using the adaptive modulation, the vital spots of the dynamic SNR range can mainly be presented for every two contiguous formats of the fixed modulation. Therefore, considering the minimum levels of the needed SNR for two suggested shapes of the higher modulation, various thresholds of the obtainable power are manipulated independently. As a result, to investigate the effect of utilizing a flexible modulation scheme on the BW efficiency, three key regions are decided, according to the channel transmission conditions, between the two fixed modulation 128 and 256 QAM with SNR levels equals to 23 dB and 26 dB respectively.

With respect to the first one of the three selected areas that is called as Low Boost (LB) area, the desired SNR threshold is located between the first threshold of the 128 QAM and the middle point of both adopted formats of modulation. Thus, the LB point SNR is recorded a higher than the 128 QAM, about 24.3 dB, but a lower than the central between the 128 and 256 QAM. As a result, the promoted SNR of this case comes up with a slight growth in the

bit-rate due to the increased ability for a quarter of the frequency subcarriers to transmit additional bits. In terms of Bit Loading Map (BLM) scenarios, the explored LB area can come from diverse arrangements of bits distribution depending on the improvement ratio in bits loading of the applied frequency subcarriers. For instance, with eight frequency subcarriers, the BLM can be equivalent to one of the following arrays, [7,7,7,8,8,7,7,7], [7,7,8,7,7,8,7,7], [7,7,7,7,7,7,8,8], etc., where the enhancement rate of the channel capacity equals to 25%.

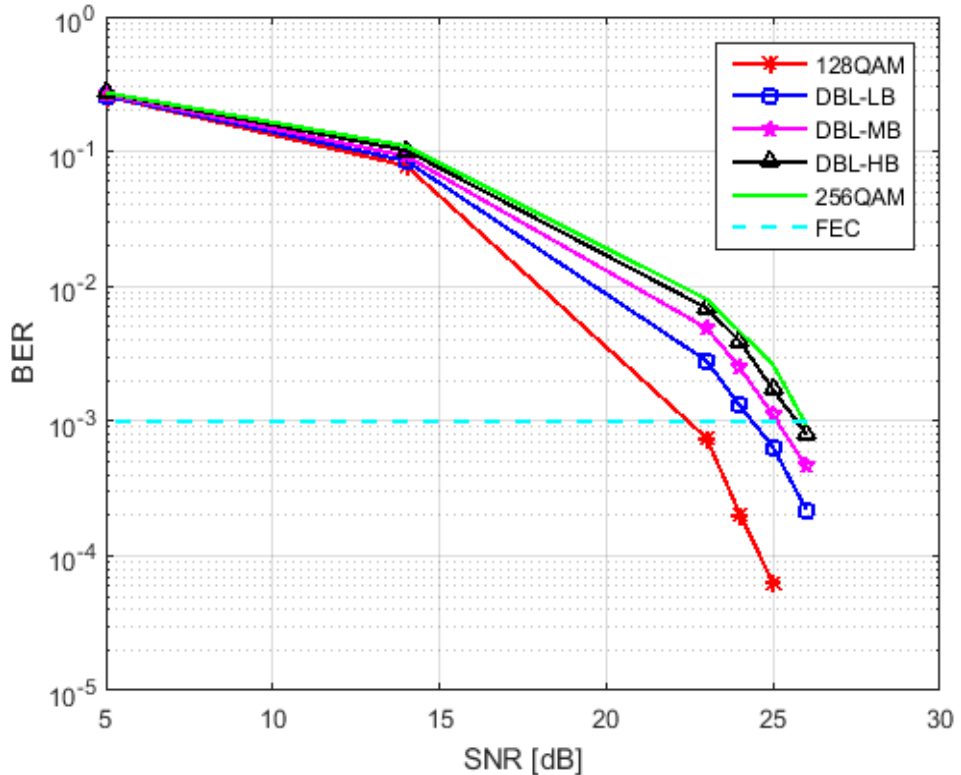


Figure 3.3.3: Apply the DBL system for induced SNR between two successive modulation formats (Kadhum, Kanakis and Crockett, 2019a).

With reference to the second tested area that is termed as Medium Boost (MB), the applicable threshold of the SNR is recorded herein higher than the middle distance between the threshold of the first modulation (128 QAM) and the second one (256 QAM). Thus, around 25.1 dB is registered for the supportive SNR of the MB case with the two adjacent formats of the higher modulation. This, as a result, leads to rising the gained level of the bit-rate due to amending the transmit capability for half of the employed frequency subcarriers. Therefore, the attained BLM of this state where 50% of the frequency subcarriers are stimulated to carry extra bits, can be constructed in one of the following styles, [8,7,8,7,8,7,8,7], [7,7,7,7,8,8,8,8], [7,8,7,8,7,8,7,8], etc. Consequently, the achieved channel capacity of this

case is larger than the LB case since the number of promoted subcarriers is higher than the first boost.

Concerning the third experienced area which is known as High Boost (HB), the valid SNR threshold of this saturated case is registered close to the second specified threshold of the fixed modulation (256 QAM) since the channel circumstance is extremely improved reaching about 25.6 dB at the acceptable limit of the BER. Accordingly, in comparison with other previously declared areas (MB, LB), the best bit-rate can be gained at this stage (HB) since the bit loading improvement can cover three-quarters of the functional subcarriers. Therefore, the organized BLM for this progressive case where 75% of the applied frequency subcarriers are able to hold more bits, can be arranged in one of the following collections, [8,8,8,8,8,7,7,8], [8,8,8,8,7,7,8,8], [7,7,8,8,8,8,8,8], etc. It's worth pointing that, all the three mentioned cases (HB, MB, LB) are obtained from the enhanced conditions of the channel status which in turn promotes the SNR thresholds between two bounded modulation formats.

As is clear in Figure 3.3.4, to clarify the variation of the maximum bit-rate of transmission for improved stages of the channel circumstance, three main channel capacities are experimentally investigated with the DBL system. Therefore, in accordance with the strength grade of the channel circumstance, the realized channel capacities between the two employed shapes of the fixed modulation (128 and 256 QAM) are diverse from the low increment (LB) with 7.25 Gb/s, to the medium increment (MB) with 7.5 Gb/s and to the high increment (HB) with 7.75 Gb/s.

This, as such, is gained since the elevated level of the SNR can give more support to promoting the channel capacity than the BER performance. Thus, for a dynamic gain of transmission, the developed SNR can increase only the maximum bit-rate between the two successive modulations yet keeping a steady level of the BER at  $10^{-3}$ . As a result, apart from the worst condition of the channel, the updated channel capacities with the DBL technique can outweigh the registered channel capacity of the first threshold term in the dynamic SNR range. Hence, compared to the fixed modulation system, the improved channel capacities of the DBL scheme can be upgraded in correspondence with the variable channel status. Consequently, in contrast with the fixed modulation, the channel capacity of the transmission can be maximized up to around 114% of the original maximum bit-rate yet sustaining a similar level of the acceptable BER.

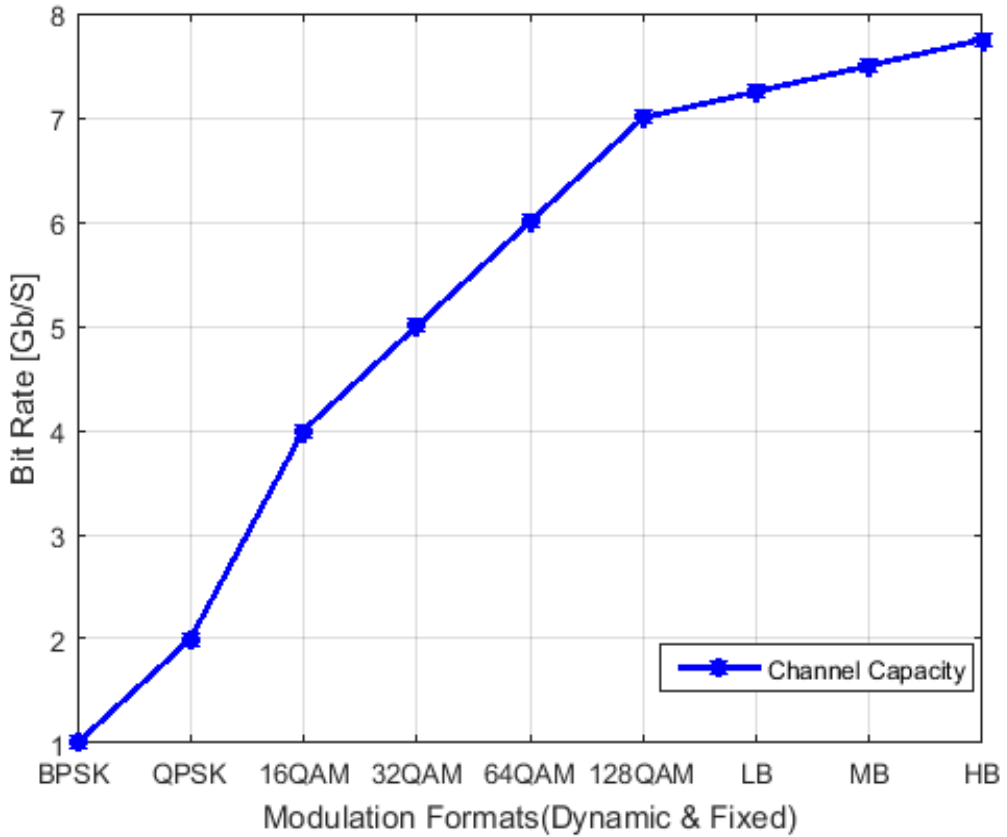


Figure 3.3.4. Maximising achieved bit-rate with the DBL system (Kadhum, Kanakis and Crockett, 2019a).

### 3.4 Summary

In this chapter, the three levels of OGFDM processing are introduced. The first level is the filtration processing that is introduced for a single frequency centre of the OGFDM. The experiment showed 2 dB gain between the channel capacity of the OGFDM and GFDM, hence, 8 Gb/s and 4 Gb/s are recorded for the OGFDM and GFDM respectively at sampling frequency equals to 2 GHz and modulation format is equivalent to 256 QAM. The doubled channel capacity resulted from utilizing the orthogonal filters (Hilbert) instead of the non-orthogonal one (RRC). In addition, a similar BER performance for both the GFDM and OGFDM at the same limits of the SNR are demonstrated. The second level is the oversampling processing that is introduced for a couple carrier system of the OGFDM. The findings showed that with the normal oversampling at 2 GHz sampling frequency and enlarged roll-off factor ( $0.5 \leq \alpha \leq 1$ ), the overall channel capacity is reduced more sharply. However, by employing the double oversampling, the overall channel capacity is improved by about 4 times due to avoiding the unwanted increment of the roll-off value. On the other hand, the roll-off values between 0 and 0.3 at the double oversampling mode (halved filter BW) causes in degrading the channel capacity in contrast with the normal oversampling. As a result, the hybrid solution

that combines both normal and double oversampling is recommended for better channel capacity. The third level is the modulation processing that is introduced for a quadruple carrier system of the OGFDM. The experimented work showed that by utilizing a flexible modulation scheme for two adjacent fixed modulation formats like (128QAM & 256QAM), three main thresholds (low, medium, high) can be invested for the dynamic SNR range. As such, apart from the worst status of the transmission, the gained channel capacities of the adaptive allocation far outweigh the obtained level of the fixed modulation. To extra support the system model description, the Visio application is used for drawing figures. In addition, the MATLAB simulation is utilized to validate the results and represent them graphically. The main parts of this chapter were published in (Kadhum et al., 2018), (Kadhum, Kanakis, and Crockett, 2019b), and (Kadhum, Kanakis, and Crockett, 2019a).

# **Chapter 4: Multi-Carrier Stages of OGFDM Waveform**

## **4.1 Preliminary Stage**

### **4.1.1 Introduction**

The future generations of mobile networks target extensively satisfying the accelerated and exceptional development of upcoming cellular applications (Breandán *et al.*, 2018). As such, the significant scenarios of the predicted wireless networks as the Bit-pipe Communication (Borkar and Pande, 2016), Machine Type Communication (Li *et al.*, 2017), Tactile Internet (Simsek *et al.*, 2016) and Wireless Regional Area Network (Agiwal, Roy and Saxena, 2016) have been explored by the wireless research community. Unfortunately, due to key technical issues with the current 4G waveform like wasted BW of the cyclic prefix, sensitivity to the frequency offset, and the OOB emission, the presently used CP-OFDM cannot be able to attain the expected necessities of the modern mobile market (Hazareena, 2018).

As a result, advanced research studies have introduced alternative waveforms that were evolved from the conventional CP-OFDM (Hwang *et al.*, 2009) to new filtered waveforms as the FBMC, the UFMC, the F-OFDM, and the GFDM. Accordingly, the sophisticated age of the mobile generations can be known as a “*filtration era*”. For more explanation, waveform developers have pursued to perform the digital filtration on various levels of frequency subcarrier arrangement. Therefore, the filtration can be applied for orthogonal frequency subcarrier like in the FBMC (He *et al.*, 2018), or for uniformed size group of orthogonal frequency subcarriers like in the UFMC (Teja, 2018), or for irregular size group of orthogonal frequency subcarriers like in the F-OFDM (Shuqi, Xin and Yongqiang, 2018). Furthermore, because of the confliction between digital filters and the orthogonal frequency subcarriers, the filtrating process is achieved for non-orthogonal frequency subcarrier as in the GFDM that has been considered as the 5G waveform of mobile (Jorswieck, 2018).

Nevertheless, due to removing the perpendicular multiplexing with the GFDM, recently, a novel technique of the transmission waveform named as single carrier OGFDM is proposed (Kadhum *et al.*, 2018). The newly presented waveform that fundamentally depends on the GFDM physical layer has obtained the orthogonality for the non-orthogonally filtered frequency subcarriers of the single carrier GFDM. Consequently, the digital orthogonal filters (Hilbert pair) have emerged as an influence addressing for the infected BW efficiency of the GFDM by realizing the orthogonality in the filtration stage rather than the subcarriers stage.

The main idea beyond this technology is changing the phase between the utilized filters that in turn keeps the applied filters working concurrently (Lu *et al.*, 2016). Due to applying the orthogonality, the frequency subcarriers of the new wireless mobile infrastructure are filtered in a dual way, hence, in comparison to the GFDM, the single carrier of the OGFDM can double the channel capacity of transmission (Kadhum *et al.*, 2018).

On the other hand, the single carrier scenario cannot be recommended for the higher wireless channel capacity of future mobile communication (Gb/s). The main reason beyond that is, the single carrier with a high transmission rate can be highly impacted by the ISI than the low bit-rate since the maximum expected delay of spread is higher than the specified time for each symbol duration. It's worth pointing that delay spread, which is defined as a dispersion in time which could cause a distortion of the spreading signal in the time domain, is responsible for any probable ISI. As such, the fading will be a frequency-selective when the delay spread is larger than the period of the symbol while a flat fading can be achieved when the delay spread is less than the symbol duration (Luo, 2013). Thus, the system performance in terms of the channel capacity and BER can be influenced by the utilized way of channel participation. From the frequency domain perspective, the frequency-selective fading is demonstrated when the channel BW is smaller than the signal BW. Thus, different signal frequencies can experience variant levels of fading. On the other hand, the flat fading can be obtained when the channel BW is larger than the signal BW, where signal frequencies can experience a similar amount of fading (Luo, 2013).

To mitigate such an issue, the multicarrier transmission is considered to improve the quality of service for developed generations of mobile (4G and beyond) (Agiwal, Roy and Saxena, 2016). Therefore, to avoid vulnerable transmission service that cannot stand against the ISI phenomena (bad quality of service), the multicarrier system is adopted with the developed mobile networks. It's worth pointing that, the ISI problem can be professionally solved by switching from the single to the multi-carrier transmission. The main idea beyond this kind of treatment is increasing the specified duration of the symbol and hence, reducing the impact of the ISI. Thus, by dividing the BW channel with a high data rate to a group of subcarriers with a low data rate, a larger symbol duration than the delay spread is mainly achieved. Consequently, by utilizing the multi-carrier system the channel is turned from the selective to the flat fading and then it can be estimated simply. Thus, an easier equalization is provided to decrease the impact of the ISI that, in turn, comes up with a simpler receiver approach.

Moreover, the remaining ISI is completely removed by depending on the time protection intervals. Therefore, optimized system performance can be gained for an increased number of frequency subcarriers that essentially able to cope up with a higher delay spread (Grover, 2013).

“As a result, to further broaden the range of waveform’s functionalities and its related applications, it is greatly beneficial if the single frequency carrier of the OGFDM is extra extended to the multiple frequency carriers of the OGFDM. Thus, an improved BW efficiency can be achieved herein with this proposed expansion” (Kadhum, 2019).

This, nevertheless, causes in escalating the induced interference level for the increased number of filtered frequency subcarriers. Therefore, depending on the transmission conditions, the wireless signal that progressively suffers from losing power experiences diverse range of attenuation (Kumar, Member and Parihar, 2018). As such, due to the declined level of the transmission power, the possibility of the interference occurrence is increased for the enlarged level of the rolled-off filters. (Kadhum, Kanakis and Crockett, 2019b). As a result, the trade-off relation between the filter roll-off factor and the aggregated channel capacity is investigated broadly herein to clarify optimally the system design guidelines under different wireless channel statuses.

To access the highest level of the BW efficiency, the adaptive modulation format is largely employed with the presented multi-carrier OGFDM system. Thus, depending on transmission circumstances, the same frequency subcarriers can potentially be reused in a more efficient than the conventional way(Kadhum, Kanakis and Crockett, 2019a).

In this part (preliminary stage), the new design of the OGFDM is basically achieved in the physical layer of the wireless transmission system. In addition, the performance in terms of the channel capacity and the BER is deliberated in an electrical back to-back system.

Regarding the simulation tools, the MATLAB and Visio software applications are utilized to validate and demonstrate graphically the achieved results. The rest of the part is planned as follows: Section 4.1.2 discusses the main concepts of the proposed system physically and mathematically. Section 4.1.3 evaluates the system performance utilizing a computer simulation.

#### 4.1.2 System Model

After the effective utilization of the orthogonal Hilbert filters with the single carrier system of the OGFDM (Kadhum *et al.*, 2018), the advanced Hilbert filters are principally employed herein for the multi-carrier system of the same waveform. The developed design of the OGFDM aims to introduce the orthogonality, avoid the internal interference, and maximize the gained bit-rate from the multi-carrier perspective. In comparison with the GFDM, the proposed scheme can improve the performance of transmission yet sustaining a similar computational complexity to the GFDM.

As is clear in Figure 4.1.1, in the transmitter side, particularly, at the modulation level of the multi-carrier OGFDM, the most common modulation shapes are employed adaptively for the applied frequency subcarriers where the bits loading operations are mainly managed.

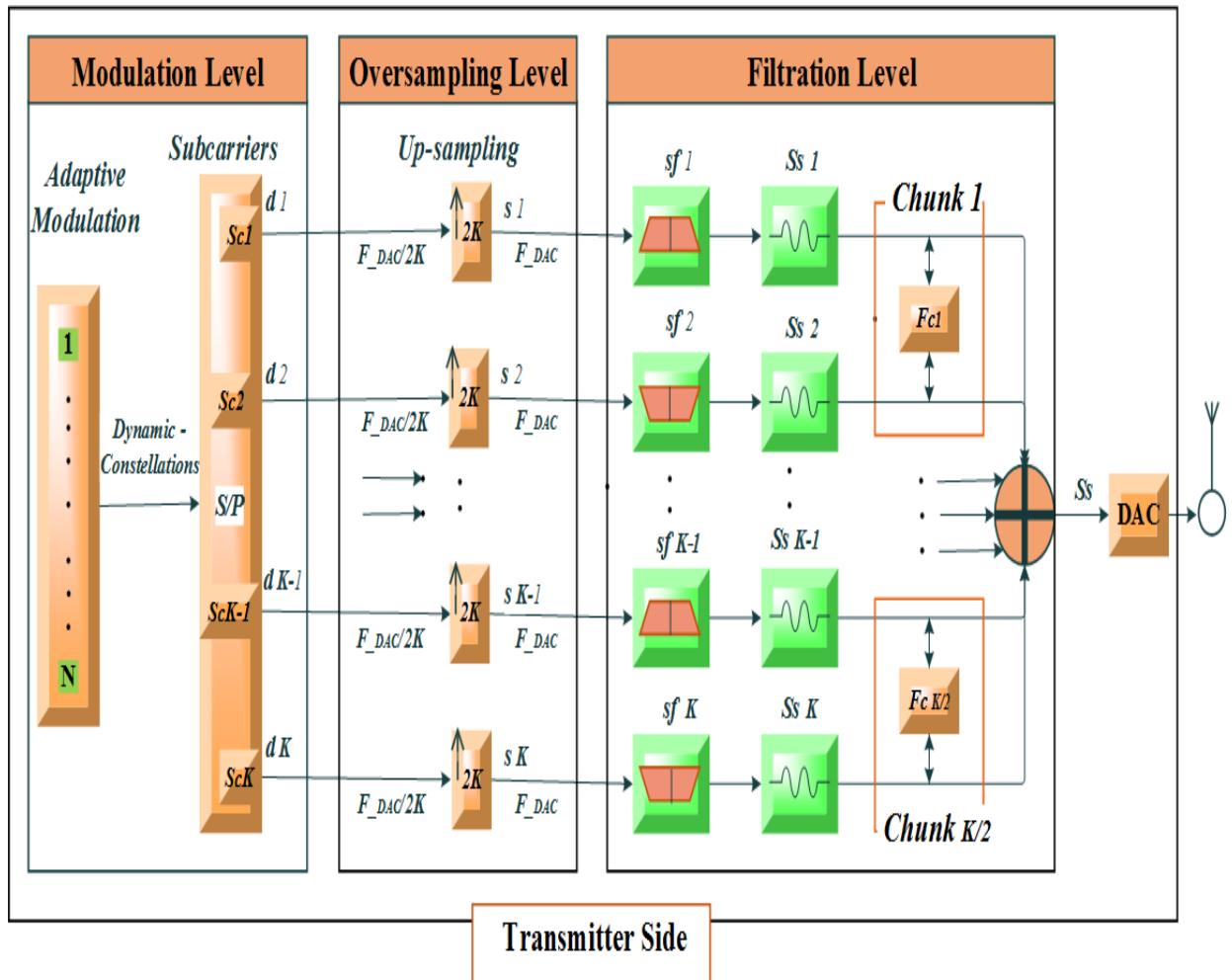


Figure 4.1.1: Wireless transmission system of the multi-carrier OGFDM (Kadhum, 2019).

Besides, depending on the different bit token size ( $N$ ) which is formerly allocated for each produced complex number, a various Gray map is presented. Consequently, with the improved channel condition, the hybrid format of the modulation can come up with a further number of bits which in turn can rise the BW efficiency. In addition, depending on the applied modulation types in the frequency domain, the consumption power of the frequency subcarriers is diverse. Nevertheless, this variation can be addressed by utilizing the normalization process where the average power of the constellation table is set to one.

At the oversampling level, where the sampling manipulation of the frequency subcarriers is performed, the oversampling factor is utilized to up-sampling appropriately the normalized subcarriers. Accordingly, the processed subcarriers are either sampled by a value of  $K$  or  $2K$ , where  $K$  represents the number of the employed subcarriers at the OGFDM system. That means, apart from the normal condition of the transmission where  $OV=K$ , the system, occasionally, needs to be up-sampled by a  $2K$  avoiding the undesirable statuses which are badly impacting the channel capacity.

At the filtration level where the shaping filters of the Hilbert pair are employed to filter the up-sampled subcarriers, each two successive frequency subcarriers are filtered and allocated orthogonally to an appropriate frequency centre. Therefore, in contrast to the GFDM, every centre of the frequency can concurrently accommodate two of the filtered subcarriers. This, as such, results in improving the BW efficiency of the promoted system due to the developed ability of the carrier to engage with a doubled number of the convoluted subcarriers for the same available BW.

After that, utilizing a suitable electrical adder, the filtered subcarriers are digitally combined in one stream of data. The DAC is used to convert the digital data sequence and pass them to the analog domain where the wireless signal is prepared for transmission by an antenna.

As is seen in Figure 4.1.2, in the receiver side, where reverse processes are principally executed to retrieve the main data, the ADC is used initially to digitize the received signal of the multicarrier OGFDM.

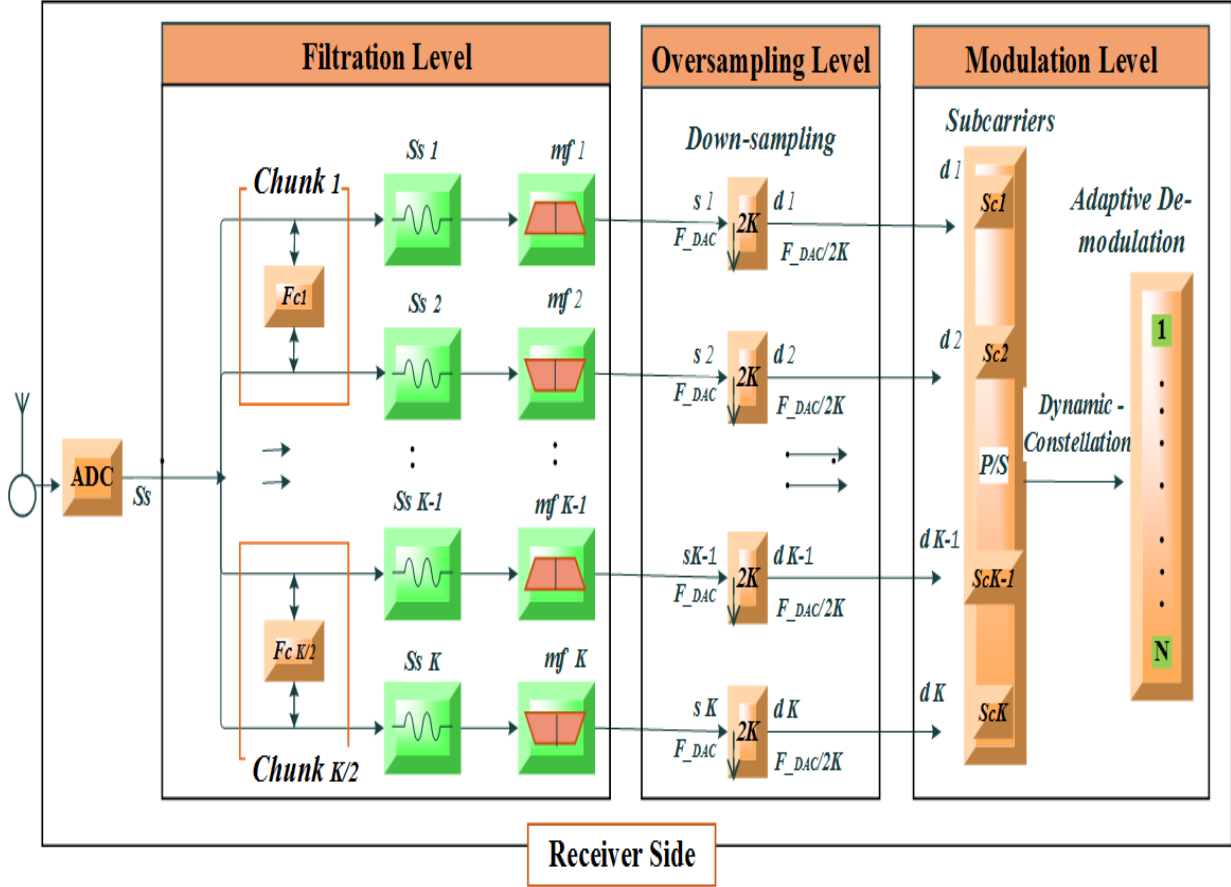


Figure 4.1.2: Wireless reception system of the multi-carrier OGFDM (Kadhum, 2019).

Then, at the filtration level, the matching filters are correspondingly applied for de-multiplexing the data stream on each used frequency centre. After that, at the oversampling level, the convoluted frequency subcarriers are fundamentally manipulated by down-sampling every applied subcarrier. Ultimately, at the modulation level, after passing through the de-normalization stage, variant formats of modulation appear for the utilized frequency subcarriers. Therefore, to dynamically translate the complex numbers into binary digits, the adaptive demodulation process is employed. From a mathematical viewpoint, the key components of the proposed multi-carrier system are expressed for both the transmitter and receiver sides.

On the transmitter side, where the Hilbert filters are utilized for the multi-carrier, the impulse responses of each  $h^h$  pair of shaping filters are represented as follows (Tao *et al.*, 2013):

$$\begin{aligned} Sf_h^A(t) &= g(t) \cos(2\pi f c_h t) \\ Sf_h^B(t) &= g(t) \sin(2\pi f c_h t) \end{aligned} \quad (1)$$

where  $f_{ch}$  signifies the frequency centre of the  $h^{th}$  Hilbert pair, and ( $1 \leq h \leq 8$ ).

In addition, the  $g(t)$  indicates the baseband pulse which is demonstrated as follows (Tao *et al.*, 2013):

$$g(t) = \frac{\sin[\pi(1 - \alpha)\Upsilon] + 4\alpha\Upsilon \cos[\pi(1 + \alpha)\Upsilon]}{\pi\Upsilon [1 - (4\alpha\Upsilon)^2]}, \quad \Upsilon = t/\Delta t, \quad (2)$$

At the receiver side, where the Hilbert filters are inversely employed for the multi-carrier, the impulse responses of each corresponding pair of the matching filters are expressed as follows (Tao *et al.*, 2013):

$$\begin{aligned} Mf_h^A(t) &= Sf_h^A(-t) \\ Mf_h^B(t) &= Sf_h^B(-t) \end{aligned} \quad (3)$$

To extract the intended signal, the convolution operation is performed between the shaping and matching filters as follows (Tao *et al.*, 2013):

$$Mf_j^C(t) \otimes Sf_i^D(t) = \begin{cases} \delta(t - t_0), & \text{if } C = D \text{ and } j = i \\ 0, & \text{if } C \neq D \text{ or } j \neq i \end{cases} \quad (4)$$

Presuming that the frequency sampling of both the ADC & DAC is identical, the frequency centre allocation of each Hilbert pair in the multi-carrier system is specified as follows:

$$f_{ch} = (2h - 1)(BW/K) \quad (5)$$

where,  $h$  represents the order of Hilbert pair for the utilized frequency centre and  $BW = F_{(DAC/ADC)}/2$ .

“Due to the optimal selection of every utilized frequency centre, the frequency responses of Hilbert filters are orthogonally accommodated and sequentially distributed in the spectral region of the available BW. It’s worth pointing that, the main problem that could be faced with the multi-carrier system is the intra-channel interference which essentially can degrade

the system performance. As a result, the relation between the frequency sampling of the employed subcarrier ( $Sub_S$ ) and the roll-off factor of the applied filter is significantly considered herein.

The impact of these two key factors on allocated BW of the filter ( $F_{BW}$ ) is expressed as follows" (Kadhum, 2019) (Kumar, Member and Parihar, 2018):

$$F_{BW} = Sub_S * (1 + \alpha) \quad (6)$$

where  $0 \leq \alpha \leq 1$ .

"It is shown from Figure 4.1.3 that with the normal oversampling ( $OV = K$ ), the interference between filtered subcarriers is decided depending on the value of the roll-off. Thus, for the ideal case system ( $\alpha = 0$ ), the allocated BW of each utilized filter is equal to the offered sampling rate of each employed subcarrier, hence, no interference occurs among adjacent filters.

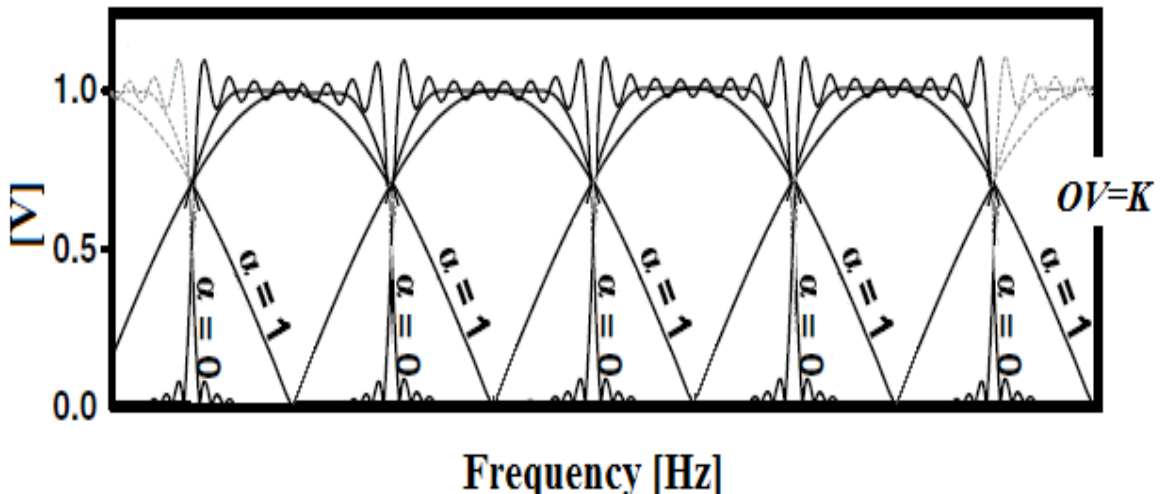


Figure 4.1.3: Normal case ( $OV=K$ ) (Kadhum, 2019).

On the other hand, for the worst situation ( $\alpha = 1$ ), the occupied size of each applied filter is doubled resulting in increasing the interference dramatically. This, as a result, comes up with escalating the level of the BER, hence, decrease the capacity of the channel at the acceptable level of error.

To address this issue, as is clear from Figure 4.1.4, the oversampling operation is reconfigured by doubling the number of generated copies for each employed subcarrier yet keeping the same allocation of the frequency centre. It worth noting that, the free band spaces which are

mainly created after doubling the  $OV$  can be considered as perfect guard areas for adjacent filters. Hence, free interference filters can be applied for the worst conditions. However, according to Shannon's theorem (Im *et al.*, 1995), the channel capacity is reduced due to the BW reduction in comparison to the best roll-off case of the normal oversampling as follows" (Kadhum, 2019):

$$\begin{aligned} Cap_{(Normal)} &= BW * \log_2(1 + SNR) \\ Cap_{(Double)} &= (BW/2) * \log_2(1 + SNR) \end{aligned} \quad (7)$$

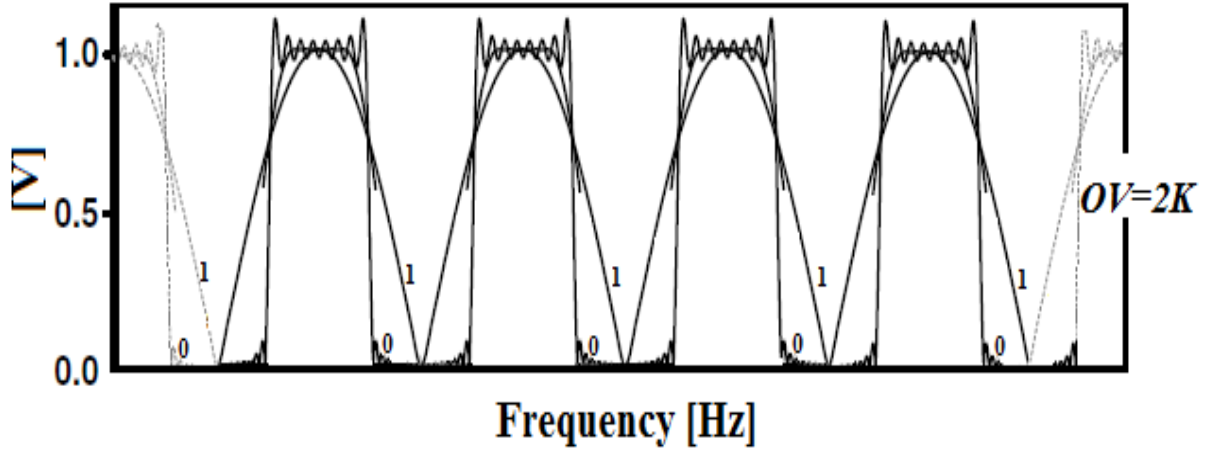


Figure 4.1.4: Double case ( $OV=2K$ ) (Kadhum, 2019).

### 4.1.3 Experimental Results

The performance features in terms of the channel capacity and BER are experimentally demonstrated herein. As such, a numerical simulation is widely undertaken in the physical layer of the proposed multicarrier system to evaluate the activity of the OGFDM waveform in an electrical back-to-back wireless transmission system. Unless explicitly stated, the applied value of the normal oversampling factor is considered in accordance with the assigned number of the utilized filters ( $OV=K$ ) which are equivalent herein to sixteen frequency subcarriers ( $K=16$ ). Since filter parameters like the coefficient number and roll-off factor can highly influence the overall system performance, the assigned values of those significant constraints are optimally managed to ensure the best channel capacity at the acceptable BER. Consequently, the effective value of the filter rolling is fixed initially at a roll-off factor equals to 0.1 and the taps number is equivalent to 32. Moreover, the adaptive modulation of the most common formats between the BPSK and the 256 QAM is utilized.

The key parameters of the experimented system are specified in Table 4.1.1. Besides, MATLAB tools that were mentioned in section 3.1.3 are utilized to represent the obtained results graphically.

Table 4.1.1: System parameters for the multi-carrier OGFDM

Parameter	Value
No. of frequency centres	8
$F_{DAC/ADC}$	4 GHz
SNR	23 dB
Roll-off	0 - 1
System mode	Multi-carrier
Number of subcarriers	16
Filter length	32
Spectral efficiency BW	1Hz
Oversampling	Normal & Double
Modulation format	Fixed & Adaptive
OGFDM symbols	2000
Filter type	Hilbert filter

As is seen from Figure 4.1.5 and Figure 4.1.6, the presented multi-carrier system aims to employ principally the whole BW rather than only a small piece of it as with the single carrier system. Hence, considering that the compared single carrier occupies partly the available BW, the introduced multi-carrier can give a great opportunity to utilize entirely the BW by supporting a set of frequency centres. Therefore, an extra BW efficiency is gained by evolving the OGFDM spectrum from one carrier concept to a regular group of carriers.

It is clear from Figure 4.1.7 that the achieved performance in terms of the channel capacity is greater with the multi-carrier OGFDM than the non-orthogonal GFDM due to the orthogonally exploiting of the developed Hilbert filters. As such, for a variant range of modulation formats, a stable 2 dB gain can be obtained between the channel capacity of the offered OGFDM and the GFDM. It's worth noting that, despite realizing a doubled channel capacity with the OGFDM, the acceptable level of the counted BER ( $10^{-3}$ ) under the AWGN is yet quite similar between the OGFDM and the GFDM. However, as the developed system tends to increase the number of the participated frequency centres for the same BW, the induced interference between the adjacent filters can occur mainly in the multi-carrier system.

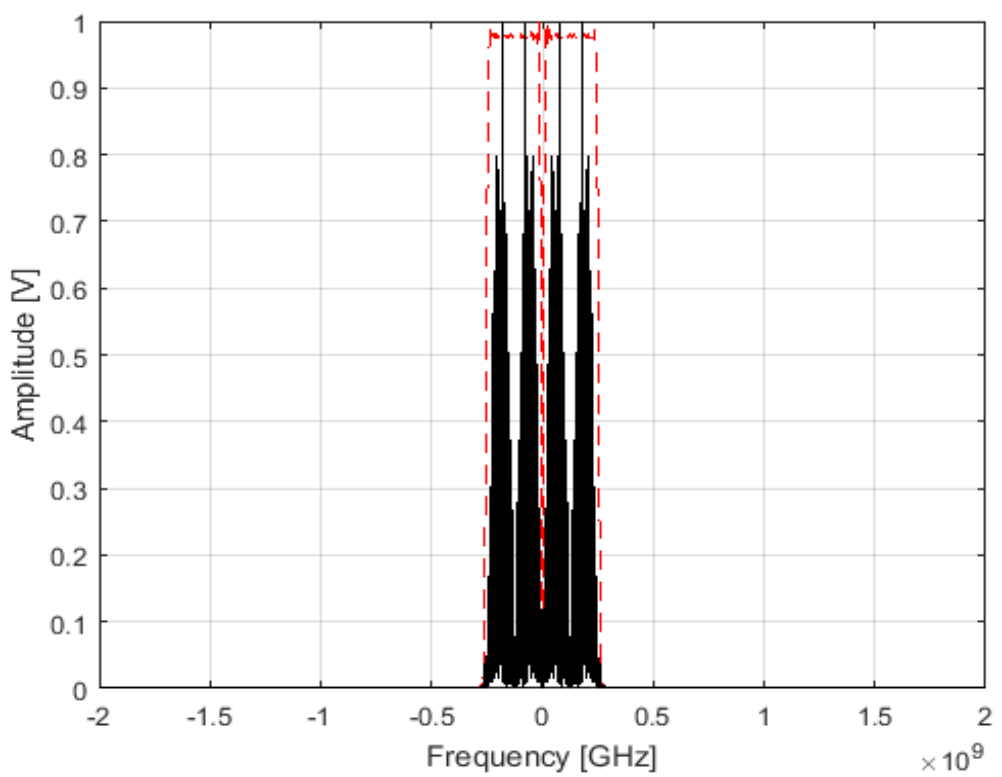


Figure 4.1.5: Transmission spectrum for a single carrier in the OGFDM system (Kadhum, 2019).

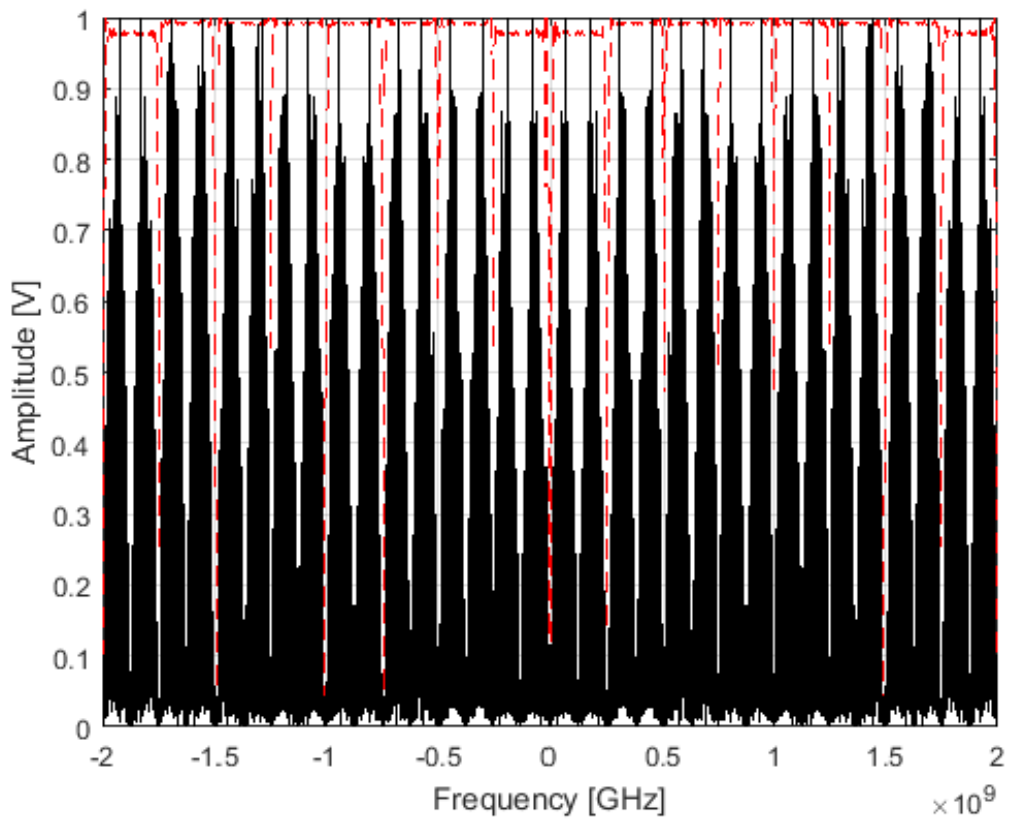


Figure 4.1.6: Transmission spectrum of the multi-carrier OGFDM (Kadhum, 2019).

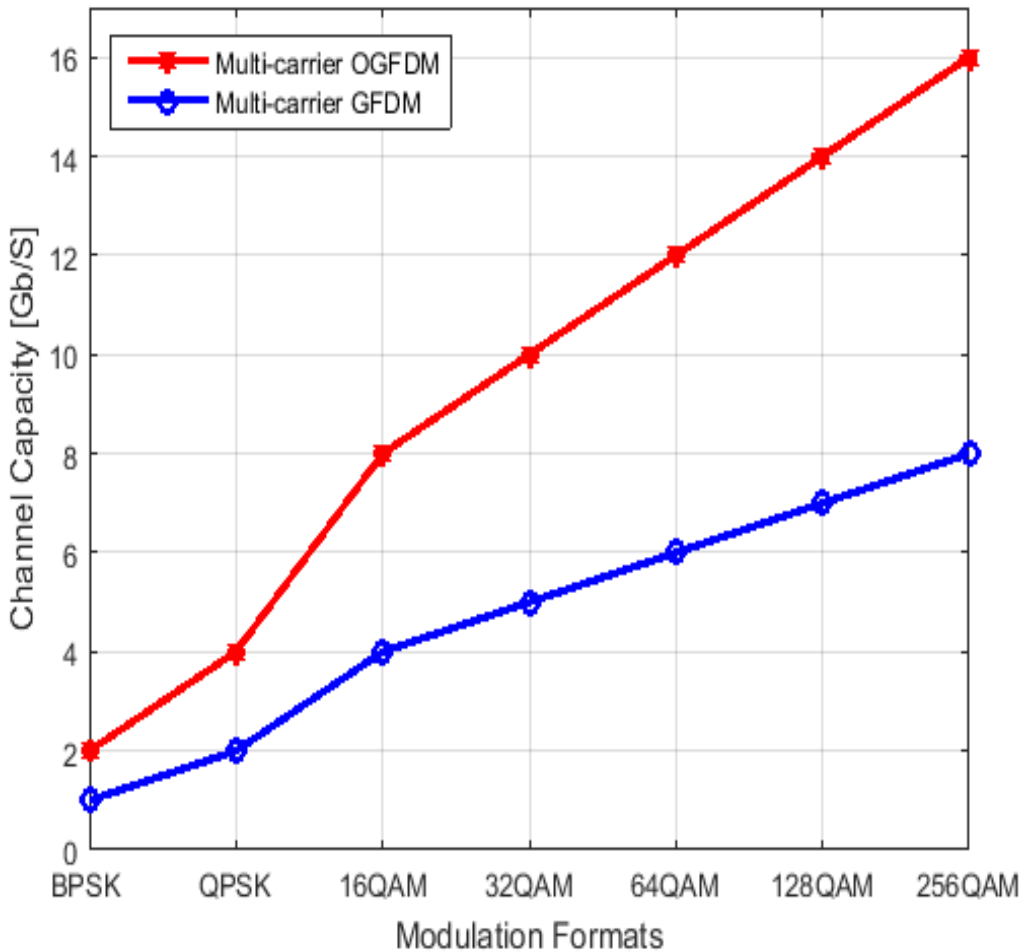


Figure 4.1.7: Channel capacity of the multi-carrier OGFDM vs GFDM. with  $F_{DAC} = 4$  GHz (Kadhum, 2019).

It is seen from Figure 4.1.8, that the interference can happen when the roll-off factor of the applied filter is gradually enlarged with the normal oversampling mode. Accordingly, the average rate of the error is relatively increased in accordance with the expanded interference between the adjacent filters that are working at the same SNR level. This, as such, causes in collapsing the capacity of the channel, particularly, with the poor transmission conditions where the roll-off factor of the same filters type (In-phase / Out-phase) can be allocated between 0.5 and 1 ( $0.5 \leq \alpha \leq 1$ ). Hence, the raised grades of the filter rolling value can play a big role in exaggerating the calculated BER which in turn can negatively impact the maximum obtained bit-rate of the transmission.

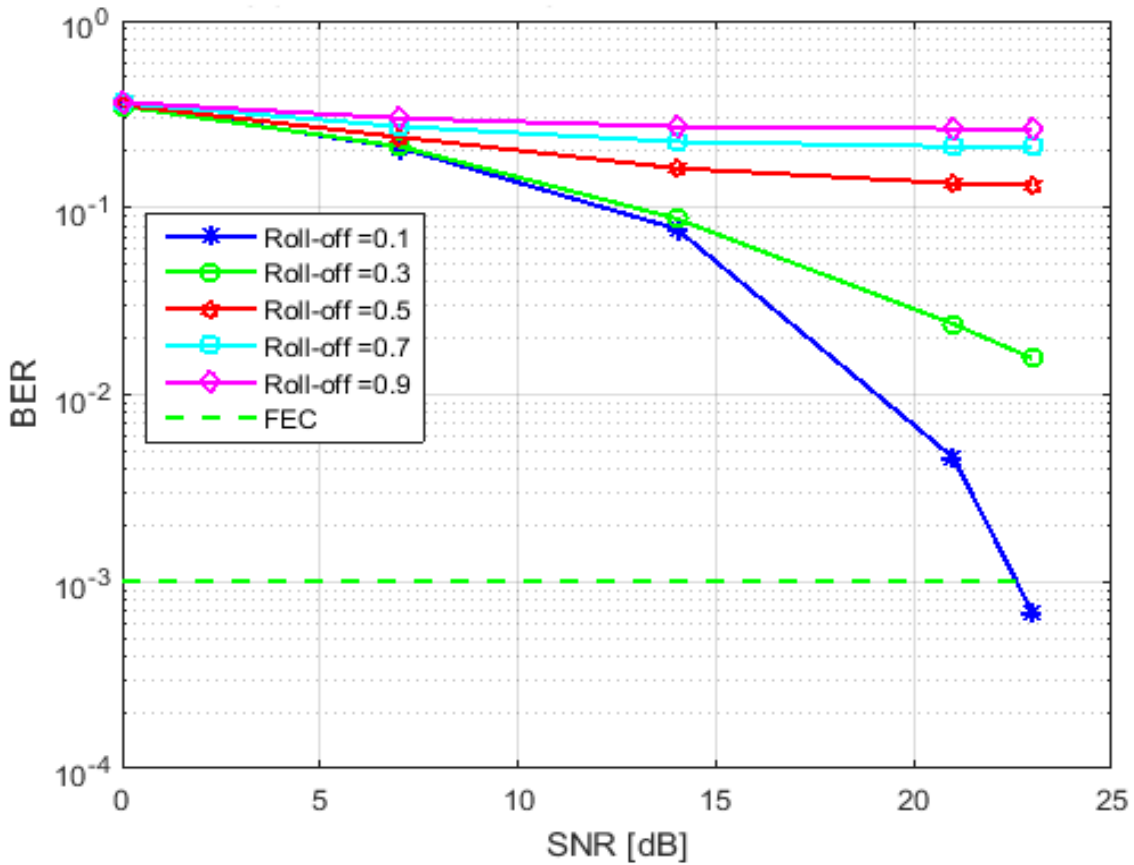


Figure 4.1.8: BER of variant roll-off factor with normal oversampling (Kadhum, 2019).

In this context, considering the minimum degree of interference for the filter roll-off factor, the maximum channel capacity can be recorded at the optimum value of the rolling where roll-off equals 0.1. Depending on the adjustable feature of the oversampling process, productive collaboration is realized between the oversampling and filtration levels to remove any possible intra-channel interference. As such, a new manipulation for the oversampling is introduced to avoid the unwanted roll-off impact between the adjacent filters.

As is shown in Figure 4.1.9, the principle of the double oversampling is utilized herein where the employed oversampling factor is twice the applied frequency subcarriers ( $OV = 2K$ ). Therefore, based on the newly accessible free bands between the neighbouring filters, the bad behaviour of the roll-off factor is accommodated.

Accordingly, regardless of the roll-off value, the calculated BER level at each comparable threshold of the SNR is obtained similarly for the entire range of the filter rolling. This, as a result, comes up with securing a higher channel capacity than the achieved bit-rate with the conventional way at the acceptable limits of errors.

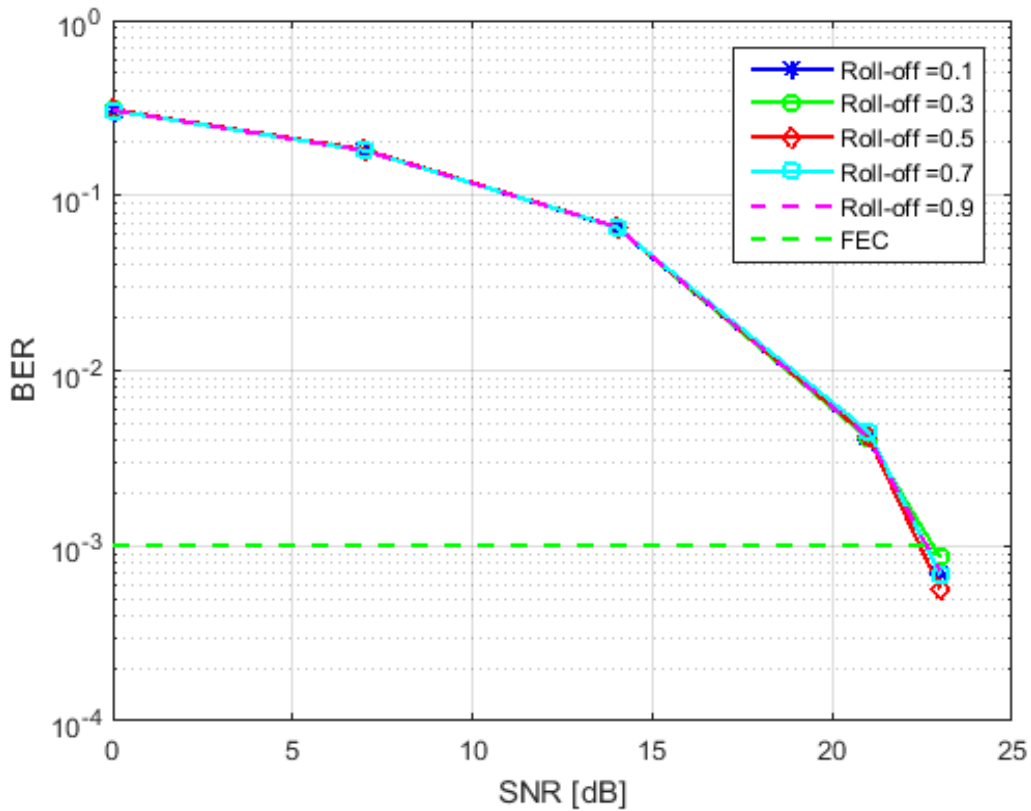


Figure 4.1.9: BER of variant roll-off factor with double oversampling (Kadhum, 2019).

It is clear from Figure 4.1.10 that, in terms of the BW efficiency, a maximum BW usage is recorded with the normal oversampling mode and the optimal value of roll-off ( $\alpha=0.1$ ) side by side with a supportive level of the SNR equals 23 dB. However, with an expanded value of the filter rolling, particularly, with a roll-off factor equals or higher than 0.5, a sharp reduction is registered for the obtained level of the BW efficiency at the same applied mode of the oversampling. Consequently, by using the normal oversampling with different stages of the roll-off factor, the system can test a severe fluctuation between the maximum and minimum levels of the BW efficiency.

This, nevertheless, can be addressed by adopting the double-mode of the oversampling where a stable level of the BW efficiency is demonstrated for both the perfect ( $\alpha = 0.1$ ) and poor ( $\alpha = 0.5$ ) values of the filter roll-off factor. However,, due to the doubled rate of the oversampling mode which in turn results in halving the available BW spaces with all roll-off cases, the BW efficiency is mainly decreased. Nonetheless, since two significant factors (SNR and BW) are essentially utilized to decide the BW efficiency, about 10% extra enhancement is gained due to the improved SNR level. Therefore, around 40% reduction is recoded rather than 50% comes from avoiding the interference of the adjacent filters.

On the other hand, the obtained channel capacity with the double oversampling is still mostly better than the calculated BW efficiency with the normal oversampling, particularly, for the roll-off values between 0.5 and 1 ( $0.5 \leq \alpha \leq 1$ ). Hence, because of the difficulty in handling the extreme interference between the adjacent filters at the normal oversampling mode, the BW efficiency is declined by around 85%. That's means, the achieved BW efficiency can reach near 60% with the double case of the oversampling against 15% with the normal one. Consequently, at worst-case scenarios ( $0.5 \leq \alpha$ ), four times higher improvement can be realized with the double oversampling than the normal one. Thus, considering the system performance in terms of the overall channel capacity, the double oversampling can be more suitable for the bad circumstances of the transmission than the normal one and vice-versa. As a result, neither normal oversampling nor double one alone can be an appropriate solution for the future wireless waveform (OGFDM). Accordingly, a combination of both (normal & double) can be recommended for the optimal manipulation of the oversampling where the highest amounts of the bit-rate are obtained.

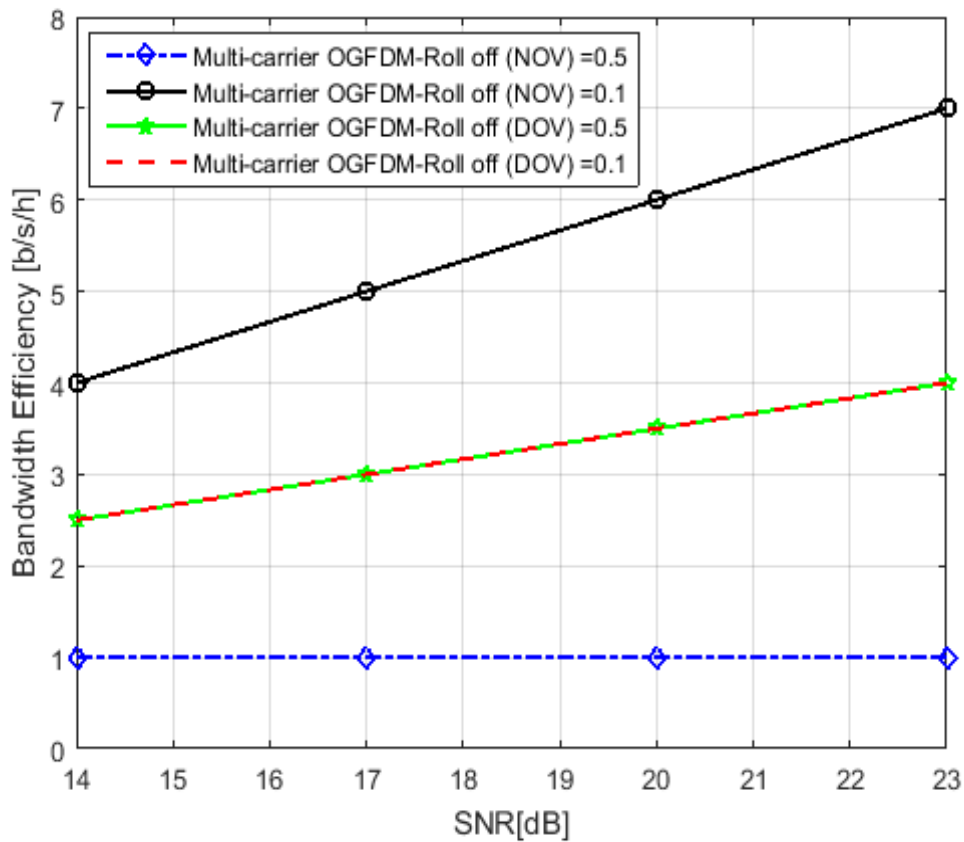


Figure 4.1.10: BW efficiency of the multi-carrier OGFDM with normal and double oversampling (Kadhum, 2019).

As is seen in Figure 4.1.11, with reference to the impact of the adaptive modulation, an extra improvement in the channel capacity is achieved in accordance with the enhanced states of the wireless channel. Therefore, the bit-rate of the transmission can be maximized up to about 14% of its initially gained channel capacity with the fixed formats. This principally occurs since the elevated stage of the SNR can support more the attained channel capacity of the adaptive modulation than improve the BER level of the fixed modulation. Consequently, a set of the amended channel capacities can be reached like C1, C2, C3 with the adaptive mode yet keeping a stable case of the BER at the  $10^{-3}$  for every two contiguous forms of the fixed modulation as with the 128 and 256 QAM.

Depending on such kind of modulation (adaptive), the resilient transmission system is established with a developed ability for bending to the real circumstances of the fading. This, hence, comes in contrast to the fixed scheme of modulation that is fundamentally designed for considering only the worst condition of the transmission. As a result, apart from the worst channel state, the adaptive system performance in terms of the channel capacity can outweigh the maximum bit-rate of the fixed modulation system.

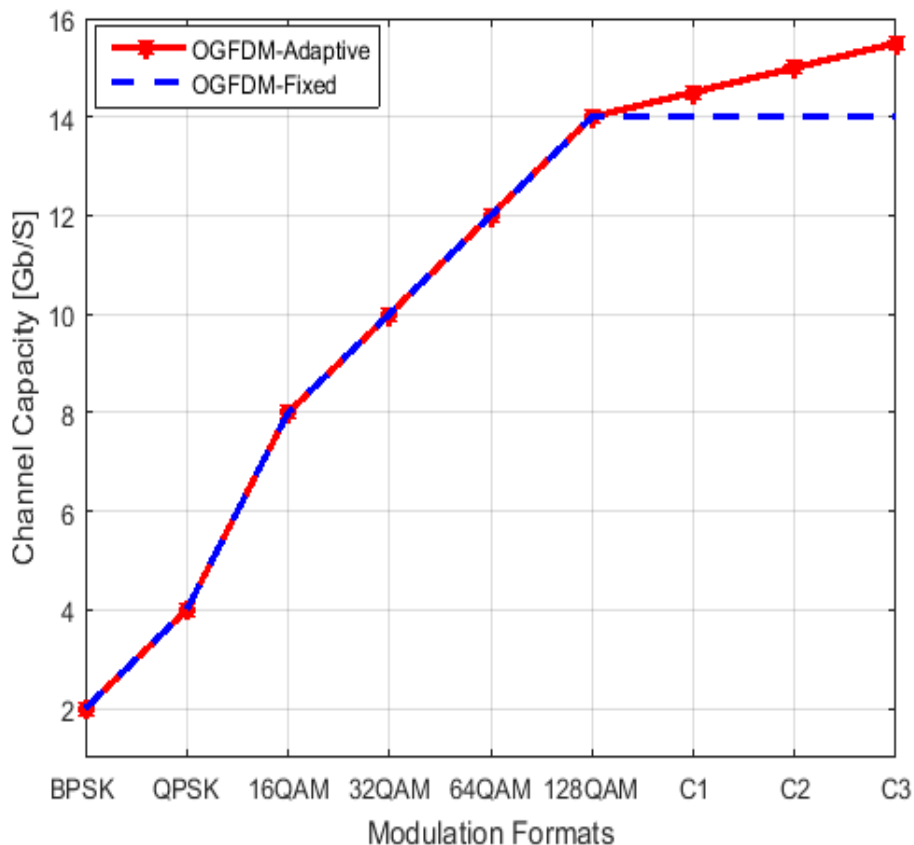


Figure 4.1.11: Improved channel capacities with the adaptive modulation of the OGFDM (Kadhum, 2019).

## 4.2 Upgraded Stage

### 4.2.1 Introduction

The upcoming generation of mobile networks tend broadly to keep up the growing requirements of future transmission (Haboobi and Kadhum, 2019a). This is, therefore, motivating the wireless research community to investigate new techniques for accommodating the key predicated scenarios of modern wireless networks like the Bit-pipe Communication (Wan *et al.*, 2018), Machine Type Communication (Walia, 2017), Tactile Internet (Simsek *et al.*, 2016) and Wireless Regional Area Network (Habibi *et al.*, 2019).

From the physical layer perspective, the currently employed CP-OFDM waveform cannot be able to achieve the future mobile market demands (Yli-kaakinen *et al.*, 2017). This is mainly because of some significant issues with the CP-OFDM that make it suffers from the OOB emission, high peak to average power ratio, frequency offset sensitivity and partially lost BW (Balint, 2018). As a result, filtered waveforms with developed features have been introduced recently for the next generation of mobile. For example, the FBMC (Gaohui, 2018), the UFMC (Saad, Al-ghouwayel and Hijazi, 2018), the F-OFDM (Wu *et al.*, 2016), and the GFDM (Towliat, Mohammad and Asgari, 2018). Consequently, the forthcoming generation of mobile networks can be described as a filtration era.

For more clarification, the digital filtration has been applied on different levels of frequency subcarrier allocation. Thus, waveform developers have utilized the filtration either for each orthogonal subcarrier as in the FBMC (Yunzheng *et al.*, 2015), or for each fixed group of orthogonal subcarriers like in the UFMC (Bochechka *et al.*, 2017), or for each flexible group of orthogonal subcarriers as in the F-OFDM (Hazareena, 2018). Furthermore, due to confliction between the employed digital filters and the orthogonal subcarriers, the filtration is applied for each non-orthogonal subcarrier like in the GFDM that has considered recently as the 5G waveform. (Hilaro-tacuri, Fortes and Sampaio-neto, 2018). However, due to removing the orthogonality with the GFDM waveform, the BW efficiency has been influenced severely.

To address this problem, lately, a single carrier waveform named as OGFDM is proposed (Kadhum *et al.*, 2018). The presented waveform has obtained the orthogonality for the non-orthogonal subcarriers of a single frequency centre of the GFDM. This, as such, comes up

with achieving the orthogonality in the filtration level rather than the subcarriers level. The core idea beyond these advanced filters is the phase change which makes them executed simultaneously. As a result, the developed Hilbert filters can be considered as an emerging solution for the degraded BW efficiency of the GFDM. From the single carrier transmission perspective, the introduced OGFDM doubled the wireless channel capacity of mobile in comparison with the GFDM (Kadhum *et al.*, 2018).

Nevertheless, the single carrier scenario cannot be recommended for the higher wireless channel capacity of future mobile communication (Gb/s). The main reason beyond this is, the single carrier with a high transmission rate can be highly impacted by the ISI than the low bit-rate since the maximum expected delay of spread is higher than the specified time for each symbol duration (Zhu *et al.*, 2010). As such, the fading will be a frequency-selective when the delay spread is larger than the period of the symbol while a flat fading can be achieved when the delay spread is less than the symbol duration. Thus, the system performance in terms of the channel capacity and BER can be highly influenced by the utilized way of channel participation.

To mitigate such an issue, very recently, the single carrier of the OGFDM has been promoted to the multi-carrier system (Kadhum, 2019). The preliminary multi-carrier OGFDM has been launched, as the first stage, with sixteen filtered subcarriers and a sampling frequency is equivalent to 4 GHz.

In this part (upgraded stage), an extended version of the multi-carrier OGFDM with a double number of filtered subcarriers (thirty-two) and enlarged size of the  $F_{DAC}$  equals to 6 GHz is experimentally demonstrated. The developed design of the OGFDM with the multi-carrier system involves three key expanded levels of processing, which are known as the filtration level, oversampling level, and modulation level.

In terms of the filtration level, the advanced Hilbert filters (Smirnov, Kharitonov and Preobrajensky, 2015) are applied proficiently on the multi-carrier system ensuring an orthogonal transmission with the upgraded design of the OGFDM. As such, comparing to the GFDM, a higher wireless channel capacity is gained due to the orthogonal filters. In addition, key filter's parameter (roll-off factor) is also adjusted optimally to obtain a maximum capacity of the channel at the acceptable level of the BER. Thus, the relation between the expanded range of roll-off factor and obtained channel capacity is investigated as well.

With respect to the oversampling level, the flexible oversampling process (Kadhum, Kanakis and Crockett, 2019b) is adopted to accommodate any probable interference among the increased filters, that in turns, can improve the attained BW efficiency. Thus, exploring the impact of both the roll-off factor and oversampling factor on increasing the aggregated channel capacity. By this level of processing, the main downside of the multi-carrier system can be manipulated efficiently.

In terms of the modulation level, the adaptive modulation scheme (Kadhum, Kanakis and Crockett, 2019a) is widely utilized with the progressive multi-carrier OGFDM system to achieve an extra enhancement for the capacity of the transmission channel. Hence, depending on the transmission conditions, the frequency subcarrier with the resilient modulation scheme can be reused in a more efficient way than the fixed modulation system (Haboobi and Kadhum, 2019b). As such, investigating the effect of the received power on improving the modulation formats.

The performance in terms of the channel capacity and the BER of the promoted OGFDM waveform is fundamentally deliberated in the physical layer of an electrical back-to-back wireless transmission system. Regarding the simulation tools, the MATLAB and Visio software applications are utilized to validate and demonstrate graphically the achieved results. The rest of the part is organized as follows: Section 4.2.2 discusses the key concepts of the proposed system physically and mathematically. Section 4.2.3 evaluates experimentally the system performance in comparison with both GFDM and CP-OFDM utilizing a computer simulation.

#### **4.2.2 System Model**

Following the successful launch of the multi-carrier OGFDM system (Kadhum, 2019), in this part, an extended design of the OGFDM waveform is explored physically and mathematically. The developed system aims to increase the number of subscribers yet keeping each user with a high level of channel capacity. As such, despite the enlarged number of the frequency subcarriers, the introduced system aims to sustain the specified bit-rate for each client by expanding the utilized BW, especially, after achieving good progress in terms of the BW efficiency (Kadhum *et al.*, 2018),(Kadhum, 2019), (Kadhum, Kanakis and Crockett, 2019b) (Kadhum, Kanakis and Crockett, 2019a).

The applied system has  $L$  layers of processing, each one has three key levels of partial management, where  $L$  equals the half number of frequency subcarriers ( $K/2$ ). As such, in terms of layer processing, the multi-carrier system must pass through three significant levels of treatment (modulation, oversampling, and filtration).

As is clear in Figure 4.2.1, on the transmitter side, particularly, at the modulation level of the multi-carrier OGFDM system, the extended group of the frequency subcarriers mainly tests a variant range of the most common modulation formats. Thus, the doubled subcarriers are adaptively managed by assigning a different size of bit token ( $N$ ) for each employed subcarrier. Worth noting that a mixed constellation map is introduced for the extended level of modulation due to applying diverse bit loading process for each produced complex number. As such, depending on the modulation type like the BPSK, QPSK, 16 QAM, etc., an irregular power consumption can be noticed for each frequency subcarrier. This, nevertheless, can be addressed by utilizing the normalization process where the average power of the constellation map is set to one.

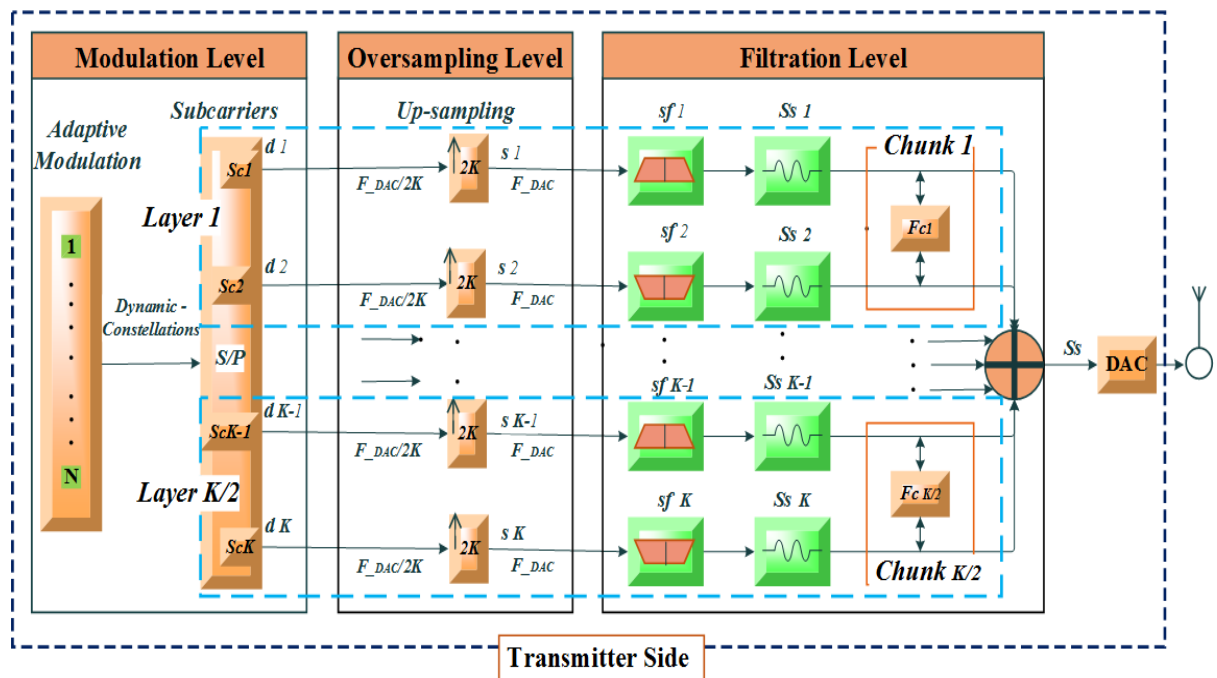


Figure 4.2.1: Wireless transmitter side of the multi-carrier OGFDM system with layer and level processing.

By adopting such a hybrid modulation shape with an enhanced channel state, an extra number of bits can be allocated for every added subcarrier at the acceptable limit of errors. Consequently, the key downside of the conventional bit loading schemes can be mitigated by alternatively employing an adaptive modulation format. This resilient kind of modulation that

is basically used for converting efficiently the assigned bits to its corresponding complex numbers is also known herein as DBL process.

At the oversampling level of the developed multi-carrier system, a double set of the modulated subcarriers is flexibly handled. Thus, the working frequency subcarriers are up-sampled by a factor of  $K$ , or  $2K$  according to the system requirements that always suppose a high channel capacity even in worse transmission statuses. Hence, inserting a set of  $K-1$  or  $2K-1$  zeros between every two adjacent samples, where  $K$  refers to the expanded number of the applied subcarriers. This form of manipulation is called herein as ICIA. It's worth pointing that the number of assigned copies for each frequency subcarrier is decided by the Oversampling stage which represents a significant base for the upcoming stage (filtration level). In addition, one copy of each used subcarrier is picked with every frequency centre that is principally specified to accommodate only two convoluted copies. As such the Oversampling layer can be considered as an important bridge between the Modulation and filtration levels.

Moving to the filtration level of the expanded OGFDM system where a double assembly of the up-sampled subcarriers is efficiently managed. At this core stage of processing, every two adjacent subcarriers of frequencies are filtered by the shaping filters of the Hilbert pair and orthogonally assigned for a similar frequency centre. Thus, the cosine and sine components of the Hilbert filters are employed effectively to multiplex orthogonally the applied subcarriers. This kind of treating is also known as DCP.

Before leaving the digital domain, it's quite vital here if the main differences between the processing in terms of layer and level are explained. As is seen in Figure 4.2.1 and Figure 4.2.2, particularly the horizontal layer block, each layer of processing includes three levels of handling (DBL, ICIA, and DCP) that can mainly improve the overall system performance of the BW efficiency. Moreover, every layer can only work on a single frequency centre, thus, two frequency subcarriers can be processed simultaneously due to the orthogonality of the applied filters. Consequently, the single carrier transmission can be considered as a good example of the layer treating.

On the other hand, as is clear in Figure 4.2.1 and Figure 4.2.2, particularly the vertical level blocks, each level of processing contains  $K/2$  layers of management and is principally in charge of performing a portion of the system activity. Thus, one kind of treatment (DBL, ICIA, or DCP) can be achieved with one level of the process. Furthermore, each level can

work on multiple frequency centres where all frequency subcarriers are partially processed. Therefore, the level of management can represent one of the three key portions of the multi-carrier transmission system. As a result, improving the level means promoting a specific portion of the multi-carrier system while developing the layer represents enhancing all levels of processing. After that, employing a proper electrical adder, the convoluted subcarriers are collected digitally and input as one sequence of data to the DAC.

At the converter stage, a promoted  $F_{DAC}$  size is utilized to mitigate the impact of system expansion where doubled subcarriers are participating in the same resource space. Hence, to avoid sharing limitations, the BW size is amended herein to be compatible with the developed system requirements. That means, without changing the channel BW size of the enlarged system, the increased number of the frequency subcarriers results in decreasing the specified BW for each filtered subcarrier. Accordingly, the  $F_{DAC}$  limit should be expanded to keep supplying a high level of bit-rate for each utilized subcarrier. The output of this operation is a transformed signal in the analog domain that is ready for transmission by a suitable antenna.

As is seen in Figure 4.2.2, on the receiver side, inverse processes are performed to recover the originally transmitted data. As such, after receiving the wireless signal, the promoted ADC is used to convert the analog signal to the digital domain.

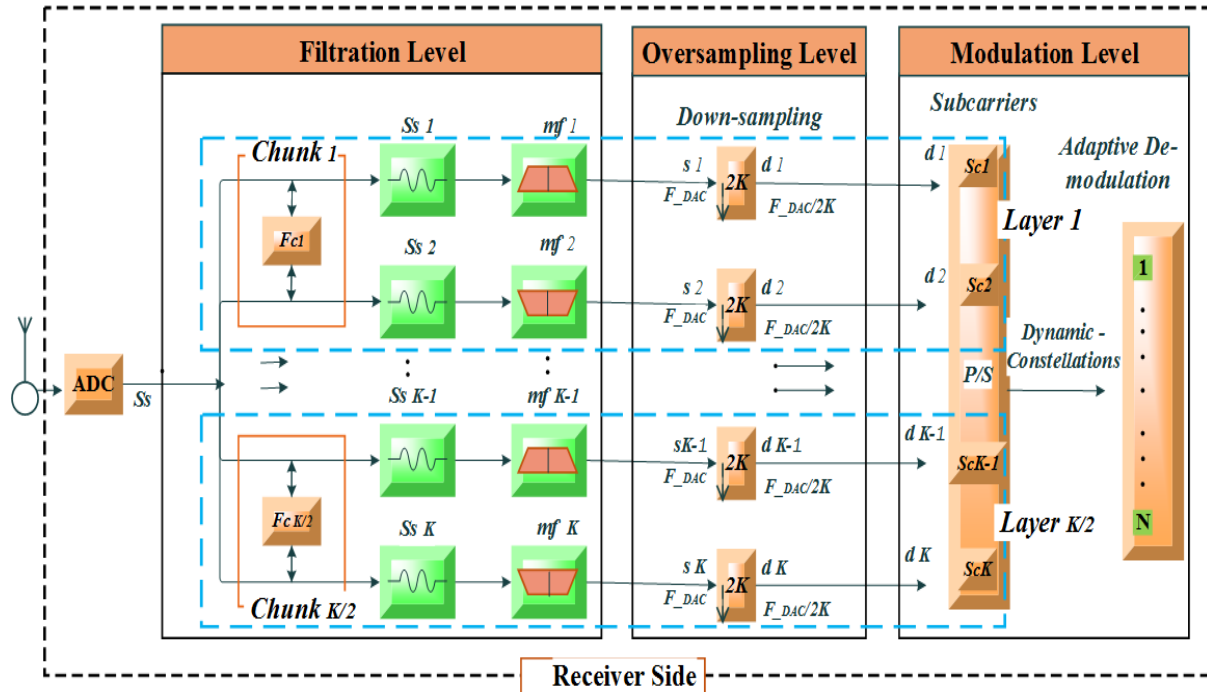


Figure 4.2.2: Wireless receiver side of the multi-carrier OGFDM system with layer and level processing.

Then, at the filtration level, the doubled set of the matching filters are employed to extract each intended subcarrier of every elected frequency centre. Hence, every two orthogonal subcarriers of a similar frequency centre are matched by the corresponding pair of the Hilbert filters. After the de-multiplexing process, the convoluted subcarriers are transferred to the oversampling level where each utilized subcarrier is down-sampled by  $K$  or  $2K$  according to the oversampling factor of the transmitter. Thus, at this stage, all the previously added zeros ( $K-1$  or  $2K-1$ ) are removed between every two adjacent samples. Subsequently, the down-sampled subcarriers are moved to the modulation level, where diffident shapes of modulation appear for the enlarged group of frequency subcarriers. Consequently, depending on the adaptive demodulation system, the complex numbers of the frequency subcarriers are converted dynamically into a stream of binary digits.

From mathematical perspective, each layer of the multi-carrier system can be expressed as follows:

In the filtration level, the impulse responses of each employed  $h^{th}$  pair of the Hilbert filters for both shaping ( $Sf$ ) and matching ( $Mf$ ) filters are represented as follows (Tao *et al.*, 2013):

$$\begin{aligned} Sf_h^A(t) &= g(t) \cos(2\pi f_{ch} t) \\ Sf_h^B(t) &= g(t) \sin(2\pi f_{ch} t) \end{aligned} \quad (1)$$

$$\begin{aligned} Mf_h^A(t) &= Sf_h^A(-t) \\ Mf_h^B(t) &= Sf_h^B(-t) \end{aligned} \quad (2)$$

where  $f_{ch}$  indicates the frequency centre of the  $h^{th}$  orthogonal pair, ( $1 \leq h \leq 16$ ), and the superscripts  $A$  and  $B$  refer to the in-phase and out-phase of the applied filter.

Besides, the  $g(t)$  signifies the baseband pulse as follows (Tao *et al.*, 2013):

$$g(t) = \frac{\sin[\pi(1-\alpha)\Upsilon] + 4\alpha\Upsilon \cos[\pi(1+\alpha)\Upsilon]}{\pi\Upsilon[1 - (4\alpha\Upsilon)^2]}, \quad \Upsilon = t/\Delta t, \quad (3)$$

Moreover, the output signal of the convolution operation between the shaping and matching filters is expressed as follows (Tao *et al.*, 2013):

$$Mf_j^C(t) \otimes Sf_i^D(t) = \begin{cases} \delta(t - t_0), & \text{if } C = D \text{ and } j = i \\ 0, & \text{if } C \neq D \text{ or } j \neq i \end{cases} \quad (4)$$

where  $t_0$  states the probable delay, the subscripts  $i$  and  $j$  represent to the order of the  $fc$ , and the superscripts  $C$  and  $D$  indicates either the in-phase or out-phase.

Considering that the expanded frequency sampling is equivalent in both sides (transmitter and receiver), the frequency centre of each filter pair is allocated as follows (Jin *et al.*, 2016):

$$fc_h = (2h - 1) (BW/K) \quad (5)$$

where,  $h$  denotes the position of the Hilbert pair and  $BW$  equals to  $F_{DAC/ADC}/2$ .

Since every applied frequency centre is optimally selected, the utilized Hilbert filters are accommodated orthogonally and distributed sequentially in the available spectrum. The specified BW of each employed filter ( $F_{BW}$ ) can be expressed as follows (Olmedo *et al.*, 2014):

$$F_{BW} = Sub_S * (1 + \alpha) \quad (6)$$

where  $0 \leq \alpha \leq 1$ , and the frequency sampling of subcarrier ( $Sub_S$ ) represents the size of generated copy for each oversampled subcarrier.

In the oversampling level, a flexible oversampling process is applied to decide the required BW size of each frequency subcarrier ( $Sub_S$ ) as follow (Olmedo *et al.*, 2014):

$$Sub_S = F_{DAC}/OV \quad (7)$$

where  $OV$  refers to the oversampling factor that mostly equals to the number of used frequency subcarriers ( $K$ ).

Besides, this important OV factor can be employed to determine the number of generated copies for each utilized subcarrier. Occasionally, the OV factor is doubled ( $2K$ ) to give extra support for the employed filters, nevertheless, this kind of manipulation can impact the overall channel capacity according to Shannon theorem as follows (Shannon, 1949):

$$Capacity = (BW) * \log_2(1 + SNR) \quad (8)$$

### 4.2.3 Experimental Results

The expanded multi-carrier OGFDM system is experimentally demonstrated herein to evaluate the performance in terms of the channel capacity and BER. Therefore, a numerical simulation is achieved for the developed design of the OGFDM including three levels of processing (filtration, oversampling, and modulation). Furthermore, to highlight the key advantages of the upgraded OGFDM, the performance comparison is performed with the formerly reported as the 5G waveform (GFDM) and LTE waveform (CP-OFDM). Moreover, the enhanced physical layer of the OGFDM is investigated in an electrical back-to-back wireless transmission system.

Prior to generating the extended design of the OGFDM, four trials are introduced and compared with the initial case. The first attempt proposed increasing the number of frequency subcarriers ( $K > 16$ ) but leaving the sampling frequency without change ( $F_{DAC} = 2$  GHz). The second try proposed improving the sampling frequency ( $F_{DAC} > 2$  GHz) without updating the number of frequency subcarriers ( $K = 16$ ). The third trial suggested enhancing both the sampling frequency ( $F_{DAC} > 2$  GHz) and the number of applied frequency subcarriers ( $K > 16$ ). The fourth trial introduced an extra enhancement in terms of the sampling frequency ( $F_{DAC} \gg 2$  GHz) improving the transmission bit-rate of each used subcarrier companied by updating the number of subcarriers ( $K > 16$ ). To clarify more about the OGFDM expansion and how the developed scenario is nominated, the following experimental cases discuss from a spectrum perspective, the assigned BW for one selected frequency centre in the examined multi-carrier OGFDM system. The key conditions of this experimented system are listed in Table 4.2.1. Besides, MATLAB tools that were mentioned in section 3.1.3 are utilized to represent the obtained results graphically.

Table 4.2.1: System parameters for the upgraded multi-carrier OGFDM.

Parameter	Value
No. of frequency centres	8-16
$F_{DAC/ADC}$	6 GHz
SNR	23 dB
Number of subcarriers	16-32
Oversampling	Normal & Double
Modulation format	Fixed & Adaptive
Filter type	RRC & Hilbert filters

In case 1(initial state), as is seen in Figure 4.2.3, with 16 frequency subcarriers and  $F_{DAC}$  corresponds to 2 GHz, the specified sampling frequency ( $F_{DATA}$ ) for one frequency centre is equalled to 125 MHz, hence, the subcarrier BW is equivalent to 62.5 MHz. As a result, the achieved bit-rate of each frequency subcarrier is 437.5 Mb/s that is gained side by side with aggregated channel capacity equals to 7 Gb/s.

In case 2 (subcarriers number increment), as is clear in Figure 4.2.4, with a steady level of sampling frequency ( $F_{DAC}= 2$  GHz) and a double number of subcarriers ( $K= 32$ ), the assigned sampling frequency for one frequency centre is affected badly ( $F_{DATA}= 62.5$  MHz). Thus, comparing to the case 1, the subcarrier BW is reduced to a half of its initial case due to doubling the applied subcarriers without expanding the speed of  $F_{DAC}$ . Despite that the overall channel capacity is still compatible with case1, the bit-rate of each applied subcarrier is descended to 218.75 Mb/s (50% decrement).

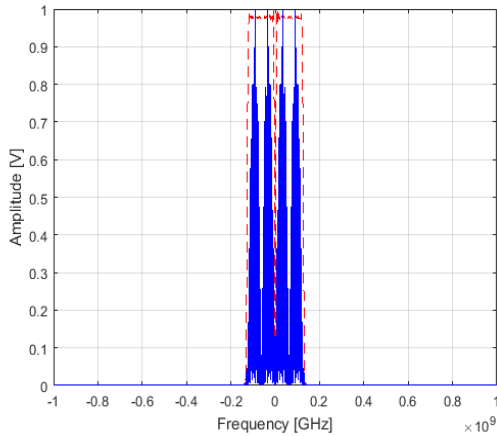


Figure 4.2.3: Case 1(initial):  $F_{DAC}= 2$  GHz,  $K=16$

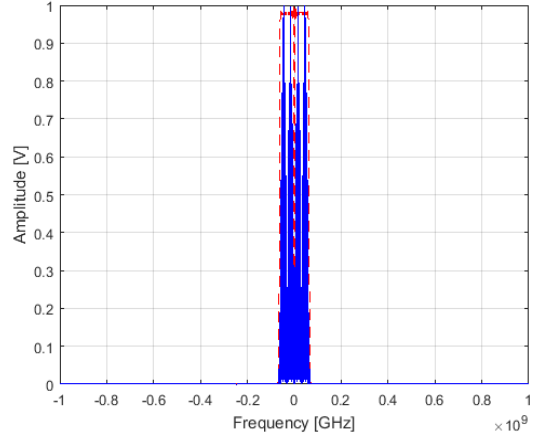


Figure 4.2.4: Case 2:  $F_{DAC}= 2$  GHz,  $K=32$

In case 3 (sampling frequency increment), as is obvious in Figure 4.2.5, with a promoted sampling frequency ( $F_{DAC}= 4$  GHz) and for the original number of the subcarriers ( $K=16$ ), a double sampling frequency, in comparative with the case 1, is given to each frequency centre ( $F_{DATA}=250$  MHz). As such, a developed BW size equals to 125 MHz is assigned for every employed subcarrier. Concerning the bit-rate of transmission, 100% increase is gained for each utilized frequency subcarrier (875 Mb/s), which in turn, raises the total channel capacity of the fixed multi-carrier system to 14 Gb/s.

In case 4 (double subcarriers number and double sampling frequency), as is shown in Figure 4.2.6, a developed multi-carrier system ( $K=32$ ) and an expanded sampling frequency ( $F_{DAC}=$

4 GHz) are achieved. Thus, relative to the case 1, the introduced case comes up with a double number of frequency subcarriers yet keeping the bit-rate of each applied subcarrier at its original value (437.5 Mb/s). Worth noting that, even with a similar level of the subcarrier bit-rate for both cases (1 and 4), the overall channel capacity of case 4 is higher than case 1 (double). Comparing to the case 2 where the number of subcarriers is elevated to 32 but unaccompanied by altering the sampling frequency, the BW decreasing issue of every utilized frequency subcarrier is mitigated herein. Thus, the allocated sampling frequency of each employed frequency centre is increased to 125 MHz against 62.5 MHz with case 2. As such, a raised level of the bit-rate (437.5 Mb/s) is recorded to every used frequency subcarrier in contradiction of 218.75 Mb/s with case 2. Moreover, due to the extended sampling frequency, the accumulated channel capacity is boosted from 7 Gb/s (case 2) to 14 Gb/s with case 4. In comparison with case 3 where the sampling frequency is promoted to 4 GHz without upraising the number of the subcarriers, a high level of sharing a resource (BW) is reached here by doubling the number of subcarriers ( $K=32$ ). Despite that the obtained bit-rate of each frequency subcarrier with case 3 is higher than the case 4, the case 3 scenario is not mostly preferred for the OGFDM system since the number of subcarriers is not permitted to increase.

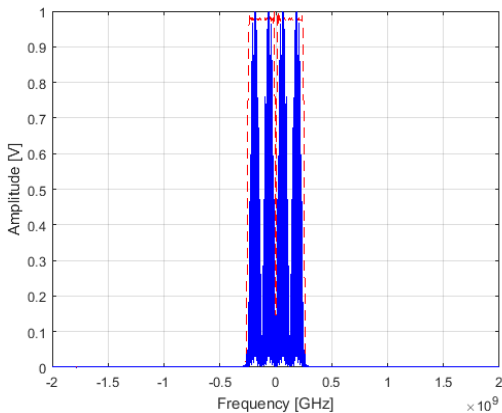


Figure 4.2.5: Case 3:  $F_{DAC} = 4$  GHz,  $K=16$

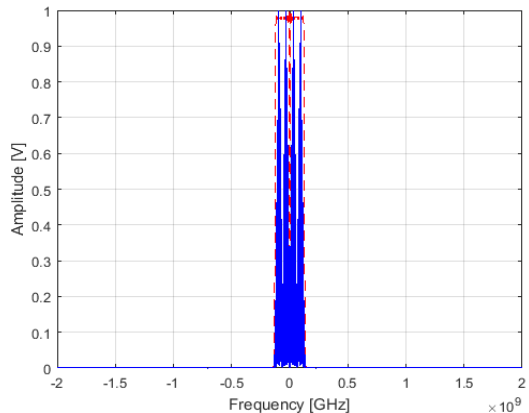


Figure 4.2.6: Case 4:  $F_{DAC} = 4$  GHz,  $K=32$

In case 5 (progressive state), as is shown in Figure 4.2.7, an advanced case of transmission is gotten herein by extra expanding the utilized sampling frequency from 4 to 6 GHz with keeping the applied number of subcarriers as in case 4. Worth noting that, the  $F_{DAC}$  of this case can be further enlarged, but as the multi-carrier OGFDM system tends currently to work at the 6 GHz band radio frequency, the employed  $F_{DAC}$  is upgraded by only 50% of the last update (case 4). In this context, a better sampling frequency (187.5 MHz) is obtained than the

previously discussed case (125 MHz). Comparing with case 4, both the number of subcarriers and the sampling frequency are developed. In addition, relative to case 3, a doable number of subcarriers is used expanding the range of resource sharing. Moreover, in contrast with case 2, three times increase is counted for the bit-rate of the frequency subcarrier. Consequently, comparing with the initial state case, neither only increasing the number of subcarriers nor rising the size of the utilized sampling frequency alone can be adopted as a vital expansion for the desired system. Since the future applications of mobile tend to increase the number of subscribers yet keeping the bit-rate of each one at a high level, the last trial can be considered as the best option for the expanded plan. As such, case 5 that combines both an improved bit-rate and an enlarged number of subcarriers is highly recommended for the expanded design of the multi-carrier OGFDM waveform.

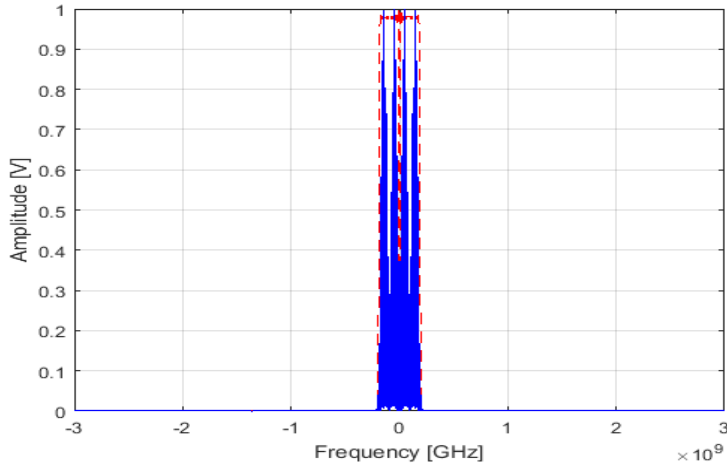


Figure 4.2.7: Case 5:  $F_{DAC} = 6$  GHz,  $K=32$

Table 4.2.2 summarizes the introduced cases of the OGFDM expansion including the initial case.

Table 4.2.2: Comparison of expansion trials for multi-carrier OGFDM system.

	$F_{DAC}$ (GHz)	$N_{Sc}$	$F_{DATA}$ (MHz)	$fc$ (MHz)	$Sc\text{-Cap}$ (Mb/s)	$T\text{-Cap}$ (Gb/s)
<b>Case 1</b>	2	16	125	62.5	437.5	7
<b>Case 2</b>	2	32	62.5	31.25	218.75	7
<b>Case 3</b>	4	16	250	125	875	14
<b>Case 4</b>	4	32	125	62.5	437.5	14
<b>Case 5</b>	6	32	187.5	93.75	656.25	21

After selecting the required scenario (case 5) for the developed OGFDM design, the main system parameters are updated accordingly. Since the intended expansion is discussed from the layer processing perspective, the impact of the upgraded physical layer on the system performance (channel capacity and BER) is explored for the three levels of management. Thus, such important parameters like the number of subcarriers and sampling frequency size can directly influence the filtration, oversampling, and modulation levels of handling.

On the topic of the filtration level, the developed multi-carrier OGFDM with 6 GHz is mainly compared with the GFDM waveform exploring the impact of Hilbert filters on the transceiver process. In addition, despite that the expanded sampling frequency is set to 6 GHz, the effect of extending the initial case of the  $F_{DAC}$  from 2 to 4 and then to settle at 6 GHz is also considered for the overall performance. Thus, investigating how the change in sampling frequency can impact the bit-rate of transmission in cooperating with the orthogonal filters that play a big role in improving the BW efficiency and then supporting the channel capacity of the upgraded system.

As is seen in Figure 4.2.8, in this experiment, a stable 2 dB gain is obtained between the aggregated channel capacity of the OGFDM and the GFDM because of the orthogonality impact of the utilized Hilbert filters on the OGFDM waveform. Thus, a higher channel capacity (double) is achieved with the orthogonal OGFDM than the non-orthogonal GFDM with the RRC for an equivalent level of the sampling frequency.

In addition, a similar improvement (2 dB) can be attained between the OGFDM / GFDM of the updated cases (3 and 4) and the OGFDM / GFDM of the primary cases (1 and 2) due to developing the applied  $F_{DAC}$  of the same waveform from 2 GHz to 4 GHz. As such, 2 dB increase can be acquired by either improving the BW efficiency (Hilbert pair) or by extra extending the used sampling frequency.

On the other hand, moving from 2 GHz to 4 GHz for different waveforms like between GFDM and OGFDM comes up with an additional variance (4 dB). Hence, the capacity of the channel can be improved four times by converting from the GFDM with 2 GHz to the OGFDM with 4 GHz. The main reason beyond this increment is the combined influence of both the advanced Hilbert filters and the improved (doubled) sampling frequency.

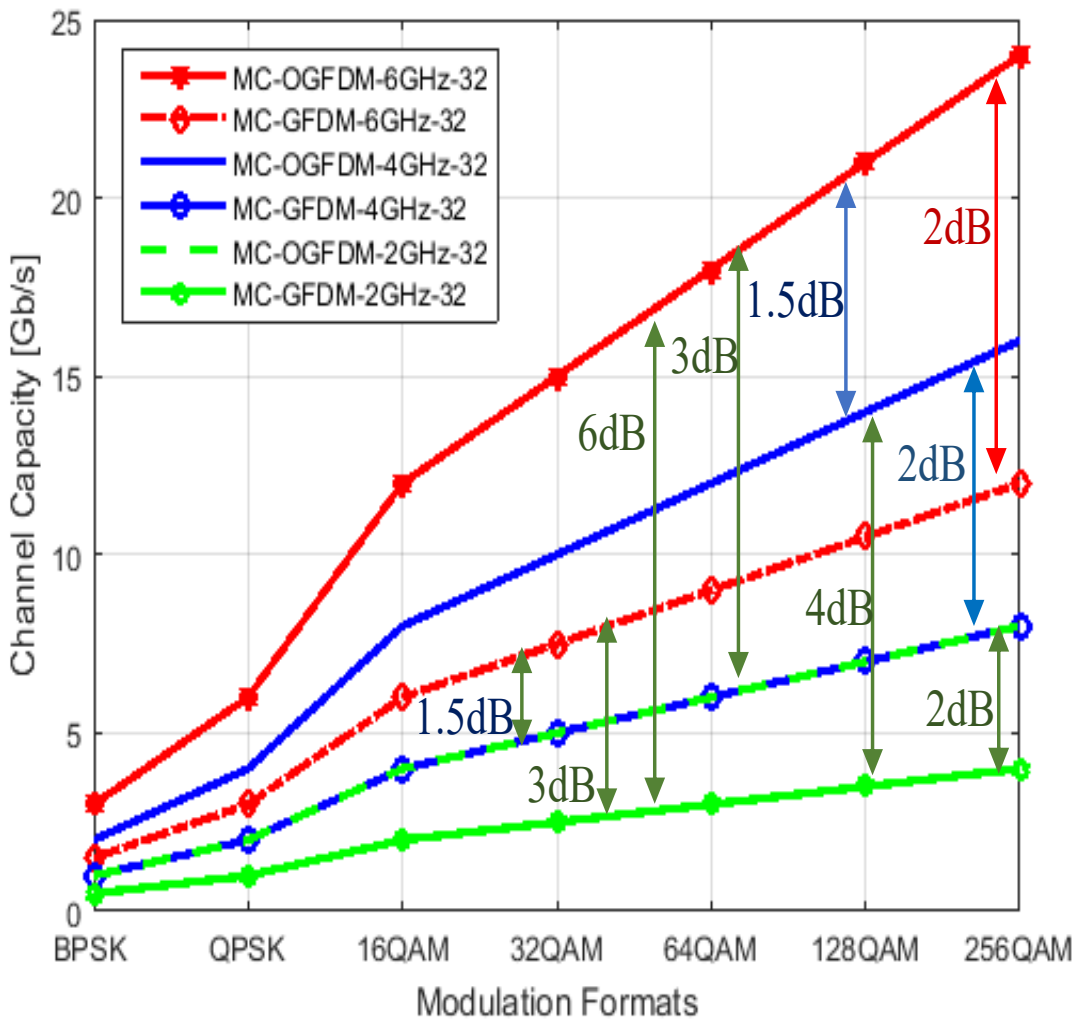


Figure 4.2.8: Channel capacity of the multi-carrier OGFDM vs GFDM with diverse sampling frequency.

Moreover, identical channel capacity can be reached between the OGFDM with 2 GHz and the GFDM with 4 GHz reflecting that the impact of the developed filters is equivalent to doubling the utilized BW. Noteworthy that, the accomplished enhancement due to expanding the employed BW is not always equated to 2 dB since the amount of improved channel capacity depends on the applied size of the sampling frequency. For example, 3 dB and 1.5 dB gains are realized for the channel capacity of the OGFDM by raising to 6 GHz the used sampling frequency of the OGFDM for both the 2 GHz and 4 GHz respectively. Besides, considering the effect of utilizing the orthogonal filters on the system performance, a double amount of boosting, 6 dB and 3 dB, are recorded for the OGFDM channel capacity with 6 GHz, in comparing with the GFDM at 2 and 4 GHz.

In terms of the relationship between the duplex channel capacity and calculated BER, it is clear from Figure 4.2.9, that even with the double bit-rate of the OGFDM system, a similar SNR is recorded for both the multi-carrier OGFDM and GFDM. Hence, the upgraded waveform under the AWGN able to double the capacity of the channel yet keeping the BER at an identical level for the GFDM.

With reference to the oversampling level, since moving from the single carrier to the multi-carrier system comes up with inducing the interference between the applied filters of the frequency subcarriers, a hybrid treatment combines between the normal oversampling and double oversampling is experimented herein on both the developed OGFDM and the GFDM. Thus, the oversampling level can supply vital support to the filtration level by avoiding the influence of the enlarged roll-off factor on the same type filters.

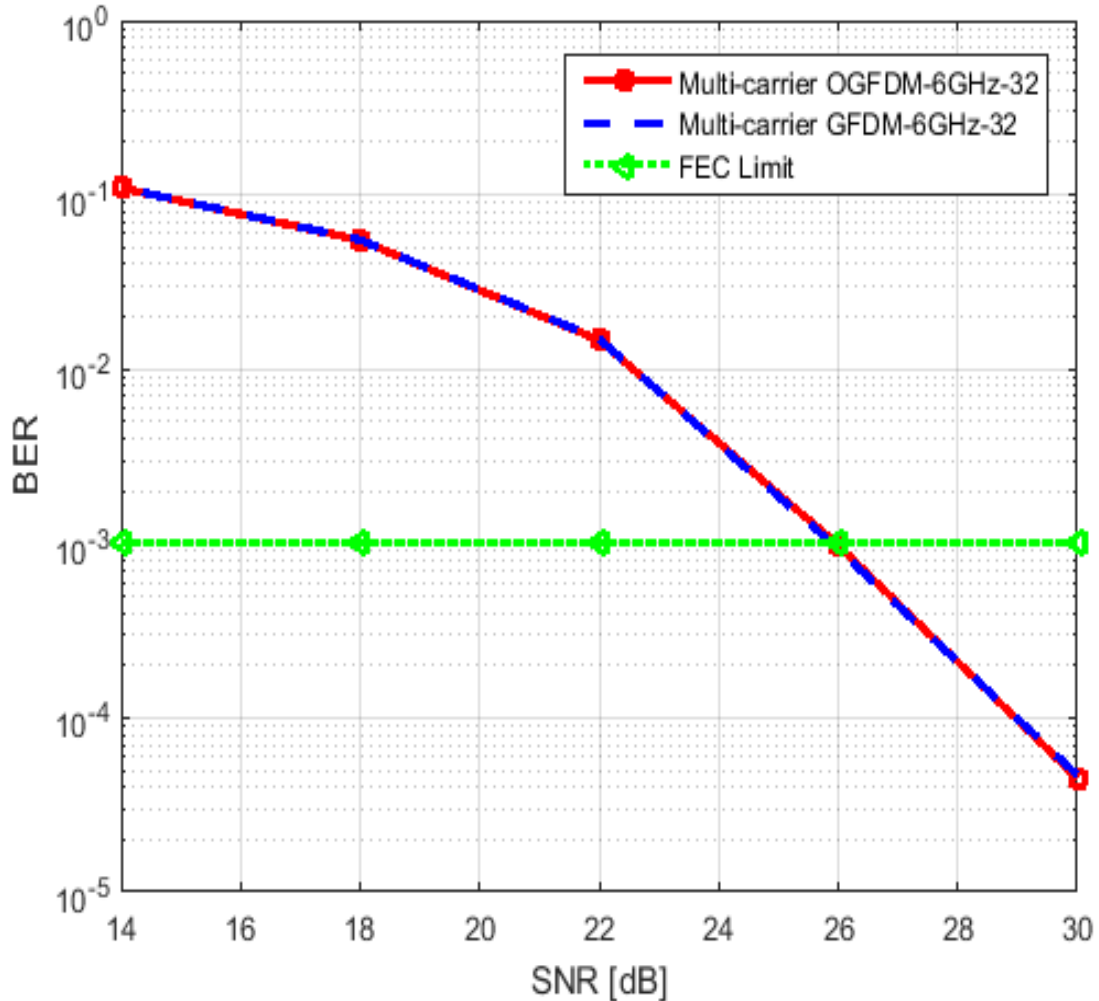


Figure 4.2.9: Similar achieved SNR for both multi-carrier OGFDM and GFDM.

From the oversampling perspective, with the normal case (normal), where the oversampling factor ( $OV$ ) equals to the number of the subcarriers ( $K$ ), the interference between filtered subcarriers is decided according to the roll-off value. For instance, with the initial rolling case ( $\alpha = 0$ ), the specified BW of the filter is equivalent to the subcarrier sampling rate (no interference), while, for the worst rolling case ( $\alpha = 1$ ), the filter BW size is doubled for each filter (maximum interference).

To mitigate such an issue, a reconfigurable oversampling process is adopted where the number of produced copies for each utilized subcarrier can be doubled ( $OV = 2K$ ) for the same allocation centres of frequencies. Therefore, the negative effect of the roll-off can be accommodated counting on the offered band intervals, which in turn, can remove any possible intra-channel interference. Hence, regardless of the roll-off factor behaviour, a better bit-rate can be secured than the traditional oversampling ( $OV = K$ ).

The upgraded OGFDM is also compared with the GFDM considering the impact of the normal and double oversampling on the system performance (channel capacity and BER) at 6 GHz sampling frequency.

As is shown in Figure 4.2.10, three key zones of the channel capacity which are known herein as the ‘Green Zone’ (GZ), ‘Yellow Zone’ (YZ), and the ‘Red Zone’ (RZ) are investigated. In the GZ, where the channel capacities are calculated for rolling values less than 0.4 ( $0 \leq \alpha < 0.4$ ), four important areas are recognized. The first area, which is counted for the OGFDM with the normal case, represents all channel capacities above the stable line of the OGFDM channel capacity with the double oversampling, where the maximum channel capacity is achieved in this zone. The second area is assigned for channel capacities that come from the OGFDM with double oversampling. The third area, which is specified for the GFDM with the normal oversampling, signifies all channel capacities above the steady channel capacity of the GFDM with the double oversampling but lower than the OGFDM with the double oversampling and the fourth area is given for channel capacities of the GFDM with double oversampling.

In the YZ which is calculated for the roll-off value of 0.4, the channel capacities for both the normal oversampling and double oversampling are equivalent at this neutral area.

In the RZ, that is introduced for all channel capacities with a rolling factor higher than 0.4 but not exceed one ( $0.4 < \alpha \leq 1$ ), four significant areas are realized. The first area is allocated for the OGFDM with the double oversampling that provides the highest amounts of channel capacities in the zone. The second area is decided for the GFDM with the double oversampling under the steady channel capacity of the OGFDM with the double oversampling. The third area is described for the OGFDM with the normal oversampling, where all channel capacities are settled down the stable line of both the OGFDM and GFDM channel capacities with the double oversampling. The fourth area is given for channel capacities that are resulted from the GFDM with the normal oversampling where the lowest amounts of channel capacities are recorded.

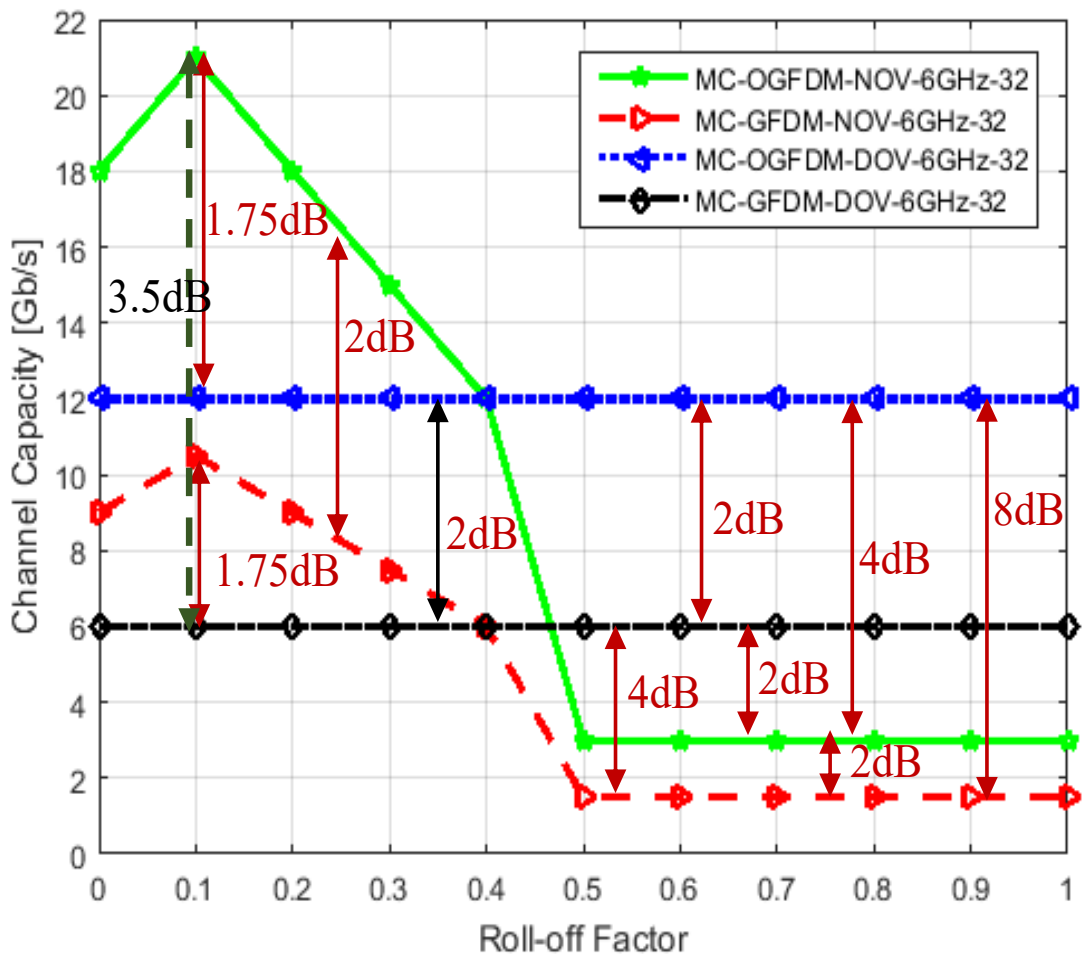


Figure 4.2.10: Channel capacity of upgraded OGFDM vs GFDM with normal and double oversampling.

The experimental work indicates that, in the GZ, a fixed 2 dB gain is attained between the channel capacity of OGFDM and GFDM under the normal oversampling condition. Besides, a similar ratio (2 dB) is calculated for the channel capacity of both the OGFDM and GFDM

with the double oversampling. This unchanged 2 dB comes principally from applying the developed Hilbert filters at the OGFDM waveform. Moreover, despite half BW usage, 1.75 dB is registered for the decrease in the bit-rate of the OGFDM with the normal oversampling at the optimum value of the rolling ( $\alpha = 0.1$ ) against the double oversampling. Also, in a similar way but with lower BW efficiency, 1.75 dB is recorded for the difference between the normal oversampling and double oversampling of the GFDM. It's worth noting that 3.5 dB gain can be obtained by moving from the channel capacities of the GFDM with the double oversampling to the maximum channel capacity of the OGFDM with the normal oversampling.

In the RZ, using the double oversampling state, a steady 2 dB gain is reached by transferring from the bit-rate of the GFDM to the OGFDM. It's also noticed that the relation between both the GFDM and OGFDM can test a comparable behaviour under the double oversampling condition. This mainly occurs due to the impact of the developed filters that continue in the doubling even with worst circumstance. Furthermore, 4 dB improvement is calculated by converting from the OGFDM / GFDM with normal oversampling to a similar waveform with the double oversampling. Noteworthy that a big achievement is recorded (8 dB gain) by moving from GFDM with normal oversampling to the OGFDM with the double oversampling reflecting the power of utilizing the double oversampling process with OGFDM waveform. As a result, for a robust transmission scenario of the OGFDM, a combination of both the normal oversampling and double oversampling is utilized, where the normal oversampling is strongly recommended for the GZ while the RZ can be highly engaged with the double oversampling.

In terms of the BW efficiency, it is clear from Figure 4.2.11 that promoting the transmission system from the GFDM to the OGFDM comes up with 2 dB gain for both the normal oversampling and double oversampling treatments. In addition, the maximum BW efficiency is recorded for the OGFDM with normal oversampling, particularly, at the GZ where  $\alpha = 0.1$ . Nevertheless, in the RZ with extra rolling expansion ( $0.5 \leq \alpha$ ), the BW efficiency of the OGFDM under the normal oversampling suffers from a severe decrease, about 7 dB comparing to the optimal value ( $\alpha = 0.1$ ). To manipulate such a dilemma, the double oversampling solution is introduced for improving the impacted level of the BW efficiency. Thus, a stable efficiency can be obtained for the utilized BW where less than 2 dB can be registered for the difference between the channel capacity of the double oversampling and the

maximum bit-rate of the normal oversampling. Concerning the modulation level, an extra BW efficiency is gained herein by applying the adaptive modulation format on the updated system which is presently composed of 32 filtered subcarriers working at 6 GHz sampling frequency. Besides, the system performance (channel capacity and BER) of the OGFDM is compared with the GFDM under the fixed and adaptive modulation schemes.

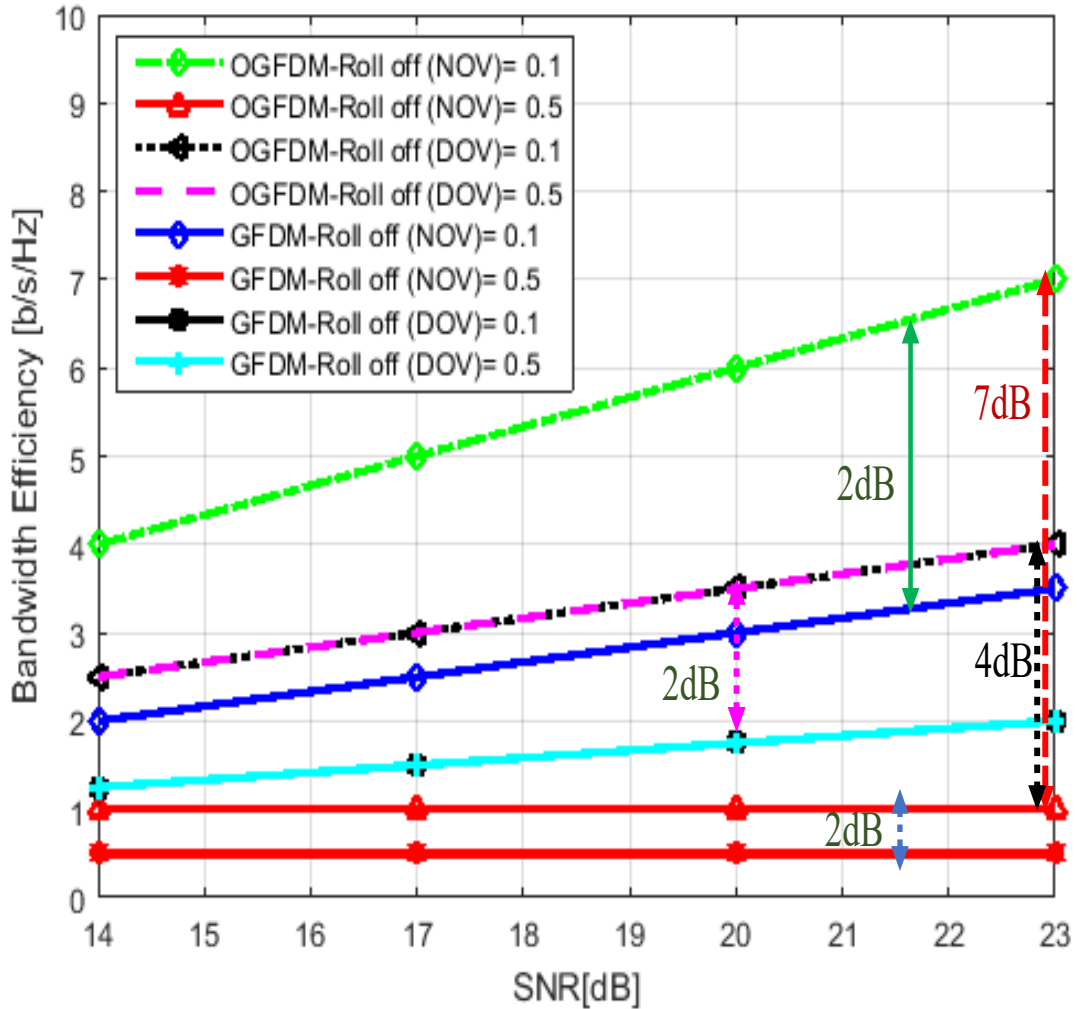


Figure 4.2.11: BW efficiency of multi-carrier OGFDM vs GFDM with normal and double oversampling.

As is seen in Figure 4.2.12, three vital areas, that are known herein as Low Boost (LB), Medium Boost (MB), and High Boost (HB), are elected between the 128 QAM and 256 QAM with minimum SNR edges equal to 23 dB and 26 dB respectively.

The first case (LB) is calculated for a 25%-bit-rate improvement with the SNR threshold equals to 24.1 dB where different possible arrangements of the Bit Loading Map (BLM) can be shown compatible with for this ratio of the enhancement. For instance, with thirty two

frequency subcarriers, the BLM can be one of the following arrays, [8,7,7,7,7,7,7,8,7,8,7,7,7,8,7,8,8,7,7,7,7,7,7,7,7,7,8,8],[8,8,8,8,8,8,8,8,7,7,7,7,7,7,7,7,7,7,7], etc. Worth noting that, compared with the previous multi-carrier system (16 frequency subcarriers), the number of improved subcarriers that can carry extra bit is increased (doubled) herein for the same ratio of the power enhancement. Thus, only four subcarriers are boosted with the preliminary multi-carrier system in comparison with eight enhanced subcarriers with the upgraded scheme. The core idea beyond these distributions is that a quarter of the subcarriers is improved by loading 8 bits rather than 7, which in turns, results in a minor channel capacity increase.

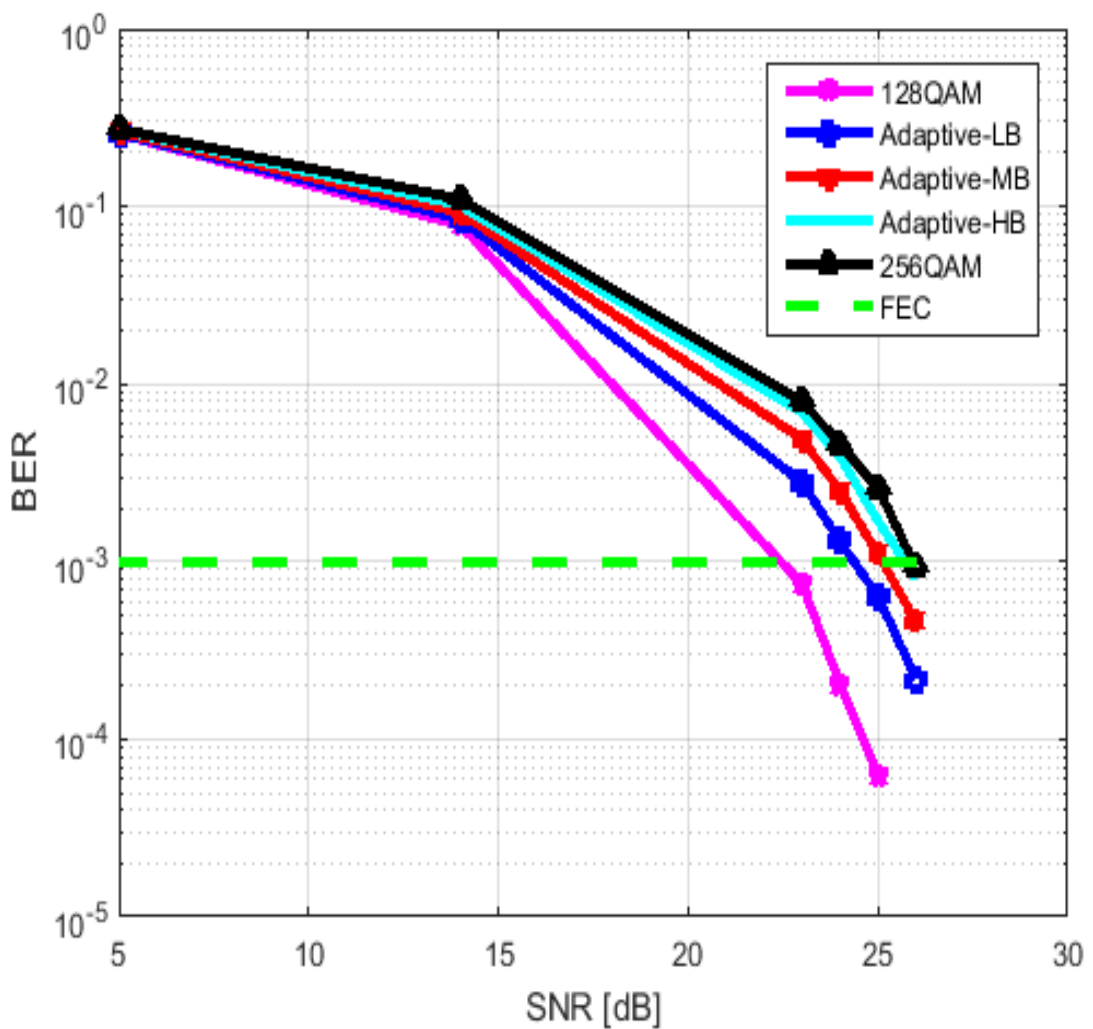


Figure 4.2.12: Three significant adaptive areas, LB, MB, and HB between 128 & 256 QAM.

In the second case (MB), the threshold of the required SNR that is equivalent to 25.1 dB can be decided between the first (128 QAM) and the second (256 QAM) modulation formats.

In the third case (HB), the promoted threshold of the SNR can come up with 75%-bit-rate development in comparison with the previously stated modes (MB, LB). The BLM of this progressive state can be compatible with one of the following styles, [8,8,8,7,7,8,8,8,7,8,8,8,8,8,8,7,7,7,7,7,7,7], etc. Therefore, at the HB where the recorded SNR equals to 25.1 dB, the number of frequency subcarriers with a further bit is enhanced to 24 improved cases with the developed OGFDIM in comparison with only 12 amended subcarriers with the earlier multi-carrier system.

As is shown in Figure 4.2.13, comparing to the GFDM, a double amount of the channel capacity (2 dB) gain is obtained for the OGFDM with both the fixed and adaptive modulation formats. Such a notable improvement is essentially acquired due to the powerful use of the orthogonal filters (Hilbert pairs) in the OGFDM waveform. In addition, the findings of the experiment declare that for the two tested schemes of the fixed modulation (128 and 256 QAM), the maximum bit-rate of transmission can be elevated up to around 114% of the overall channel capacity yet keeping the BER at steady state ( $10^{-3}$ ). Consequently, in comparison with the fixed modulation format, the modified level of the SNR for the adaptive schemes grants a greater priority for supporting the channel capacity of the OGFDM than improving the BER of it. Accordingly, the adaptive bit loading can mainly support the real fading conditions of the transmission than only back the worst circumstances which are principally treated by the fixed modulation schemes.

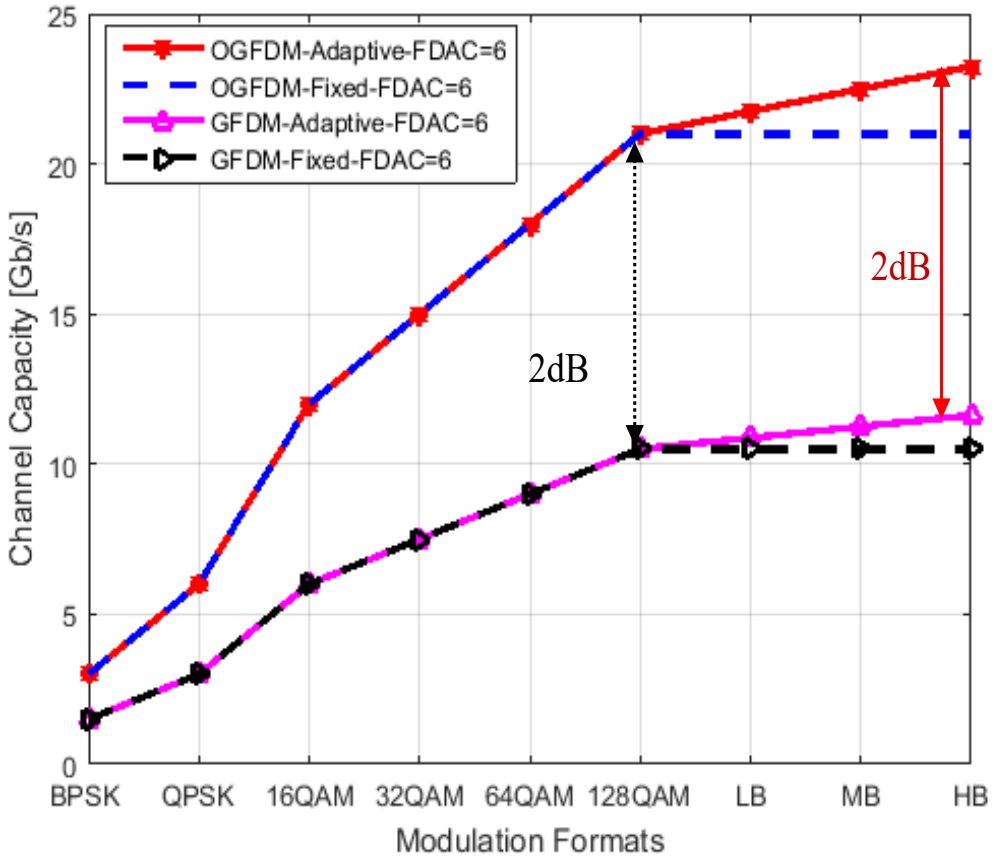


Figure 4.2.13: Utilization of adaptive modulations in the multi-carrier OGFDM and GFDM .

After comparing the upgraded OGFDM waveform with the filtered 5G waveform (GFDM), another important comparison is applied herein with the non-filtered LTE waveform (CP-OFDM) that have been proposed recently for the 5G networks by the Ericsson telecommunications company (Zaidi *et al.*, 2018). Hence, demonstrating experimentally the difference in wireless channel capacity between employing filtered and orthogonal waveform like OGFDM and non-filtered but orthogonal one like CP-OFDM. As such, exploring the developed features of the OGFDM that combine proficiently both the orthogonality of CP-OFDM and flexible filtration of GFDM in one orthogonal, filtered, and flexible system.

As is seen in Figure 4.2.14, regarding the filtration level, the OGFDM can obtain a better level of SNR by about 3 dB difference in comparison with the Ericsson waveform (CP-OFDM). As such, the OGFDM receiver requires lower power (26 dB) than the CP-OFDM (29 dB) to secure a similar amount of channel capacity at the acceptable limits of BER. This is mainly achieved due to utilizing the advanced Hilbert filters that reduce efficiently the effect of the OOB emission decreasing unwanted side lobes between frequency subcarriers (Smirnov, Kharitonov and Preobrajensky, 2015).

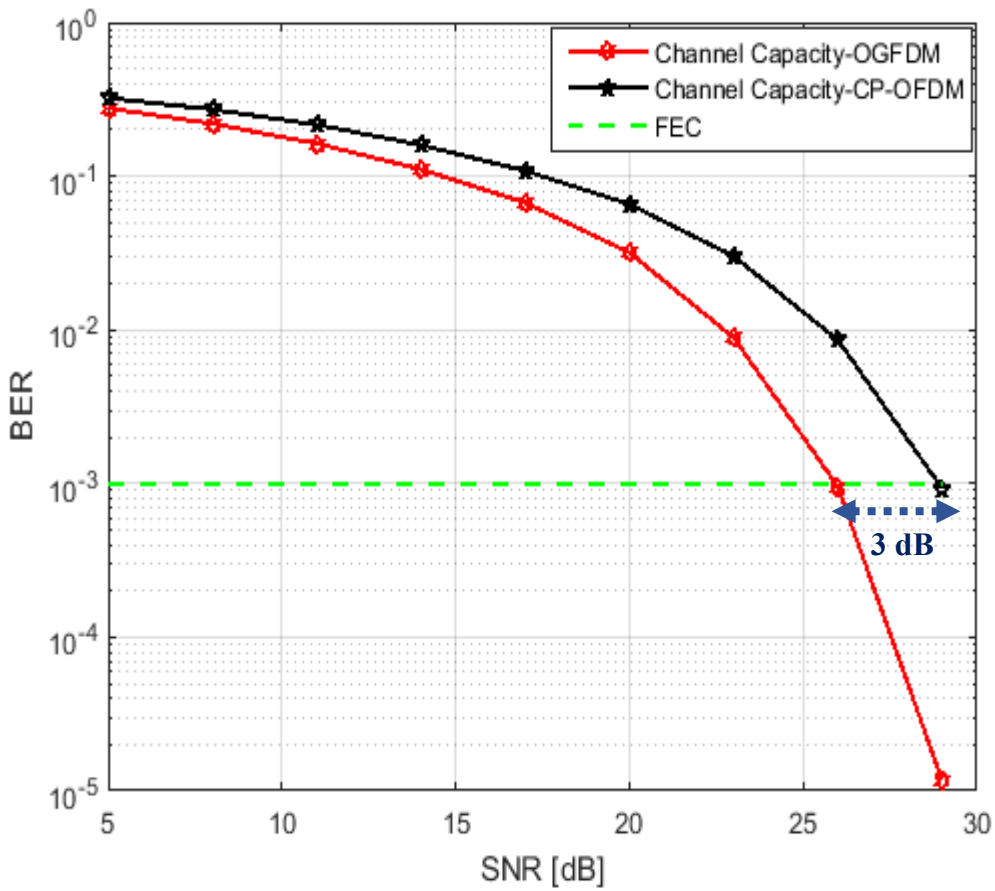


Figure 4.2.14: SNR level difference between the OGFDM and the CP-OFDM (Ericsson technology).

As is shown in Figure 4.2.15, for the same SNR threshold, higher channel capacity is achieved with OGFDM than the proposed Ericsson CP-OFDM waveform. Thus, due to improving the SNR level with filtered OGFDM, a better BW efficiency than the non-filtered CP-OFDM is obtained at the acceptable BER limit ( $10^{-3}$ ). This, as a result, comes up with increasing the number of carried bits for the OGFDM frequency subcarrier improving the wireless channel capacity by about 115% relative to the CP-OFDM. It's worth noting that despite both OGFDM and CP-OFDM are orthogonal waveforms, higher channel capacity is reached with OGFDM than CP-OFDM due to utilizing a developed filtration process (Hilbert filters) in OGFDM multiplexing stage. The efficient use of the filtered frequency centres with OGFDM comes up with supplying extra non-interfered rooms in the accessible BW that mainly increase the calculated channel capacity according to Shannon's theory. As such, by reducing the OOB emission for the OGFDM frequency subcarriers, a lower level of SNR is required for recognizing the received wireless signal in comparison with the Ericsson technology CP-OFDM.

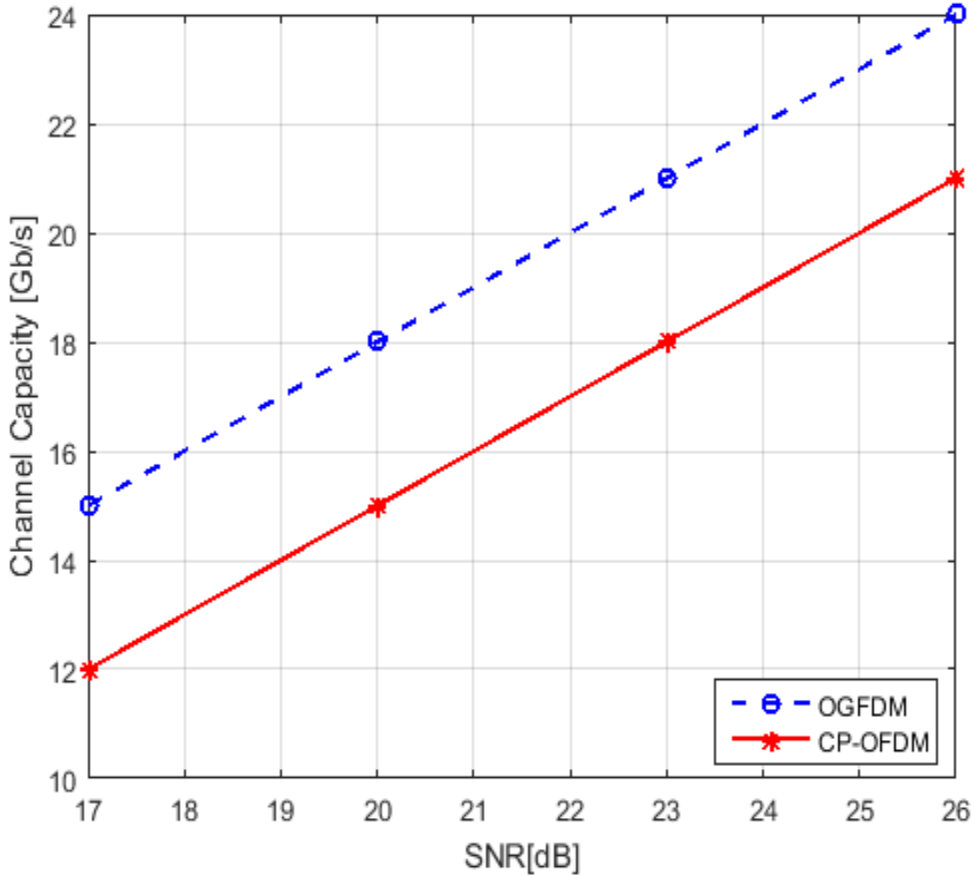


Figure 4.2.15: Channel capacity difference between multi-carrier OGFDM and CP-OFDM (Ericsson technology).

In terms of the BER performance, the OGFDM waveform gains an improved level of BER in comparison with the Ericsson waveform CP-OFDM at a similar transmission bit-rate. That means, by adopting a similar modulation scheme for both the OGFDM and CP-OFDM at the same limits of the SNR, a higher level of BER is recorded with the CP-OFDM than the OGFDM. Therefore, by using, for example, 256 QAM as a modulation format, the OGFDM can carry 8 bits while only 7 bits (128 QAM) can be carried by the CP-OFDM at the acceptable BER level.

Regarding the oversampling level, the assigned sampling frequency ( $F_{DATA}$ ) of each OGFDM frequency subcarrier is determined by either depending on the original number of frequency subcarriers ( $K$ ) or double number of them ( $2K$ ). However, in the CP-OFDM Ericsson technology, due to restriction of the IFFT, only one normal mode is used to regulate the allocated  $F_{DATA}$  of frequency subcarrier (Chen *et al.*, 2015). As is shown in Figure 4.2.16, in the good condition (GC) of transmission where higher modulation format is applied with the assigned SNR, the OGFDM with NOV gains a better BW efficiency than both the Ericsson

waveform (CP-OFDM) and the OGFDM with DOV. On the other hand, as is seen in Figure 4.2.17, in bad condition (BC) of transmission where lower modulation format is applied with specified SNR, the OGFDM with DOV can achieve a higher BW efficiency, around 4 dB gain than both the CP-OFDM (Ericsson waveform) and the OGFDM with NOV. This is mainly obtained due to utilizing a flexible oversampling mode with OGFDM where the allocated subcarrier BW can be decided either normally (NOV) or doubly (DOV).

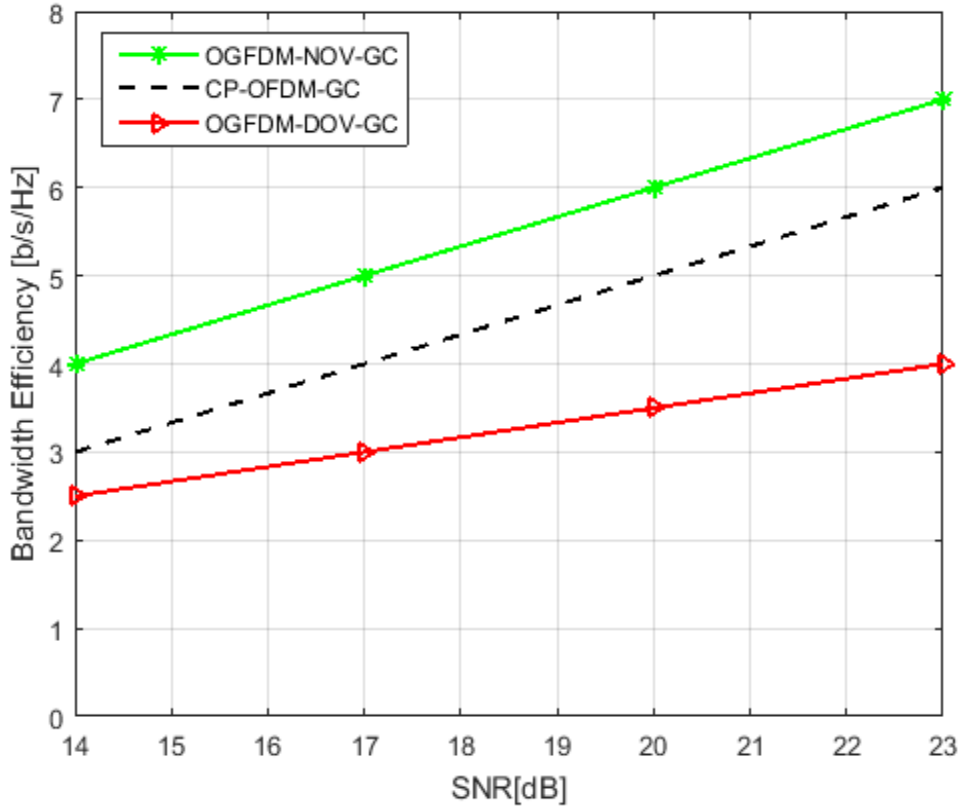


Figure 4.2.16: BW efficiency difference between the OGFDM and CP-OFDM (Ericsson technology) in good transmission condition.

Regarding the modulation level, as is clear in Figure 4.2.18, since the filtration process reduces the OOB emission, the transmission bit-rate of OGFDM with adaptive modulation can be maximized up to around 133% of the CP-OFDM transmission rate (Ericsson waveform) with fixed modulation format. As such, due to 3 dB difference of SNR between OGFDM and CP-OFDM, the channel capacity of OGFDM with fixed modulation can exceed the CP-OFDM channel capacity with DBL. Hence, the bit-rate of the OGFDM that is assigned for the worst transmission condition (fixed modulation) is higher than the bit-rate of the Ericsson waveform (CP-OFDM) specified for the best transmission condition (adaptive modulation).

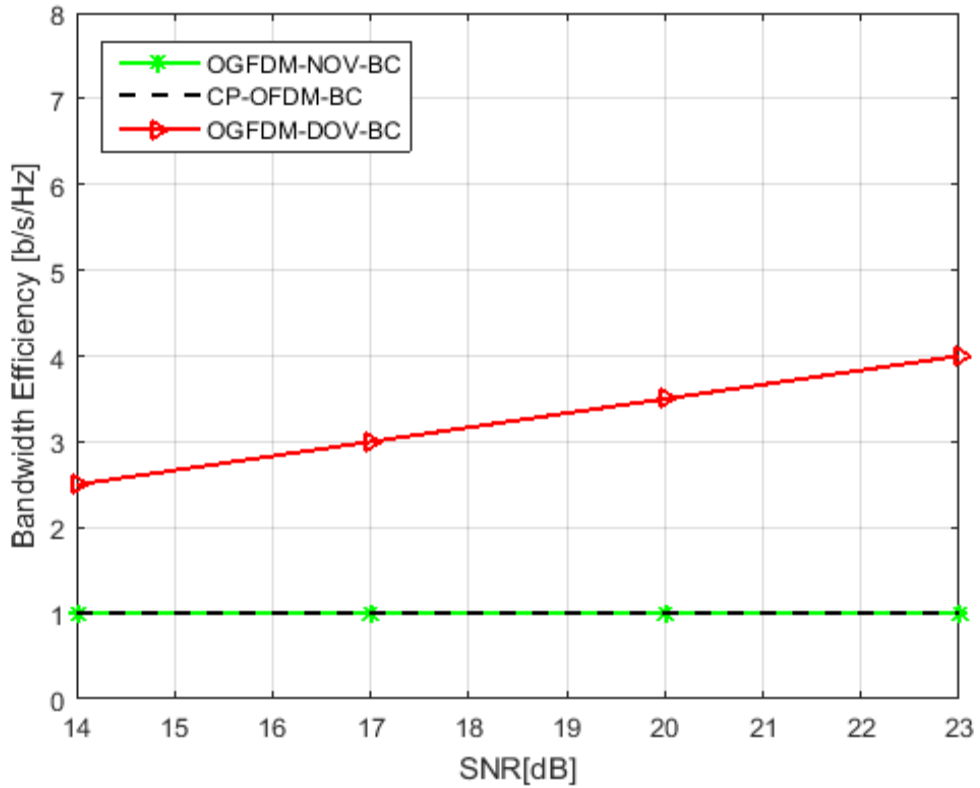


Figure 4.2.17: BW efficiency difference between the OGFDM and CP-OFDM (Ericsson technology) in bad transmission condition.

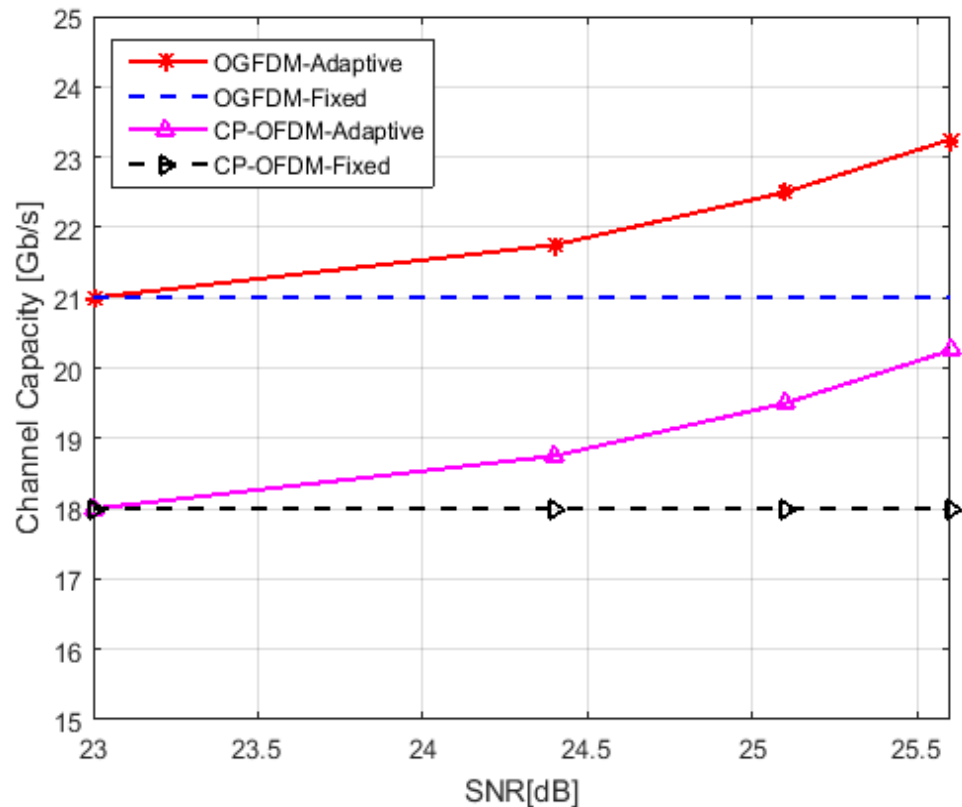


Figure 4.2.18: Difference in channel capacity between the OGFDM and CP-OFDM (Ericsson technology) for adaptive and fixed modulations.

### **4.3 Summary**

In this chapter, the developed stages (preliminary and upgraded) of the multi-carrier OGFDM system are introduced. For a better BW efficiency, the three levels of processing (filtration, oversampling, and modulation) are combined in one efficient system (preliminary multi-carrier OGFDM). The applied system provides higher channel capacity and wider resource sharing than the previously mentioned systems of the OGFDM (single, couple, and quadruple carrier). The preliminary system is then upgraded where both the number of frequency subcarriers and the speed of sampling frequency are improved. In addition, the extended OGFDM (32 subcarriers and 6 GHz sampling frequency) can extra support a higher overall channel capacity than both the 5G waveform (GFDM) and the LTE Ericsson waveform (CP-OFDM). In comparing with the GFDM, the experiment showed 2 dB improvement because of utilizing the Hilbert filters. Besides, due to the combined influence of both the orthogonal filters and, double sampling frequency, the OGFDM channel capacity is improved by about four times. In the RZ, 8 dB gains are obtained by changing from the GFDM with NOV to the OGFDM with DOV. Nevertheless, in the GZ, 3.5 dB gains can be obtained by moving from the channel capacities of the GFDM with the DOV to the maximum channel capacity of the OGFDM with the NOV. With both DBL and fixed modulation, the OGFDM still supplies 2 dB gain relative to GFDM. In comparison with the CP-OFDM, the OGFDM gains 3 dB difference in the SNR level demonstrating the impact of employing a resilient filtration process with orthogonality. Besides, the OGFDM with both NOV at good transmission condition and DOV at bad transmission condition records a higher channel capacity than CP-OFDM. Furthermore, the OGFDM with DBL can maximize the bit-rate up to around 133% of the CP-OFDM bit-rate with fixed modulation formats. To extra support the system model, the Visio application is used for drawing figures side by side with the MATLAB simulation that is utilized to validate the results and represent them graphically. The main parts of this chapter were published in (Kadhum, 2019), and (Kadhum, 2020).

# **Chapter 5: Conclusion and Future Work**

## **5.1 Conclusion**

In this research, a novel technique of the communication waveform for improving the channel capacity of future mobile networks yet keeping them at the acceptable limits of errors is proposed, investigated and evaluated in the physical layer of an electrical back-to-back wireless transmission system. The proposed waveform (OGFDM) that is explored from different levels of processing (filtration, oversampling, and modulation) is demonstrated for the single carrier, couple carrier, quadruple carrier and ultimately for the multi-carrier system.

As demonstrated in section 3.1, with respect to the single carrier OGFDM system (Kadhum *et al.*, 2018), particularly, at the filtration level, since the traditional filter (RRC) of the GFDM caused in decreasing the efficiency of the BW, the developed Hilbert filters are applied for the OGFDM presenting a high level of the BW efficiency. The experimental results of one frequency centre introduced 2 dB gain between the channel capacity of the OGFDM and GFDM for different modulation formats. Thus, utilizing sampling frequency equals to 2 GHz and modulation format is equivalent to 256 QAM, 8 Gb/s and 4 Gb/s are recorded for the OGFDM and GFDM respectively. This is principally resulted from counting on the Hilbert pairs that combine and separate orthogonally the frequency subcarriers of the OGFDM frequency centre. The core idea behind these developed filters is the perpendicular change in phase between adjacent frequency subcarriers that comes up with cancelling any probable interference. The findings also showed a similarity between the intended SNR for both the OGFDM and GFDM which in turns make the presented system able to attain double channel capacity at the same acceptable level of the BER. This, as such, makes the improved filtering process able to address optimally the drawbacks of the conventional GFDM filters, hence, doubling the OGFDM channel capacity of each transmitted frequency centre. The obtained results were achieved firstly for the single carrier system and then promoted gradually for the multi-carrier system. In addition, such a kind of manipulating that ends up with convoluting two filtered subcarriers for every utilized frequency centre is called as digital chunk processing.

As explained in section 3.2, with reference to the couple carrier OGFDM system (Kadhum, Kanakis and Crockett, 2019b), specially, at the oversampling level, as interference handling is a significant operation for the digital filters of the OGFDM system, the relationship between

the oversampling factor and roll-off factor of the filter is investigated thoroughly. The preliminary improvement in the oversampling stage was applied firstly for two frequency centres that are used to examine the induced interference between neighbouring subcarriers work at 2 GHz sampling frequency. The experimental output showed that with the traditional scheme of oversampling which fundamentally works in the normal oversampling mode, the overall channel capacity is reduced more sharply with comparatively enlarged roll-off factor ( $0.4 < \alpha$ ). As such, due to extremely overlap between adjacent filters of the same kind (in-phase/quadrature-phase), the interference is further increased. On the other hand, with the amplified values of the roll-off ( $0.5 \leq \alpha \leq 1$ ), the achieved results declared that employing the double oversampling mode, the overall channel capacity is amended. Therefore, by implementing a double oversampling, the unwanted increment of the roll-off value is avoided professionally. However, in contrast with the normal oversampling, the roll-off values between 0 and 0.3 of the double oversampling mode causes in degrading the channel capacity due to the halved BW of the applied filters. Consequently, neither the normal oversampling nor the double oversampling mode alone can reach the best management of the interference. As such, the hybrid manipulation that combines both normal and double oversampling is recommended to extra support a better channel capacity, higher transmission reliability and larger resources sharing than the traditional way. This type of handling that accommodates two oversampling modes together is named as intra-channel interference avoidance.

As illustrated in section 3.3, in relation to the quadruple carrier OGFDM system (Kadhum, Kanakis and Crockett, 2019a), particularly, at the modulation level, due to the restricted BW efficiency of the fixed modulation shapes, an improved technique of bits mapping is applied. Consequently, rather than the limited formats of the modulation like the 128 QAM, an adaptive modulation scheme is alternatively employed for the four frequency centres that operate in 2 GHz sampling frequency. By adopting such kind of treatment, the adjusted modulation can maximize the performance in terms of the channel capacity without requiring for use a higher static modulation like the 256 QAM. This, mainly, leads to achieving a further enhancement in the BW usage yet maintaining an appropriate BER level. The experimented work demonstrated that employing the resilient modulation format, three significant thresholds (low, medium, high) can be decided for the dynamic SNR range of any two adjacent forms of the fixed modulation. That's means, with variable channel status, better transmission bit-rates can be realized in contrast with the traditional modulation formats. As a result, apart from the undesirable circumstances of the transmission, the achieved channel capacities of the

flexible configuration far outweigh the stationary threshold of the calculated channel capacity with the fixed modulation. This is principally obtained due to the adaptive allocation of the applied bit-stream in accordance with the updated channel conditions. Such form of assigning that allocates bits according to the amended power of the frequency subcarrier is termed as dynamic bit loading.

As seen in section 4.1, on the topic of the multi-carrier OGFDM system (Kadhum, 2019), the introduced configuration with 8 frequency centres, and 16 frequency subcarriers, that are sampling at 4 GHz, can extra provide a higher channel capacity and broader sharing resource than the previous systems (single, couple and quadruple carrier) of the OGFDM. In addition, from a functional perspective, the developed multi-carrier scheme combines all three levels of the processing (filtration, oversampling, and modulation) in one uniform scheme. In terms of the filtration level, the findings indicate that using the Hilbert filters, that are orthogonally multiplexing a set of frequency subcarriers, the overall channel capacity of the OGFDM is doubled achieving 14 Gb/s in compared with 7 Gb/s for GFDM. The best capacity of the channel is gained for the filter with roll-off equals to 0.1, while, the worst channel capacities are recorded for roll-off equals to or larger than 0.5 at normal oversampling ( $OV = 16$ ). In terms of the oversampling level, the influence of the double oversampling ( $OV = 32$ ) accommodates the negative reaction of the enlarged roll-off factor perfectly. Thus, the calculated BER for all expected values of the increased roll-off ( $0 \leq \alpha \leq 1$ ) comes up with a similar level of the acceptable errors ( $10^{-3}$ ) at SNR corresponds to 23 dB. Nevertheless, compared to the normal case ( $OV = 16$ ) with roll-off values less than 0.4, the channel capacity of the double oversampling is mainly decreased due to the reduced BW. This, as a result, make the combination between the normal and double oversampling is more suitable than adopting just one mode. In terms of the modulation level, by utilizing the adaptive modulation with both the filtration and hybrid oversampling (normal and double), better bit-rates are reached than the conventional modulation. This, therefore, improves the performance by maximizing the wireless channel capacity to around 14% of its aggregated bit-rate with the fixed modulation formats. Thus, without a complete transfer to a higher fixed modulation system, a further BW efficiency is realized yet keeping the error average at the acceptable standard ( $BER = 10^{-3}$ ). It's worth noting that, compared to the multi-carrier system, the preceding systems can associate only two processes at most in their systems. For example, the filtration process in the single carrier, the filtration and oversampling processes in the couple carrier and the filtration and modulation processes in the quadruple carrier.

As clarified in section 4.2, concerning the extended version of the multi-carrier OGFDM system (Kadhum, 2020), the upgraded scheme with 32 frequency subcarriers and sampling frequency equals to 6 GHz can further support a wider number of mobile users and a higher overall channel capacity than the preliminary multi-carrier OGFDM. Experimentally speaking, each layer of processing has three levels of management (filtration, oversampling, and modulation) that directly impact the performance of the introduced system. In terms of the filtration level, the experiment shows that 2 dB rise can be gained by either enhancing the BW efficiency (Hilbert pair) or by extra increasing (double) the used sampling frequency. In addition, moving from the GFDM to the OGFDM with transferring the speed from 2 GHz to 4 GHz comes up with an additional variance (4 dB) which in turns results in improving the channel capacity of the OGFDM by about four times in comparing with the GFDM. Furthermore, similar channel capacity can be recorded for the OGFDM with 2 GHz and the GFDM with 4 GHz reflecting principally the influence of the advanced filters. Worth noting that, the realized upgrading due to extending the utilized BW is not necessarily matching to 2 dB gain. Consequently, by rising the OGFDM sampling frequency to 6 GHz, 3 dB and 1.5 dB gains are recognized for the channel capacity of the OGFDM with both the 2 GHz and 4 GHz respectively. Also, due to the orthogonality of the OGFDM, 6 dB and 3 dB increase, are registered with 6 GHz, in comparing with the GFDM at 2 and 4 GHz. In the oversampling level, mainly at the GZ, the findings indicate that due to the Hilbert filters, a stable 2 dB gain is reached between the channel capacity of OGFDM and GFDM under the normal oversampling and double oversampling conditions. In addition, despite the halved BW with the double oversampling, a lower decrease (1.75 dB) is recorded for the bit-rate of the OGFDM and GFDM with the normal oversampling at the optimum rolling ( $\alpha = 0.1$ ). Moreover, by moving from the channel capacities of the GFDM with the double oversampling to the maximum channel capacity of the OGFDM with the normal oversampling, 3.5 dB gain can be obtained. In the RZ, 4 dB gain is counted by changing from the OGFDM / GFDM with normal oversampling to a similar form with the double oversampling. Besides, 8 dB improvement is calculated for moving from GFDM with normal oversampling to the OGFDM with the double oversampling. In the modulation level, particularly, at the adaptive level of the upgraded system, the results declare that, in comparison with the preliminary multi-carrier system, the number of the amended subcarriers that can carry additional bit is increased (doubled) for the same ratio of the SNR threshold. Therefore, eight, sixteen and twenty-four improved subcarriers are recorded for 25%, 50%, and 75% enhancement rate respectively. Worth noting that, the aggregated bit-rate of the transmission can be maximized up to around

114% of the overall channel capacity yet keeping a steady level of the BER at  $10^{-3}$ . Additionally, in comparing to the GFDM, 2 dB gain is obtained for the channel capacity of the OGFDM with both the fixed and adaptive modulation formats. Furthermore, the upgraded OGFDM is compared with the CP-OFDM (LTE Ericsson technology) where 3 dB difference in SNR level is recorded for the OGFDM than CP-OFDM at the acceptable BER limit. In addition, the OGFDM with both NOV and DOV demonstrates a higher channel capacity than CP-OFDM in good and bad transmission conditions respectively. Moreover, bit-rate of the OGFDM with DBL is maximized by up to around 133% of the CP-OFDM bit-rate with fixed modulation shapes.

## 5.2 Future Work

- After successfully launching the new waveform OGFDM for the single input single output (SISO) transceivers, it would be great if the OGFDM system is introduced for the multiple-input multiple-output (MIMO) transceivers. The proposed system aims to obtain an extra improvement in wireless channel capacity.
- Since wireless technology includes, in addition to the mobile systems (LTE, 5G and beyond), variant range of transmission systems like wifi, WiMAX, Bluetooth, etc., it would be interesting to consider the OGFDM for other wireless networks like the LAN, MAN, and WPAN. As such, investigating the effect of changing the area of transmission on the overall channel capacity and how this can be addressed by the developed OGFDM waveform.

## References

- Agiwal, M., Roy, A. and Saxena, N. (2016) 'Next Generation 5G Wireless Networks: A Comprehensive Survey', *IEEE Communications Surveys Tutorials*, 18(3), pp. 1617–1655. doi: 10.1109/COMST.2016.2532458.
- Aijaz, A. (2016) 'Towards 5G-enabled Tactile Internet: Radio resource allocation for haptic communications', *2016 IEEE Wireless Communications and Networking Conference Workshops, WCNCW 2016*, pp. 145–150. doi: 10.1109/WCNCW.2016.7552690.
- Al-mawali, K. S. *et al.* (2011) 'Simple Discrete Bit-loading for OFDM Systems in Power Line Communications', *2011 IEEE International Symposium on Power Line Communications and Its Applications*. IEEE, pp. 267–270. doi: 10.1109/ISPLC.2011.5764405.
- Alexander, E. and Poullikas, D. (1999) *Formulas and Tables for Signal Processing*.
- Bai, Z. *et al.* (2010) 'On the Physical Layer Performance with Rank Indicator Selection in LTE / LTE-Advanced System', *2010 IEEE 21st International Symposium on Personal, Indoor and Mobile Radio Communications Workshops*. IEEE, pp. 393–398. doi: 10.1109/PIMRCW.2010.5670402.
- Balint, C. (2018) 'OFDM-Based Multi-Carrier Waveforms Performances in 5G', *2018 International Symposium on Electronics and Telecommunications (ISETC)*. IEEE, pp. 1–4.
- Ballal, B. R., Chadha, A. and Satam, N. (2013) 'Orthogonal Frequency Division Multiplexing and its Applications', *International Journal of Scientific Engineering and Research (IJSER)*, 1(1–3), pp. 325–328.
- Barry, E. J. R., Lee, E. A. and Messerschmitt, D. G. (2004) 'Digital Communication Edition John R. Barry, Edward A. Lee, David G. Messerschmitt 3rd ed. 2004', p. 2004.
- Bochechka, G. *et al.* (2017) 'Comparative analysis of UFMC technology in 5G networks', *2017 International Siberian Conference on Control and Communications (SIBCON)*. IEEE, pp. 1–6. doi: 10.1109/SIBCON.2017.7998465.
- Borkar, S. and Pande, H. (2016) 'Application of 5G next generation network to Internet of Things', *2016 International Conference on Internet of Things and Applications, IOTA 2016*, pp. 443–447. doi: 10.1109/IOTA.2016.7562769.
- Boshehba, S. A., Badran, E. F. and Mahmoud, M. (2013) 'A Modified Blind Deterministic Carrier Frequency Offset Estimator for OFDM Systems', *2013 Second International Japan-Egypt Conference on Electronics, Communications and Computers (JEC-ECC)*. IEEE, pp. 18–22. doi: 10.1109/JEC-ECC.2013.6766378.
- Boute, R. T. (1985) 'On The Equivalence of Time-Division and Frequency-Division Multiplexing', C(1), pp. 97–99.
- Breandán, Ó. *et al.* (2018) 'Devices and Sensors Applicable to 5G System Implementations', *2018 IEEE MTT-S International Microwave Workshop Series on 5G Hardware and System Technologies (IMWS-5G)*. IEEE, pp. 1–3.
- Casas, E. F. and Leung, C. (1992) 'OFDM for Data Communication Over Mobile Radio FM Channels', 40(4), pp. 680–683.
- Chen, B. *et al.* (2015) 'Research on Synchronization Issues of CP-OFDM Receiver', *2015 IEEE 5th International Conference on Electronics Information and Emergency Communication*. IEEE, pp. 126–130. doi: 10.1109/ICEIEC.2015.7284503.

- Chiumento, A. *et al.* (2014) ‘Scalable LTE interference mitigation solution for HetNet deployment’, *2014 IEEE Wireless Communications and Networking Conference Workshops, WCNCW 2014*, pp. 46–51. doi: 10.1109/WCNCW.2014.6934859.
- Debbabi, N., Siala, M. and Boujema, H. (2005) ‘Optimization of the OFDM prototype waveform for highly time and frequency dispersive channels through a maximization of the SIR’, *2005 12th IEEE International Conference on Electronics, Circuits and Systems*. IEEE, (1), pp. 1–4. doi: 10.1109/ICECS.2005.4633470.
- Demel, J., Bockelmann, C. and Dekorsy, A. (2017) ‘Evaluation of a software defined GFDM implementation for industry 4.0 applications’, *Proceedings of the IEEE International Conference on Industrial Technology*, pp. 1283–1288. doi: 10.1109/ICIT.2017.7915548.
- Ding, Z., Wang, X. and Yang, W. (2016) ‘A Dynamic Load Balancing Algorithm in Heterogeneous Network’, *2016 7th International Conference on Intelligent Systems, Modelling and Simulation (ISMS)*. IEEE, pp. 337–342. doi: 10.1109/ISMS.2016.41.
- Feig, E. (1990) ‘FREQUENCY DIVISION MULTIPLEXING WITH CHANNEL CONSTRAINTS’, pp. 287–291.
- Gaoxui, L. (2018) ‘Research on a Modulation Recognition Method for the FBMC-OQAM Signals in 5G Mobile Communication System’, *2018 13th IEEE Conference on Industrial Electronics and Applications (ICIEA)*. IEEE, (3), pp. 2544–2547. doi: 10.1109/ICIEA.2018.8398139.
- Gaspar, I. *et al.* (2014) ‘LTE-compatible 5G PHY based on Generalized Frequency Division Multiplexing’, *2014 11th International Symposium on Wireless Communications Systems (ISWCS)*. IEEE, pp. 209–213. doi: 10.1109/ISWCS.2014.6933348.
- Gaspar, I., Mendes, L., *et al.* (2015) ‘GFDM - A Framework for Virtual PHY Services in 5G Networks’, pp. 1–8.
- Gaspar, I., Gaspar, I., *et al.* (2015) ‘Synchronization using a Pseudo-Circular Preamble for Generalized Frequency Division Multiplexing in Vehicular Communication Synchronization using a Pseudo-Circular Preamble for Generalized Frequency Division Multiplexing in Vehicular Communication’, *Vehicular Technology Conference, 2013. VTC Spring 2013, IEEE 82nd*. doi: 10.1109/VTCFall.2015.7391164.
- Geng, S., Xiong, X. and Cheng, L. (2015) ‘UFMC System Performance Analysis for Discrete Narrow-band Private Networks’, *2015 IEEE 6th International Symposium on Microwave, Antenna, Propagation, and EMC Technologies (MAPE)*. IEEE, pp. 303–307. doi: 10.1109/MAPE.2015.7510319.
- Gessner, C. *et al.* (2012) ‘UMTS Long Term Evolution ( LTE ) - Technology Introduction Application Note Products ’:
- Ghogho, M. *et al.* (2005) ‘Channel estimation and symbol detection for block transmission using data-dependent superimposed training’, *IEEE Signal Processing Letters*, 12(3), pp. 226–229. doi: 10.1109/LSP.2004.842283.
- Grover, A. (2013) ‘ML and MMSE Equalizers in Frequency selective and Flat fading Channels’, *2013 1st International Conference on Artificial Intelligence, Modelling and Simulation*. IEEE, 1, pp. 413–415. doi: 10.1109/AIMS.2013.75.
- Habibi, M. *et al.* (2019) ‘A Comprehensive Survey of RAN Architectures Toward 5G Mobile Communication System’, *IEEE Access*. IEEE, 7, pp. 70371–70421. doi: 10.1109/ACCESS.2019.2919657.
- Haboobi, H. and Kadhum, M. R. (2019a) ‘Impact Study and Evaluation of Higher Modulation Schemes on

- Physical Layer of Upcoming Wireless Mobile Networks', *International Journal of Advanced Computer Science and Applications(IJACSA)*, 10(5).
- Haboobi, H. and Kadhum, M. R. (2019b) 'Utilise Higher Modulation Formats with Heterogeneous Mobile Networks Increases Wireless Channel Transmission', in *Proceeding of computing conference 2019, London*.
- Han, S., Sung, Y. and Lee, Y. H. (2017) 'Filter Design for Generalized Frequency-Division Multiplexing', *IEEE Transactions on Signal Processing*, 65(7), pp. 1644–1659. doi: 10.1109/TSP.2016.2641382.
- Hao, W., Hongwen, Y. and Jun, T. (2012) 'A Novel Adaptive Bit Loading Algorithm for BICM-OFDM System', pp. 311–315.
- Hazareena, A. (2018) 'A SURVEY : ON THE WAVEFORMS FOR 5G', *2018 Second International Conference on Electronics, Communication and Aerospace Technology (ICECA)*. IEEE, (Iceca), pp. 64–67. doi: 10.1109/ICECA.2018.8474641.
- He, Z. et al. (2018) 'A Novel RAPF Algorithm and Its PAPR Reduction Performance Based DFT Spreading in FBMC-OQAM System', *2018 10th International Conference on Communication Software and Networks (ICCSN)*. IEEE, 1(1), pp. 334–338. doi: 10.1109/ICCSN.2018.8488253.
- Hilario-tacuri, A., Fortes, J. M. P. and Sampaio-neto, R. (2018) 'Analytical spectral evaluation of GFDM systems over non-linear channels with memory', *2018 IEEE 10th Latin-American Conference on Communications (LATINCOM)*. IEEE, (3), pp. 1–5.
- Howald, R. L., Kesler, S. and Kam, M. (1998) 'BER Performance Analysis of OFDM-QAM in Phase Noise', p. 19104.
- Hwang, T. et al. (2009) 'OFDM and Its Wireless Applications : A Survey', 58(4), pp. 1673–1694.
- Im, G. H. et al. (1995) '51.84 Mb/s 16-CAP ATM LAN Standard', *IEEE Journal on Selected Areas in Communications*, 13(4), pp. 620–632. doi: 10.1109/49.382153.
- Ingle, V. K. and Proakis, J. G. (2012) *Digital Signal Processing Using MATLAB*. USA.
- Jayan, G. and Nair, A. K. (2018) 'Performance Analysis of Filtered OFDM for 5G', *2018 International Conference on Wireless Communications, Signal Processing and Networking (WiSPNET)*. IEEE, pp. 1–5.
- Jiang, Z. and Mao, S. (2015) 'Energy Delay Tradeoff in Cloud Offloading for Multi-Core Mobile Devices', *IEEE Access*, 3, pp. 2306–2316. doi: 10.1109/ACCESS.2015.2499300.
- Jin, W. et al. (2016) 'Improved Performance Robustness of DSP-Enabled Flexible ROADM Free from Optical Filters and O-E-O Conversions', *Journal of Optical Communications and Networking*. OSA, 8(8), p. 521. doi: 10.1364/JOCN.8.000521.
- Jorswieck, E. (2018) 'Transceiver Design for GFDM with Index Modulation in Multi-user Networks', (March), pp. 14–17.
- Junhui, Z., Guan, S. and Gong, Y. (2011) 'Performance Analysis of Adaptive Modulation System over Mobile Satellite Channels', pp. 3–6.
- Kadhum, Kanakis, T. and Crockett, R. (2019a) 'Dynamic Bit Loading with the OGFDM Waveform Maximises Bit-Rate of Future Mobile Communications', *Advances in Intelligent Systems and Computing*, 998, pp. 242–252. doi: 10.1007/978-3-030-22868-2\_19.
- Kadhum, Kanakis, T. and Crockett, R. (2019b) 'Intra Channel Interference Avoidance with The OGFDM Boosts Channel Capacity of Future Wireless Mobile Communication', in *Proceeding of computing conference 2019, London*.

- Kadhum, M. R. *et al.* (2018) ‘Digital Chunk Processing with Orthogonal GFDM Doubles Wireless Channel Capacity’, in *Proceeding of computing conference 2018, London*, pp. 1–6.
- Kadhum, M. R. (2019) ‘New Multi-Carrier Candidate Waveform For the 5G Physical Layer of Wireless Mobile Networks’, *2019 Wireless Days (WD)*. IEEE, pp. 1–7.
- Kadhum, M. R. (2020) ‘Upgrading Physical Layer of Multi-Carrier OGFDM Waveform for Improving Wireless Channel Capacity of 5G Mobile Networks and Beyond †’, *information Article*, 11(1). Available at: <https://www.mdpi.com/2078-2489/11/1/35>.
- Kawamura, T. *et al.* (2006) ‘Investigations on Optimum Roll-off Factor for DFT-Spread OFDM Based SC-FDMA Radio Access in Evolved UTRA Uplink’, (1).
- Kim, H. and Rautio, T. (2016) ‘Weighted selective mapping algorithm for FBMC-OQAM systems’, *2016 International Conference on Information and Communication Technology Convergence, ICTC 2016*, pp. 214–219. doi: 10.1109/ICTC.2016.7763471.
- Kim, J. *et al.* (2018) ‘A New Filter-Bank Multicarrier System : The Linearly Processed FBMC System’, *IEEE Transactions on Wireless Communications*. IEEE, 17(7), pp. 4888–4898. doi: 10.1109/TWC.2018.2832646.
- Kim, S.-Y. *et al.* (2014) ‘OLT Receiver for Power Normalization of Burst’, *IEEE Photonics Technology Letters*. IEEE, 26(24), pp. 2469–2472. doi: 10.1109/LPT.2014.2359016.
- Kumar, L., Member, S. and Parihar, M. S. (2018) ‘A Wide Stopband Low-Pass Filter With High Roll-Off Using Stepped Impedance Resonators’, 28(5), pp. 404–406.
- Kundu, P. (2014) ‘Comparison of Peak to Average Power Reduction Techniques in OFDM’, *2014 International Conference on Advances in Computing, Communications and Informatics (ICACCI)*. IEEE, 2(1), pp. 875–879. doi: 10.1109/ICACCI.2014.6968456.
- Li, F. *et al.* (2016) ‘A interference-free transmission scheme for GFDM system’, *2016 IEEE Globecom Workshops, GC Wkshps 2016 - Proceedings*. doi: 10.1109/GLOCOMW.2016.7848815.
- Li, X. *et al.* (2017) ‘Carrying MTC service in 5G - A network management perspective’, *IEEE Vehicular Technology Conference*. doi: 10.1109/VTCFall.2016.7880928.
- Liu, G. and Jiang, D. (2016) ‘5G: Vision and Requirements for Mobile Communication System towards Year 2020’, *Chinese Journal of Engineering*, 2016(March). doi: 10.1155/2016/5974586.
- Liu, Y. *et al.* (2017) ‘Waveform Design for 5G Networks: Analysis and Comparison’, *IEEE Access*, 3536(c), pp. 1–1. doi: 10.1109/ACCESS.2017.2664980.
- Lizárraga, E. M., Dowhuszko, A. A. and Sauchelli, V. H. (2012) ‘Improving Out-of-Band Power Emissions in OFDM Systems using Double-length Symbols’, 10(3), pp. 1710–1718. doi: 10.1109/TLA.2012.6222575.
- Lu, W. *et al.* (2016) ‘Simultaneous wireless information and power transfer based on joint subcarrier and power allocation in OFDM systems’, *IEEE Access*, 5, pp. 2763–2770. doi: 10.1109/ACCESS.2017.2671903.
- Luo, D. (2013) ‘Optimum Power Allocation for OFDM in Physical-Layer Network Coding over a Flat Frequency-selective Fading Channel’, *2013 9th International Conference on Information, Communications & Signal Processing*. IEEE, (61201148), pp. 1–5. doi: 10.1109/ICICS.2013.6782897.
- Maham, B. (2006) ‘DSP Implementation Aspects of an OFDM Based Wireless MAN Modem’, *2006 International Conference on Wireless Communications, Networking and Mobile Computing*. IEEE, pp. 1–4. doi: 10.1109/WiCOM.2006.76.
- Mera, M. I. and Estrada, R. L. (2009) ‘Model Based Design of an Adaptive Transmission Module for Non-

- Line of Sight OFDM System ( WiMAX )', 00(C), pp. 204–206.
- Michailow, N. *et al.* (2014) ‘Generalized Frequency Division Multiplexing : A Flexible Multi-Carrier Modulation Scheme for 5th Generation Cellular Networks’, *Proceedings of the German Microwave Conference(GeMiC'12)*, 62(9), pp. 1–4.
- Mukumoto, K. and Wada, T. (2014) ‘Realization of Root Raised Cosine Roll-Off Filters Using a Recursive FIR Filter Structure’, *IEEE Transactions on Communications*. IEEE, 62(7), pp. 2456–2464. doi: 10.1109/TCOMM.2014.2329672.
- Naga Rani, P. and Santhi Rani, C. H. (2017) ‘UFMC: The 5G modulation technique’, *2016 IEEE International Conference on Computational Intelligence and Computing Research, ICCIC 2016*. doi: 10.1109/ICCIC.2016.7919714.
- Nimr, A. *et al.* (2018) ‘Extended GFDM Framework : OTFS and GFDM Comparison’, pp. 0–5.
- Nusairat, A., Li, X. and Member, S. (2012) ‘WiMAX / OFDMA Burst Scheduling Algorithm to Maximize Scheduled Data’, *IEEE Transactions on Mobile Computing*. IEEE, 11(11), pp. 1692–1705. doi: 10.1109/TMC.2011.211.
- Olmedo, M. I. *et al.* (2014) ‘Multiband Carrierless Amplitude Phase Modulation for High Capacity Optical Data Links’, 32(4), pp. 798–804.
- Ouzzif, M. (2009) ‘Statistical analysis of the cyclic prefix impact on indoor PLC capacity’, pp. 285–289.
- Prabu, R. T. *et al.* (2016) ‘Millimeter Wave for 5G Mobile Communication Application’, *International Conference on Advances in Electrical, Electronics, Information, Communication and Bio-Informatics (AEEICB16)*, pp. 1–5. doi: 10.1109/AEEICB.2016.7538280.
- Prommee, P., Thongdit, P. and Angkeaw, K. (2017) ‘Log-domain high-order low-pass and band-pass filters’, *AEUE - International Journal of Electronics and Communications*. Elsevier GmbH, 79, pp. 234–242. doi: 10.1016/j.aeue.2017.06.014.
- Saad, M., Al-ghouwayel, A. and Hijazi, H. (2018) ‘UFMC Transceiver Complexity Reduction’, *2018 25th International Conference on Telecommunications (ICT)*. IEEE, pp. 295–301. doi: 10.1109/ICT.2018.8464863.
- Sacchi, C. *et al.* (2017) ‘Millimeter-Wave Transmission for Small-Cell Backhaul in Dense Urban Environment : a Solution Based on MIMO-OFDM and Space-Time Shift Keying ( STSK )’, 5.
- Schaich, F. *et al.* (2014) ‘Waveform contenders for 5G &#x2014; OFDM vs. FBMC vs. UFMC’, *2014 6th International Symposium on Communications, Control and Signal Processing (ISCCSP)*. IEEE, pp. 457–460. doi: 10.1109/ISCCSP.2014.6877912.
- Schwartz, M. (2009) ‘INTRODUCTION TO “ THE HISTORY OF OFDM ”’, (November).
- Shannon, C. E. (1949) ‘Communication in the Presence of Noise \*’, *Proceedings of the IEEE*. IEEE, 72(9), pp. 1192–1201. doi: 10.1109/PROC.1984.12998.
- Shuqi, W., Xin, M. and Yongqiang, C. (2018) ‘Design and Implementation of F-OFDM Filter’. doi: 10.1109/SNSP.2018.00044.
- Simsek, M. *et al.* (2016) ‘5G-Enabled Tactile Internet’, *IEEE Journal on Selected Areas in Communications*. IEEE, 34(3), pp. 460–473. doi: 10.1109/JSAC.2016.2525398.
- Smirnov, P. N., Kharitonov, S. A. and Preobrajensky, E. B. (2015) ‘Synthesis Methods of Hilbert Filters for Control Systems of Static Converters’, *2015 16th International Conference of Young Specialists on Micro/Nanotechnologies and Electron Devices*. IEEE, (5), pp. 486–489. doi: 10.1109/EDM.2015.7184590.

- Son, B. S. *et al.* (2002) ‘A high-speed fft processor for ofdm systems’, pp. 281–284.
- Stern, S. and Fischer, R. F. H. (2014) ‘OFDM vs . Single-Carrier Modulation : A New View on the PAR Behavior’, (Section V), pp. 112–119.
- Tao, L. *et al.* (2013) ‘Experimental demonstration of 10 Gb/s multi-level carrier-less amplitude and phase modulation for short range optical communication systems’, *Optics Express*, 21(5), p. 6459. doi: 10.1364/OE.21.006459.
- Tarchi, D., Corazza, G. E. and Vanelli-coralli, A. (2013) ‘Analysis of a State Based Approach for Adaptive Coding and Modulation in Mobile Satellite Environments’, *2013 IEEE 77th Vehicular Technology Conference (VTC Spring)*. IEEE, pp. 1–5. doi: 10.1109/VTCSpring.2013.6691888.
- Teja, R. (2018) ‘Review of UFMC Technique in 5G’, pp. 115–120. doi: 10.1109/ICICS.2018.00034.
- Torrea-duran, R. *et al.* (2012) ‘Adaptive Energy Efficient Scheduling Algorithm for LTE Pico Base Stations Rodolfo’, *2012 Future Network & Mobile Summit (FutureNetw)*. IEEE, pp. 1–8.
- Towliat, M., Mohammad, S. and Asgari, J. (2018) ‘GFDM Interference Mitigation Without Noise Enhancement’, *IEEE Communications Letters*. IEEE, 22(5), pp. 1042–1045. doi: 10.1109/LCOMM.2018.2813393.
- Tran, G. K., Shimodaira, H. and Sakaguchi, K. (2016) ‘Evaluation of mmWave overlaid 5G heterogeneous cellular networks - Suitable frequency bands for different 5G KPIs’, in *13th IEEE VTS APWCS 2016*.
- Umatani, T., Ohno, K. and Itami, M. (2010) ‘A Study on Schemes of Reducing Influence of Impulse Noise in OFDM under Multi-path Channel’, *2010 Digest of Technical Papers International Conference on Consumer Electronics (ICCE)*. IEEE, (2), pp. 119–120. doi: 10.1109/ICCE.2010.5418903.
- Walia, J. S. (2017) ‘Future Scenarios and Value Network Configurations for Industrial 5G’, pp. 79–84.
- Wan, L. *et al.* (2018) ‘4G / 5G Spectrum Sharing’, *IEEE Vehicular Technology Magazine*. IEEE, 13(december), pp. 28–39. doi: 10.1109/MVT.2018.2865830.
- Wang, Z. *et al.* (2012) ‘Frequency-Domain Oversampling for Zero-Padded OFDM in Underwater Acoustic Communications’, *IEEE Journal of Oceanic Engineering*. IEEE, 37(1), pp. 14–24. doi: 10.1109/JOE.2011.2174070.
- Weitkemper, P. *et al.* (2016) ‘On regular resource grid for filtered OFDM’, *IEEE Communications Letters*, 20(12), pp. 2486–2489. doi: 10.1109/LCOMM.2016.2572183.
- Wen, J., Hua, J. and Lu, W. (2018) ‘Design of Waveform Shaping Filter in the UFMC System’, 6.
- Wu, D. *et al.* (2016) ‘A field trial of f-OFDM toward 5G’, *2016 IEEE Globecom Workshops, GC Wkshps 2016 - Proceedings*. doi: 10.1109/GLOCOMW.2016.7848810.
- Wunder, G. *et al.* (2014) ‘5GNOW: Non-orthogonal, asynchronous waveforms for future mobile applications’, *IEEE Communications Magazine*, 52(2), pp. 97–105. doi: 10.1109/MCOM.2014.6736749.
- Yang, L., Cheng, S. and Wang, H. (2005) ‘EFFECTS OF CYCLIC PREFIX ON OFDM SYSTEMS OVER TIME-VARYING CHANNELS’, (a 1), pp. 750–753.
- Yang, Q. *et al.* (2009) ‘Real-time reception of multi-gigabit coherent optical OFDM signals’, 17(10), pp. 873–879.
- Yli-kaakinen, J. *et al.* (2017) ‘Efficient Fast-Convolution-Based Waveform Processing for 5G Physical Layer’, *IEEE Journal on Selected Areas in Communications*. IEEE, 35(6), pp. 1309–1326. doi: 10.1109/JSAC.2017.2687358.

- Yu, M. (2011) ‘Adaptive Bit Loading Algorithm of Shortwave Broadband OFDM System’, pp. 49–52.
- Yunzheng, T. *et al.* (2015) ‘A Survey : Several Technologies of Non-Orthogonal Transmission for 5G’, *China Communications*. China Institute of Communications, 12(October), pp. 1–15. doi: 10.1109/CC.2015.7315054.
- Zaidi, A. A. *et al.* (2018) ‘OFDM Numerology Design for 5G New Radio to Support IoT, eMBB, and MBSFN’, *IEEE Communications Standards Magazine*, 2(2), pp. 78–83. doi: 10.1109/mcomstd.2018.1700021.
- Zhang, Z. *et al.* (2017) ‘Universal filtered multi-carrier transmission with adaptive active interference cancellation’, *IEEE Transactions on Communications*, 65(6), pp. 2554–2567. doi: 10.1109/TCOMM.2017.2681668.
- Zhu, L. *et al.* (2010) ‘On Maximum Achievable Information Rates of Single-Carrier and Multi-Carrier Systems over the Ultra Wideband Channels’, *2010 IEEE International Conference on Ultra-Wideband*. IEEE, 2, pp. 1–4. doi: 10.1109/ICUWB.2010.5616837.

## Appendix

### Multiple IMRaD

Overview of PhD

Literature survey(?)

#### Topic one

- Introduction
- Methods
- Results
- Discussion

#### Topic two

- Introduction
- Methods
- Results
- Discussion

#### Topic three

- Introduction
- Methods
- Results
- Discussion

Conclusion/drawing strands together